Seismic Performance Assessment of Multi-Storey Buildings with Cold Formed Steel Shear Wall Systems

by

Joel Martínez Martínez

A thesis presented to the

University of Waterloo

in fulfilment of the thesis

requirement for the degree of

Doctor of Philosophy

in

Civil Engineering

Waterloo, Ontario, Canada, 2007

I hereby declare that I am the sole author of this thesis. This is a true copy of the thesis, including any required final revisions, as accepted by my examiners.

I understand that my thesis may be made electronically available to the public.

AKNOWLEDGEMENTS

I would like to express my sincere appreciation to my supervisors, Prof. Lei Xu and Prof. D.E. Grierson, for their support, guidance, and many hours of supervision required to complete this research. Their knowledge in the subjects involved in this research played an important role in the completion of this research.

I would like to thank the National Council on Science and Technology of Mexico (CONACYT) for providing financial support for my PhD studies.

Thanks are due to the Natural Sciences and Engineering Research Council of Canada (NSERC) for providing financial support.

Thanks are due to Prof. Colin Rogers for providing experimental data that was of enormous value to my research, and also for participating as the external-to-the-university member of the examining committee.

Thanks are due to all the members of the examining committee, Prof. Jeff West, Prof. Sanjeev Bedi, and especially to Prof. Reinhold Schuster who also taught me the theory and applications of cold formed steel.

I am very grateful to my lovely wife Cinthia Escalera, for her love, support and patience during these years. Also, I am very grateful to my parents and siblings for their support during my studies. Especially, to my elder sister Ernestina and her husband Omar.

Finally, I would like to express my appreciation to everyone who made these years in Waterloo a wonderful experience.

To Cinthia and Joelito

ABSTRACT

Cold-Formed Steel (CFS) is a material used in the fabrication of structural and non-structural elements for the construction of commercial and residential buildings. CFS exhibits several advantages over other construction materials such as wood, concrete and hot-rolled steel (structural steel). The outstanding advantages of CFS are its lower overall cost and non-combustibility. The steel industry has promoted CFS in recent decades, causing a notable increase in the usage of CFS in building construction. Yet, structural steel elements are still more highly preferred, due to the complex analysis and design procedures associated with CFS members. In addition, the seismic performance of CFS buildings and their elements is not well known.

The primary objective of this study is to develop a method for the seismic assessment of the lateral-load resistant shear wall panel elements of CFS buildings. The Performance-Based Design (PBD) philosophy is adopted as the basis for conducting the seismic assessment of low- and mid-rise CFS buildings, having from one to seven storeys. Seismic standards have been developed to guide the design of buildings such that they do not collapse when subjected to specified design earthquakes. PBD provides the designer with options to choose the performance objectives to be satisfied by a building to achieve a satisfactory design. A performance objective involves the combination of an earthquake (i.e., seismic hazard) and a performance level (i.e., limit state) expected for the structure. The building capacity related to each performance level is compared with the demand imposed by the earthquake. If the earthquake demand is less than the building capacity, the structure is appropriately designed.

The seismic performance of a CFS building is obtained using pushover analysis, a nonlinear method of seismic analysis. This study proposes a Simplified Finite Element Analysis (SFEA) method to carry out the nonlinear structural analysis. In this study, lateral drifts associated with four performance levels are employed as acceptance criteria

for the PBD assessment of CFS buildings. The lateral drifts are determined from experimental data.

In CFS buildings, one of the primary load-resistant elements is Shear Wall Panel (SWP). The SWP is constructed with vertically spaced and aligned C-shape CFS studs. The ends of the studs are screwed to the top and bottom tracks, and structural sheathing is installed on one or both sides of the wall. For the analysis of CFS buildings, Conventional Finite Element Analysis (CFEA) is typically adopted. However, CFEA is time consuming because of the large number of shell and frame elements required to model the SWP sheathing and studs. The SFEA proposed in this study consists of modeling each SWP in the building with an equivalent shell element of the same dimensions; that is, a complete SWP is modeled by a 16-node shell element. Thus, significantly fewer elements are required to model a building for SFEA compared to that required for CFEA, saving both time and resources. A model for the stiffness degradation of a SWP is developed as a function of the lateral strength of the SWP. The model characterizes the nonlinear behaviour of SWP under lateral loading, such that a realistic response of the building is achieved by the pushover analysis.

The lateral strength of a SWP must be known before its seismic performance can be assessed. In current practice, the lateral strength of a SWP is primarily determined by experimental tests due to the lack of applicable analytical methods. In this investigation, an analytical method is developed for determining the ultimate lateral strength of SWP, and associated lateral displacement. The method takes into account the various factors that affect the behaviour and the strength of SWP, such as material properties, geometrical dimensions, and construction details.

To illustrate the effectiveness and practical application of the proposed methodology for carrying out the PBD assessment of CFS buildings, several examples are presented. The responses predicted by the SFEA are compared with responses determined experimentally for isolated SWP. In addition, two building models are analyzed by SFEA, and the results are compared with those found by SAP2000 (2006). Lastly, the

PBD assessment of two buildings is conducted using SFEA and pushover analysis accounting for the nonlinear behaviour of the SWP, to demonstrate the practicality of the proposed technology.

TABLE OF CONTENTS

LIST OF TABLES

LIST OF FIGURES

SYMBOLS

α_B	Sheathing's bending stiffness reduction coefficient
α_V	Sheathing's shear stiffness reduction coefficient
β	Nonlinear exponent given as function of the screw edge spacing
Δ	Shear wall panel lateral deformation, at its maximum strength
Δ_C	Maximum deformation of a sheathing-to-framing connection
ΔU	Structure displacement increment vector
δ_y	Distance from the elastic centre to the instantaneous centre of rotation
ϕ	Rotation about the x local axis of the shell element
γ	Rotation about the y local axis of the shell element
η	Shear wall panel strength modification factor
η_s	Frequency parameter, given as function of k_p
κ	Exponent depending on the period of the structure
λ	Stiffness degradation coefficient
ρ	Cross section shape factor
τ	Cauchy stress matrix
$\hat{\tau}$	Cauchy stress vector
ν_x, ν_y	Sheathing's Poisson ratios in the x and y directions, respectively
ν_{xeq}, ν_{yeq}	Equivalent shell element's Poisson ratios in the x and y directions, respectively
A	Profile's cross section area
A_b	Beam's cross section area
A_c	Column's cross section area
A_F	Stud's cross section area
AISI	American Iron and Steel Institute
A_S	Sheathing's cross section area
B_L	Linear strain-displacement matrix
B_{NL}	Nonlinear strain-displacement matrix

C	Constitutive matrix
CFEA	Conventional finite element analysis
CFS	Cold-Formed Steel
CP	Collapse Prevention
CSP	Canadian Soft Plywood
C_u	Ultimate strength factor
C_{vx}	Vertical load distribution coefficient
c	Distance from the stud's centroid to sheathing's mid-plane
D	Shell's bending rigidity
DFP	Douglas Fir Plywood
Drift	Inter-storey drift: displacement of the floor above minus the displacement of the floor below
D_x, D_y	Shell's bending rigidities along the x and y directions respectively
d	Normalized deformation
d_f	Distance from the column's centroid to floor plan's centroid
d_i	Distance from the screw i to the centre of rotation
d_{max}	Distance between the centre of rotation and the farthest screw connection
d_s	Screw diameter
d_{xi}, d_{yi}	x and y components of d_i
E	Modulus of elasticity (Young modulus)
E_b	Beam's modulus of elasticity
E_c	Column's modulus of elasticity
E_F	Steel framing studs modulus of elasticity
E_{Sx}, E_{Sy}	Sheathing's modulii of elasticity in the x and y directions, respectively
E_x, E_y	Reduced sheathing's modulii of elasticity
E_{xeq}, E_{yeq}	Equivalent shell's modulii of elasticity in the x and y directions, respectively
e_2	Unit vector in the direction of a shell's local y axis
e_y	y component of the distance from the load to the elastic centre of rotation
F	Vector of unbalanced internal forces
F_a	Site coefficient

F_{gx}	Unbalanced force in the fastener group
F_u	Material tensile strength
F_v	Site coefficient
F_x	Vector lateral forces in a building
F_y	Material tensile yield strength
f_b	Building's shear frequency
f_s	Building's shear frequency
f_g	Frames' bending frequency
G_b	Column's shear modulus of elasticity
G_S	Sheathing's shear modulus of elasticity
GWB	Gypsum Wall Board
G_{xyeq}	Equivalent shell's shear modulus of elasticity
g	Gravity constant, 9.81 m/s^2
H	Building's height
h	Storey height
h_x	Height from the ground to the storey level x
h_z	Height from the ground to the storey level z
I	Cross section moment of inertia (Second moment of area)
I_3	3x3 identity matrix
I_b	Beam's cross section moment of inertia
I_c	Column's cross section moment of inertia
I_F	Steel stud's cross section moment of inertia
IP	Iterative procedure
IO	Immediate occupancy
I_S	Sheathing's cross section moment of inertia of
i	Counter
J	Polar moment of inertia of a fastener group
J_m	Jacobian matrix
k	Node number
K_a	SWP stiffness at load increment q
K_b	Frame global shear stiffness

K_c	Columns' shear stiffness
K_e	Building's effective shear stiffness
K_F	Steel framing studs' lateral stiffness
K_i	SWP initial stiffness (elastic)
K_L	Structure's elastic stiffness matrix
K_{NL}	Structure's nonlinear stiffness matrix
K_S	Sheathing's lateral stiffness associated
K_t	Steel stud's effective length factor for torsion
$K_{x,y}$	Steel stud's effective length factors for x and y axes, respectively.
k_L	Shell element's elastic stiffness matrix
k_{NL}	Shell element's nonlinear stiffness matrix
k_p	Non-dimensional parameter
L	Floor live load
L_r	Roof live load
LDR	Lateral drift ratio for SWP
LS	Life Safety
l	Shear wall panel length
M	Moment strength of the fasteners group
M_o	Moment produced by the unitary force about the elastic centre of rotation
M_p	Moment produced by the unitary force about the instantaneous centre of rotation
m	Mass density per unit of building height
N	Shell element shape functions
$NEHRP$	National Earthquakes Hazards Reduction Program
N_x, N_y	Shell axial rigidity along the x and y directions, respectively
n	Number of nodes in a shell element
n_C	Total number of screws on the panel, used to attach the sheathing
nd	Number of nodes per node line of the shell element
n_e	Number of shell elements
n_F	Number of studs
n_o	Number of columns

n_p	Number of shear wall panels
n_s	Number of screws along the top of the shear wall (i.e, l/s_C)
n_t	Number of building storeys
OP	Operational
OSB	Oriented Strand Board
P	Shell axial rigidity
P_a	Lateral load on the SWP in consideration at load increment q
PBD	Performance-Based Design
P_F	SWP steel framing lateral strength
P_{fc}	Shear wall panel lateral strength due to failure of the end-stud
PL	Performance level
P_n	Nominal compressive strength of the end-stud
PO	Performance objective
P_R	Shear wall panel lateral strength
P_S	Sheathing lateral strength
P_x	Lateral unitary force applied in the location of the actual force
q	Load increment index for the nonlinear structural analysis
R	Vector of external loads on the structure
R_i / R_u	Normalized force on the screw connection i
r	Shell element natural coordinate, along the Cartesian x coordinate
r_c	Stiffness combination factor
r_f	Reduction factor, given as function of the number of storeys
S_1	Response acceleration parameter at one-second period
S_a	Spectral acceleration
SFEA	Simplified finite element analysis
SLI	Strength loss index of shear wall panels
S_{M1}	Design spectral response acceleration parameter at one second period
S_{MS}	Design short-period spectral response acceleration parameter
SP	Simplified procedure
S_S	Short period response acceleration parameter
SWP	Shear wall panel

s	Shell element natural coordinate, along the Cartesian y coordinate
s_C	Edge screw spacing
T	Fundamental period of the structure
T_φ	Transformation matrix for the shell element direction vectors
T_o	Characteristic period
t_{eq}	Equivalent shell thickness
t_S	Sheathing's thickness
U	Structure's displacements vector
u	Shell element's displacement in the x direction
v	Shell element's displacement in the y direction
V_1	Direction vector of the shell element local x axis
V_2	Direction vector of the shell element local y axis
V_a	Building base shear at load increment q
V_b	Base shear
$V_{b\,\max}$	Maximum target base shear
V_n	Direction vector normal to the shell element surface
V_r	Strength of a single sheathing-to-framing connection
W	Structure's seismic weight
W_g	Gravitational loads
w	Shell element's displacement in the z direction
w_{SF}	Tributary width of a stud
w_x	Seismic weight corresponding to the storey level x
w_z	Seismic weight corresponding to the storey level z
x	Cartesian coordinate in the x direction
x_{Ci}, y_{Ci}	Coordinates of the i screw with respect the elastic centre of rotation
y	Cartesian coordinate in the y direction
z	Cartesian coordinate in the z direction

Chapter 1

Introduction

1.1. General

The construction of low-rise buildings using light-gauge materials such as Cold-Formed Steel (CFS) is a common practice in North America, even in seismic areas. CFS has numerous advantages over traditional construction materials such as wood, hot rolled (structural) steel, and concrete. CFS framing is simpler to erect, reducing the construction time and labour cost, and, consequently, the building overall cost. In addition, CFS is durable and has a large strength-to-weight ratio. Homebuilders and consumers alike have a general understanding of the benefits of CFS and are receptive to the use of steel framing. This has led to a tremendous growth of the application of CFS in residential and commercial construction that has long been predicted. Despite CFS virtues and its growing application, however, opposition still exists to use CFS for structural elements in the construction of mid-rise CFS buildings in seismic areas. The primary reasons are the lack of information about the seismic performance of CFS buildings, and the complicated structural analysis and design procedures associated with CFS members and systems. Therefore, research and development, for the technical and practical aspects to eliminate or substantially mitigate the impact of these barriers, is of primary importance.

Typically, the structural system of CFS buildings is different than that of structural steel buildings. In CFS buildings, the primary structural elements are Shear Wall Panels (SWP), load-bearing wall panels, and floor and roof panels; while in structural steel buildings, the primary structural elements are columns, beams, and cross-bracings. The functions of SWP, in addition to maintaining the stability and integrity of the structural system, are to resist in-plane lateral and gravity loads, and out-of-plane wind loads if the SWP are used as exterior walls. In general, SWP in CFS framing are constructed with

vertically spaced and aligned C-shape CFS studs. The ends of the studs are screwed to the top and bottom tracks. The structural sheathing can be installed on one or both sides of the wall. Load-bearing wall panels are built similarly to SWP, except that no structural sheathing is attached to the framing. Consequently, load-bearing wall panels lack the lateral strength and, therefore, are only capable to resist gravity loads. Although the floor and roof panels are built in the same fashion as the SWP, a concrete slab poured on the CFS deck can be used instead of wood sheathing. The primary loads on the floor and roof panels are gravity loads, and in-plane lateral loads associated with wind, or earthquakes when the panels serve as horizontal diaphragms.

The seismic assessment of CFS buildings is not addressed by the National Building Code of Canada (NBCC, 2005), nor by the North American Specification for the Design of Cold-Formed Structural Members (S136-01). Therefore, engineers are not provided with guidelines for the seismic assessment of CFS buildings. The seismic design of CFS buildings is carried out in accordance with seismic design standards. Traditionally, the principal objective of seismic design standards is to prevent the collapse of structures subjected to design earthquakes, disregarding the associated economical losses. In the last decade, a new philosophy of seismic design known as Performance-Based Design (PBD) was introduced by the Federal Emergency and Management Agency (FEMA 273, 1997) for the seismic assessment and rehabilitation of existing structures. FEMA combines multiple building performance levels with seismic hazards, represented by design earthquakes, to "assure" the expected behaviour of the structure. For a building subjected to a design earthquake, a performance level refers to a limit damage state. A limit damage state is represented by displacements, inter-storey drifts, base shears, loads, stresses, accelerations, or by other limit states (Ghobarah, 2001). Using PBD assessment procedures, designers and building owners are aware of the damage in a building that satisfies the specified performance levels for the design earthquake. Therefore, PBD assessment can provide a better understanding of the behaviour of CFS buildings, resulting in safer and more economical designs.

The PBD assessment of buildings is carried out by different analysis methods, such as linear static, linear dynamic, nonlinear static, and nonlinear dynamic analyses (FEMA 273, 1997). As such, the accuracy of the results and the complexity of the structural analysis of a building vary, depending on the chosen method. In this study, the nonlinear static analysis method, also known as pushover analysis, is employed due to its simplicity and accuracy for multi-storey buildings with a predominant fundamental mode of vibration in their response (Krawinkler and Seneviratna, 1998). Essentially, pushover analysis consists of transforming the building under consideration into an equivalent single degree of freedom system. Then, the seismic loads are applied on the building in small increments and structural analysis is carried out after each load increment, and the results are accumulated over the loading history.

Pushover analysis for PBD assessment has been successfully implemented for buildings constructed of different materials such as concrete, steel, and wood. However, PBD assessment has not yet been implemented in CFS buildings. To do this, it is first necessary to characterize force-displacement response curves, develop acceptance criteria associated with the performance levels, and establish a procedure for the analysis and design of the lateral-load resistant elements.

In this study, the acceptance criteria (limit damage state) for CFS buildings are established as a function of the lateral drift and lateral strength of the SWP. Although FEMA 273 (1997) provides limit drift ratios as acceptance criteria for different performance levels and types of structural systems, FEMA does not provide such limit drift ratios for CFS SWP. The limit drift ratios for SWP are determined from experimental data. The acceptance criteria include account for the lateral strength of SWP, which must be checked to assure that the SWP do not fail prior to satisfying the specified performance objectives.

Since SWP exhibit a nonlinear behaviour when subjected to lateral loads, as demonstrated in experimental investigations (Gad et al., 1999; Branston et al., 2006; Serrette et al., 2002), a stiffness degradation model to characterize the nonlinear response

of CFS buildings is needed for the pushover analysis. Only then can the response of CFS buildings be accurately predicted. The stiffness degradation model represents the loss of the lateral strength of the SWP as the lateral loads applied on the building are increased. Several models characterizing the nonlinear behaviour of SWP are found in the literature, including those developed by Branston et al. (2006), and by Fulop and Dubina (2004). These models are determined from experimental testing on SWP. This study proposes a general model, defined by a function of the lateral strength of the SWP and the spacing of the screws at the edge of the panel.

Due to the nature of the structural elements used for CFS buildings, the structural analysis of such buildings should be carried out by Conventional Finite Element Analysis (CFEA). However, CFEA is time-consuming and cumbersome for a mid-rise CFS building because it requires a large number of elements to generate the structural model. In addition, if conventional nonlinear pushover analysis is employed for the PBD assessment of a CFS building, the computation time is significant. Therefore, the development of a simplified analysis method which is also practical to use is of primary importance.

Only a few methods to simplify the analysis of SWP are published in the literature. Fulop and Dubina (2004) have proposed a simplified method that involves replacing the sheathing by equivalent cross-bracing. The method provides accurate results for isolated SWP under seismic loads, but not for SWP subjected to gravity or out-of-plane loads. In this study, the simplification is carried even further by recognizing that the individual modeling of the studs and sheathing plates in a building is not needed. Instead, the SWP are transformed into flat shell elements with equivalent properties for modeling complete panels. The equivalent shell elements account for the properties of the studs and sheathing, and are modeled by using a sixteen-node shell element for each panel. Then, a nonlinear finite element method is employed to perform the structural analysis. This procedure is called Simplified Finite Element Analysis (SFEA), for which the number of elements required to model a mid-rise CFS building is significantly less than that for

CFEA. As a result, less, time and resources are required to generate the model and conduct the analysis of a mid-rise CFS building.

In the PBD assessment of a CFS building, the lateral strength and stiffness of the SWP must be computed and checked with applicable acceptance criteria. Due to the complexity of the interaction among wall components, evaluating the lateral strength and stiffness of a SWP has challenged structural engineers. The lateral strength of a SWP cannot be determined by the strength of the sheathing alone, as the interaction among the sheathing, studs and fasteners affect considerably both the behaviour and lateral strength of SWP. Typically, due to the lack of analytical methods, the lateral strength of a SWP must be determined by experimental testing.

The American Iron and Steel Institute (AISI, 2004) has published design tables for the lateral strength of SWP having different characteristics, such as sheathing materials, screw diameter and spacing, and stud thickness. However, the tables are derived from experimental testing, so that their application is limited to the types of SWP tested. In this study, a method for determining the lateral strength of SWP is developed, which is versatile because SWP with different configurations and material properties can be analyzed. The principal characteristics and properties of SWP are accounted for, such as thickness and material properties of the sheathing, cross-section and material properties of the studs, spacing of the studs, and diameter and spacing of the screws. The proposed method is an extension of that developed by Brant (1982), which is currently used in steel standards such as CSA S16-01 (2003) to calculate the moment strength of steel bolted connections with eccentric loads. Brant's method is employed because of the similarity of SWP with steel moment connections, in that both are composed of arrays of fasteners subjected to eccentric loads.

1.2. Objective of Study

The primary objective of this study is to develop a methodology for conducting the PBD assessment of mid-rise CFS buildings. The accomplishment of this objective involves achieving a number of particular goals that are described in the following:

- Development of a method for determining the lateral strength of SWP
- Development of an equivalent shell formulation to transform CFS panels into shell elements with equivalent properties
- Establishment of a formulation for SFEA of CFS buildings
- Validation of the proposed SFEA
- Development of a stiffness degradation model for SWP
- Establishment of an appropriate pushover analysis procedure
- Establishment of acceptance criteria related to specified performance levels for SWP
- Presentation of example applications of PBD assessment of CFS buildings using the proposed methodology

1.3. Scope

The method for determining the lateral strength of SWP accounts for the failure of the sheathing-to-framing connections, and the failure of the end-studs in compression due to in-plane loads. The method can be used to calculate the lateral deformation of isolated SWP. However, the failure of a SWP due to the possible local buckling of sheathing material is not considered in the strength evaluation.

The panels in a CFS building are transformed into flat shell elements, with equivalent properties that account for the axial and bending stiffness of the SWP. It is assumed that the studs are uniformly distributed along the length of the wall, and that a continuous bond exists between the studs and sheathing.

The SFEA employs sixteen-node shell elements to model the CFS panels. One or more sixteen-node shell elements are used to model each panel. An updated Lagrangian formulation is adopted for the nonlinear finite element analysis, accounting for the geometric and material nonlinearities. The geometric nonlinearities are accounted for in the nonlinear analysis procedure by updating the nodal coordinates and member forces at each load increment. The material nonlinearities are accounted by using a stiffness degradation model for the SWP.

The stiffness degradation model characterizes the lateral nonlinear behaviour of a SWP. This is accomplished by reducing SWP lateral stiffness as the lateral loads on the building increase. The model is a function of the lateral strength of the SWP, and the screw spacing at the edge of the SWP. It is noted that the model does not account for axial or bending stiffness degradation of a SWP.

A single-mode pushover analysis is applicable for low- and mid-rise buildings whose seismic response is governed by the first mode of vibration. Thus, high-rise buildings may not be appropriately analyzed with this method as account for the influence of higher vibration modes may required for such buildings. Spectrum-based (also known as force-controlled) pushover analysis is employed. The lateral loads are applied on the building in a pre-defined pattern in load increments of 1% of the total loading applied on the building.

The acceptance criteria for CFS buildings are established as a function of the SWP inter-storey drifts and lateral strength. This study relates the inter-storey drifts to the four performance levels defined by FEMA 273 (1997).

1.4. Assumptions and Idealizations

The following assumptions and idealizations are adopted to determine the lateral strength of SWP:

- Two types of failure are considered in the prediction of SWP lateral strength: 1) failure of the sheathing-to-framing connections, and 2) failure of the end-studs under axial forces.
- The proposed procedure does not account for the effect of local or shear buckling in the sheathing; thus, it is not applicable for SWP with thin sheathing such as CFS sheets or soft plywood.
- It is assumed that the hold-down anchors have been property designed to resist the uplift forces in the SWP. Thus, hold-down anchor failure is not accounted for in the determination of the SWP lateral strength.
- Lateral deformation due to hold-down anchor rotation is not accounted for in the prediction of the SWP lateral drifts, nor in the finite element analysis.
- It is assumed that the strength of the sheathing-to-framing connection is the same in all directions.
- The lateral deformation of a SWP is computed at the load level corresponding to the lateral strength of the SWP.

The following assumptions and idealizations are adopted for determining the properties of the equivalent shell elements:

- The studs are spaced uniformly along the length of the panel.
- A continuous bond exists between the sheathing and the studs.
- The gross cross-section properties of the CFS studs are used in the calculations.

The following assumptions and idealizations are adopted for the SFEA:

- The normal stresses transverse to the equivalent panel are disregarded for plane stress analysis.
- When a SWP fails under lateral loads, the vertical stiffness contributed by the studs is accounted for in the analysis.
- The sixteen-node shell element used to model CFS panels has five degrees of freedom; i.e., three translations along the x, y and z axes, and two rotations about the x and y axes in the plane of the shell.
- An updated Lagrangian formulation is adopted for carrying out the SFEA.

The following assumptions and idealizations are adopted for the pushover analysis:

- The pushover analysis procedure is only used for low-rise and mid-rise CFS buildings.
- The seismic loads are distributed over the height of the building using the distribution pattern specified by FEMA 273 (1997).
- The degradation of the stud-track and stud-joist connections is not taken into consideration for the pushover analysis.

1.5. Thesis Overview

Chapter 1 briefly describes the problem to be solved by this study, and the proposed methodology to solve it. The assumptions, idealizations and scope of the methodology for carrying out the PBD assessment of CFS buildings are described.

Chapter 2 presents a literature review of PBD and pushover analysis for seismic assessment. Their features, background, development and current trends are summarized.

Chapter 3 develops the methodology for determining the lateral strength of SWP. The chapter describes the SWP modes of failure that are accounted for in the proposed methodology. An iterative and simplified method for computing the lateral strength of shear wall panels is introduced. A hand-worked example application of the method is presented. Finally, the strengths and deformations of isolated SWP are compared using predicted and experimental results.

Chapter 4 develops the methodology for carrying out the simplified finite element analysis (SFEA) of CFS buildings, including: the formulation for transforming the panels into equivalent shell elements, the stiffness degradation model for the SWP, the equations for estimating the axial force in studs, and the nonlinear finite element formulation for the sixteen-node shell elements. The results of linear SFEA of isolated SWP are compared with the results computed using SAP2000 (2006). Finally, the experimental results for

isolated SWP obtained by Branston et al. (2006) are compared with the numerical predictions obtained using the SFEA proposed by this study.

Chapter 5 develops the methodology for carrying out the PBD assessment of CFS buildings using spectrum-based pushover analysis. The acceptance criteria for SWP are derived from experimental data. A step-by-step procedure for the PBD assessment of CFS buildings is presented along with a corresponding flowchart. Finally, a computer program created for carrying out the PBD assessment of CFS buildings is described.

Chapter 6 presents two simplified building models analyzed using linear SFEA and CFEA. The results from the two analyses are compared. Pushover analysis is carried out for the two building models to demonstrate the practical application of PBD assessment for CFS buildings. Finally, the results from the linear analyses are compared to those from the pushover analyses to evaluate the differences between the various approaches.

Chapter 7 discusses the findings and conclusions of this study. Several recommendations are given for future studies regarding the PBD assessment of CFS buildings.

Appendix A provides a simplified method for computing the fundamental period of vibration for buildings comprised of frameworks and shear walls.

Chapter 2

Background and Literature Review on Performance-Based Design and Pushover Analysis

2.1. Introduction

The seismic assessment of existing structures and the seismic design of new structures have taken a step forward since the publication of the National Earthquake Hazards Reduction Program (NEHRP) guidelines for the seismic rehabilitation of buildings (FEMA 273, 1997). These guidelines introduced the Performance-Based Design (PBD) philosophy, which provided designers and building owners more options to design buildings than seismic codes. For instance, with PBD, a building can be designed to remain operable, or to undergo limited damage after an earthquake. Also, FEMA's guidelines have introduced nonlinear static analysis, better known as pushover analysis, as an alternative to dynamic analysis, which is a convenient tool for seismic analysis. An earthquake is simulated by applying lateral forces on the structure, in small increments, in a predefined pattern. The pattern of lateral forces remains constant throughout the analysis, which is determined assuming that the response of the building is controlled by a single mode of vibration, usually the fundamental mode (Krawinkler and Senervitna, 1998). As such, this method of analysis is appropriate for low and mid-rise structures, including CFS buildings, the objective of study in this research.

Discussed in the first part of this chapter, is the background of PBD, mainly based on FEMA (1997, 2003), SEAOC (1995), and ATC (2003, 2005) documents. Summarized in this chapter is the background of pushover analysis, including the primary considerations and assumptions in the application of the method. Also described is the so-called second-generation PBD. The guidelines of this latter, new, philosophy have not been completed, but they are expected to be completed by 2010 (ATC, 2005). At this time, a draft with 25% of the guidelines has been published by ATC (2005). An overview of the second-

generation PBD objectives and characteristics is given. Described in the last part of the chapter is the current situation for the seismic assessment of CFS buildings.

2.2. Performance-Based Design

After several major seismic events that occurred in the recent past, such as the 1989 Loma Prieta and the 1994 Northridge earthquakes, the structural engineering community and building owners began to question the effectiveness of current building codes to protect property (Gong, 2003). Seismic codes at that time were prescriptive and primarily concerned with life safety, their primary objective being to protect building occupants and pedestrians from life threatening situations. Thus, buildings that did not collapse during an earthquake and did not generate large amounts of falling debris, were considered to fully comply with seismic code requirements. This said, however, there are many buildings for which it is desirable that they be functional after an earthquake event, such as hospitals, shelters, and important facilities (ATC 58-2, 2003).

In recognition of the different performance demands possible for different building types, in 1993 the Federal Emergency Management Agency (FEMA) provided funding to various organizations to develop the NEHRP guidelines; namely FEMA 273 (1997) and FEMA 274 (1997), for Seismic Rehabilitation of Buildings (ATC 58-2, 2003). The organizations in charge of developing the guidelines were the Applied Technology Council (ATC), American Society of Civil Engineers (ASCE), and the Building Seismic Safety Council (BSSC). These guidelines laid down the foundation for the PBD philosophy, which were primarily created for seismic assessment and rehabilitation of existing structures. Later in 1994, FEMA also awarded the Structural Engineers Association of California (SEAOC) a project to develop a framework for the PBD of new buildings, extending the concepts of FEMA 273. The project was known as VISION 2000 (ATC 58-2, 2003).

Currently, the PBD philosophy is widely accepted and used for assessing the performance of existing and new buildings, subjected to seismic loads. PBD assessment provides a

good understanding of a structure's behaviour, and allows building owners to have a better idea of a building's damages at different levels of earthquake intensity. The PBD philosophy can be defined as multi-level design that not only has explicit concern for the performance of a building at the ultimate-strength limit states, but also at intermediate and serviceability limit states (Hasan et al., 2002). In this philosophy, the design criteria are expressed in terms of the specified performance objectives that are chosen depending on the performance expected for the structure. A performance objective involves the combination of the structure's expected performance level with a seismic hazard (Bertero and Bertero, 2002). That is, a performance objective dictates the intensity of the seismic hazard that the building will be subjected to, and the limit damage the building should experience.

A performance level is a discrete damage state, selected from among a number of damage possibilities (Gong, 2003). FEMA 273 (1997) describes three performance levels for structural components and four for non-structural components, which are combined to generate four performance levels for the assembled building. For the latter, the most common and representative performance levels in the design and rehabilitation of buildings are Operational (OP), Immediate Occupancy (IO), Life Safety (LS), and Collapse Prevention (CP).

At the OP level, the building is expected to be suitable for normal use and occupancy after an earthquake, and the risk to life safety in the building is extremely low, but some non-essential services may not function (FEMA 273, 1997). Buildings at the IO performance level are safe to reoccupy after an earthquake. However, non-structural systems may not function due to either lack of electrical power or damage of the equipment. Although the building may require some reparations before re-occupancy, minimal or no damage to structural elements is expected and only minimal damage to non-structural components is expected (FEMA 273, 1997). Buildings at the LS level undergo extensive damage to structural and non-structural components, and reparations must be done before re-occupancy. Although reparations may be costly, risk to life safety is low in buildings meeting this performance level (FEMA 273, 1997). Buildings in the

CP level have reached a state of impeding partial or total collapse, and they may have suffered a significant loss of strength and stiffness with some permanent lateral deformation. Yet, the major components of the gravity load carrying system should continue carrying the gravity load demands (Gong, 2003). This building may be dangerous to life safety due to the failure of non-structural components. Most buildings at this performance level are considered complete economical losses.

A seismic hazard at a given site is represented by ground motions and its associated probability of occurrence (Bertero and Bertero, 2002). FEMA 273 (1997) identifies four seismic hazard levels with different mean return periods rounded to 2500, 500, 225 and 75 years, respectively. These seismic hazard levels are usually represented by their probability of exceedance in a 50 year period (i.e. 2%/50, 10%/50, 20%/50, and 50%/50 for severe to light ground motion intensities, respectively).

Performance objectives can be generated by combining the aforementioned performance levels and earthquake hazards. Typically, multiple performance objectives are selected for the design of new structures and the rehabilitation of existing structures. In the design of new structures, the performance objectives can be established in accordance with the importance of the building and the budget available to build it. The performance objectives can range from minimum code requirements (e.g., the OP performance level for a 50%/50 year seismic hazard, and the LS performance level for a 10%/50 year seismic hazard) to high performance requirements (e.g., the OP performance level for a 2%/50 year seismic hazard) (Bertero and Bertero, 2002). The described high performance objective, poses high demands on buildings, since the building must remain operational for the largest seismic hazard. FEMA 273 (1997) proposes three different performance objectives for the rehabilitation of structures: basic, enhanced and limited safety. These are based on the performance and damage expected for the structure rather than the type of structure. On the contrary, the performance objectives established by SEAOC (1995), for new structures, are established depending on the importance of the structure.

Shown in Table 2.1 are different performance objectives for the design of new structures. Each cell represents a performance objective which is the result of combining a performance level with a seismic hazard. Also shown in the table are the different multi-performance objectives that should be satisfied by a structure in accordance with its importance, such as ordinary building, essential building or hazardous facility. For instance, a hazardous facility should meet the OP and IO performance levels for 10%/50 and 2%/50 earthquake hazards, respectively. Although different performance objectives can be created combining other performance levels with earthquake hazards, the performance objectives shown in Table 2.1 are suitable for most buildings.

Table 2.1. Performance Objectives, SEAOC (1995)

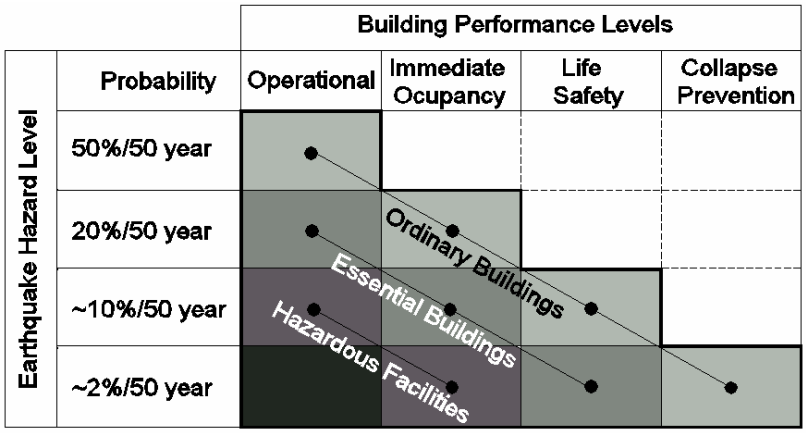

Once the multiple performance objectives are selected for designing a structure, they need to be transformed into damage targets and acceptance criteria to facilitate the analysis. The procedure to transform a performance objective into a damage target involves consideration of factors such as the building location and natural period of vibration, among others (this is discussed for CFS buildings in Chapter 5). Typically, the damage targets are established as a function of the lateral displacement and base shear for each earthquake hazard. The acceptance criteria represent the capacity of the structural elements in the building at the different performance levels, given as a function of plastic hinge rotation capacity, shear distortion capacity, and inter-storey drift capacity (FEMA 274, 1997). Once the damage targets are established, the analysis of the building is then

carried out to determine the displacement demand of the building and compare it to the limit drifts.

FEMA 273 (1997) has established four structural analysis procedures that can be used with the PBD assessment: linear static analysis, linear dynamic analysis, nonlinear static analysis, and nonlinear dynamic analysis. The advantages and disadvantages of each approach should be assessed to determine which procedure is appropriate for each particular building to be analyzed. Although the linear static analysis procedure is the simplest applicable method, its capabilities are very limited. It gives wrong answers when used for analyzing buildings that have inelastic responses, such as buildings with highly irregular structural systems or with energy dissipating devices (FEMA 273, 1997). On the other hand, the dynamic analysis procedures (linear and nonlinear) can be used for most structures and generate good results. However, the main disadvantage of dynamic methods is that their application is complicated, and the designer needs to have a deep knowledge of the mathematics of the method (FEMA 273, 1997).

The nonlinear static analysis procedure, better known as pushover analysis, is simple to apply and often yields good results for structures with a predominant fundamental period of vibration. However, pushover analysis should not be used for analyzing structures for which higher-mode vibration effects are significant, such as structures of irregular plan, structures with irregular distribution of their mass along their height, and structures with seismic isolation devices (FEMA 273, 1997).

2.3. Pushover Analysis.

Pushover analysis consists in subjecting a building's model to constant gravity loads and monotonically increasing lateral forces or displacements, until either the specified damage target is exceeded or the building collapses. This method accounts for inelastic behaviour and provides a reasonable approximation of the response of the building when subjected to the design earthquake (FEMA 273, 1997). The inelastic response of a building is the consequence of geometric and material nonlinear behaviour of its

structural elements. Geometric nonlinearities are obtained from the analysis procedure by updating the nodal coordinates of the building's model at each load increment. Depending on the chosen formulation for the structural analysis, geometric stiffness matrices can be used to consider second-order geometric effects. Material nonlinearities are accounted for in the nonlinear behaviour of the lateral-load resistant elements in the building.

Pushover analysis is employed to evaluate the demand of a building subjected to design earthquakes associated with the specified performance objectives. Then, the building's demand is compared to the building's capacity. Here, the designer can determine if the building is appropriately designed to satisfy the acceptance criteria associated with the performance levels.

Single-mode pushover analysis is based on the assumption that a structure can be modeled as a single degree of freedom system. The building response is typically assumed to be dominated by only the first mode shape, which is assumed to remain constant throughout the analysis. Although these assumptions are somewhat simplistic, studies have indicated that the response of multi-degree of freedom systems that have one dominant mode shape is modeled quite well (Krawinkler and Seneviratna, 1998). A structure that has more than 75% of its mass participating in its first vibration mode is considered to have a predominant mode shape (FEMA 273, 1997). If other mode shapes also have a high participation in the structure response, multi-mode (modal) pushover analysis should be employed (Chopra and Goel, 2002).

When assessing the behaviour of a building using pushover analysis, the designer first must transform each performance objective into a corresponding damage target. The most common damage targets are displacements and forces. For example, suppose a damage target is represented by a displacement that is the maximum roof-level displacement likely to be experienced by the structure during the design earthquake. The target displacement is compared to the displacement measured at a roof-level control node, as the lateral loads or displacements are incrementally applied on the building. If the

displacement at the control node exceeds the target displacement of any of the performance levels, the analysis is terminated, because the performance objective has been exceeded. Otherwise, the acceptance criteria for the structural elements are checked. Usually, the control node is typically located at the centre of mass at the roof level of the building (FEMA 273, 1997). This analysis approach is known as the displacement-based pushover analysis.

In the so-called spectrum-based approach, the base shear of the building is selected as the damage target: i.e., the maximum base shear most likely to be experienced by the building subjected to the design earthquake. In this approach, the incremental lateral loads are applied in the same fashion as those for the displacement-based approach, and the base shear of the building is evaluated after each load increment. When the base shear in the building is equal or greater than the target base shear for any of the specified performance objectives, the analysis is "paused" and the acceptance criteria of the structural elements are checked. Thus, it can be determined if the structural elements satisfy the specified performance levels. Although both methods have pros and cons, the displacement-based method has been shown to be more convenient for existing structures, whereas the spectral method has proven to be better for new structures (Gong, 2003).

FEMA 273 (1997) provides limit drift ratios for several types of structures, including steel moment frames, concrete walls, masonry infill walls, and wood stud walls (see Section 5.4). The drift ratios are associated with the four performance levels discussed previously, and are provided as a means to estimate the lateral drift of buildings depending on the type of structure. It is common to use the drift ratios to compute target displacements for the displacement-based PBD assessment of buildings (Hasan et al., 2002; Gong, 2003). However, pushover analysis becomes complex, when the drift ratios for the structure analyzed are not provided; for example, for CFS shear wall panels. Although CFS buildings are built in a similar fashion as wood buildings, the drift ratios for wood-framed buildings cannot be used to carry out the PBD of CFS buildings, since

there is no proof of equal behaviour. Therefore, it is necessary and appropriate to determine the drift ratios for CFS buildings from experimental test results.

2.4. New Generation Performance-Based Design.

The PBD guidelines published in the mid-nineties, such as FEMA 273 (1997) and SEAOC (1995), are referred to by ATC (2005) as first-generation PBD (PBD-1). In 2001, FEMA provided funding to ATC to develop second-generation PBD guidelines (PBD-2) for new and existing buildings, in accordance with the FEMA 445 program plan (ATC, 2005). The Pacific Earthquake Research Center (PEER) is in charge of developing the theoretical basis for these new guidelines.

One of the objectives of PBD-2 is to provide guidelines for the seismic assessment of buildings considering their unique design and construction characteristics. Another objective is to present the guidelines in terms of the risk associated with earthquake-induced losses (ATC, 2005). Using earthquake-induced losses, building owners have a better sense of the cost of repairing a building after an earthquake. These risks relate to casualties, economic losses, and downtime of the building. Casualties refer to the risk of loss of life and serious injury to occupants as a consequence of earthquake-induced damage. Economic losses include the cost of repairing or replacing damaged elements or components after an earthquake. Downtime refers to the time that buildings are closed due to repairs, inspections, cleaning, and re-occupation preparation. Establishing the performance objectives in terms of these three types of risks, not only the expected behaviour of the building is considered, but also the associated losses can be translated into an economic loss.

According to the PBD-2 philosophy, three types of procedures can be followed to perform the seismic assessment of buildings. The first is an intensity-based assessment, in which the risk is estimated for a specific seismic hazard, defined by a response spectrum. The second is a scenario-based assessment that estimates the risk from a specific earthquake scenario, as defined by earthquake magnitude and distance from the site. The

third is a time-based assessment which measures the risk over a period of time, where all the earthquakes that may occur in that period and their associated probability are considered. To date, 25% of the guidelines for the seismic performance assessment of buildings have been completed; they are expected to be fully completed around 2010 (ATC, 2005).

2.5. Seismic Assessment of Cold Formed Steel Buildings.

Research on PBD has been carried out for the design of new structures, such as structural steel frames (Gong, 2003; Liew and Chen, 2004; Lee and Foutch, 2002), and concrete structures (Zou and Chan, 2005). Also, investigations of PBD assessment for lightweight wood-frame buildings have been conducted (Filiatrault and Folz, 2002), though not as extensively as for conventional steel or concrete buildings. Conversely, this study reveals that there is neither a corresponding design standard available nor any reported research results for the seismic assessment of cold-formed steel buildings. Presently, therefore, a designer has only one option for the seismic design of a CFS building; that is, carrying out the seismic design in accordance with the seismic provisions contained in the applicable seismic codes. However, the designers are unable to assess the seismic behaviour of CFS buildings because there are no guidelines in the literature for this purpose.

Since PBD has advantages over seismic design standards and it has been successfully employed for the seismic assessment of steel and concrete structures, in this study PBD is used for carrying out the seismic assessment of CFS buildings. The procedure for conducting the PBD assessment of CFS buildings is adapted from PBD guidelines, such as FEMA 273 (1997), and FEMA 450 (2003). As described in Section 2.2, the PBD assessment of a building can be carried out in a number of ways. Thus, an appropriate analysis method and damage targets should be established in accordance with CFS buildings structural systems.

Chapter 3

Analytical method for determining the lateral strength of shear wall panels in cold formed steel buildings

3.1. Introduction

SWP are the primary structural component of CFS buildings, determining the SWP lateral strength is crucial prior to carrying out PBD assessment of a CFS building. The reason is that the lateral strength of the SWP is employed to design or review the design of the SWP. In addition, the lateral strength of SWP is employed in this study for evaluating the stiffness degradation of SWP, which characterizes their nonlinear behaviour during the pushover analysis (the stiffness degradation model and pushover analysis procedure are described in Sections 4.6 and 5.3, respectively).

In recent years, extensive experimental investigations have been carried out to understand the behaviour, and to determine the lateral strength, of SWP. Serrette et al. (1996, 2002) have conducted series of tests on SWP in CFS framing with different sheathing materials, such as Gypsum Wall Board (GWB), Oriented Strand Board (OSB), plywood, and thin CFS plates. The outcome of the tests has contributed to the development of the Standard for Cold-Formed Steel Framing-Lateral Design, published by the American Iron and Steel Institute (AISI, 2004). More recently, Branston et al. (2006) have extensively tested SWP using American and Canadian wood-based sheathing materials, such as Canadian Softwood Plywood (CSP), Douglas Fir Plywood (DFP), and OSB. The objective of Rogers's testing program is to develop guidelines for the seismic design of CFS SWP for use with the National Building Code of Canada (Branston et al., 2006). Also, Fulop and Dubina (2004, 2004b) have conducted series of tests on SWP, to generate a hysteretic model and a simplified modeling method for the SWP.

In current design practice, structural engineers obtain the lateral strength of SWP primarily from the published values in design standards and guidelines, such as AISI (2004, 1998). The nominal lateral strengths of SWP, presented in a tabulated form in the standards, are convenient to use. They are determined on the basis of experimental tests, which provide degree of confidence to practitioners. However, the application of design tables is limited by the number of tests carried out on SWP with different material characteristics and construction details, such as the type and thickness of the sheathing material, the size and configuration of the stud, and the size and spacing of the fastener. The values given in design tables for certain SWP cannot be applied or extrapolated to other SWP with different configurations or construction details. Although research has been carried out by using numerical simulations to determine the lateral strength of SWP, the approach is time consuming and may not be suitable for daily engineering practice. The development of a practical and reliable analytical method for determining the lateral strength of SWP is of primary importance to practitioners concerned with CFS framing construction.

Presented in this Chapter is an analytical method for determining the ultimate lateral strength of SWP, and their lateral displacement. Both, the lateral strength and lateral displacement, are predicted for isolated SWP. The proposed method takes into account a broad range of factors that affect the behaviour and strength of SWP, namely: material property, thickness and geometry of sheathing and studs, spacing of studs, and construction details such as size and spacing of the sheathing-to-stud fasteners. A hand-worked example is presented to demonstrate the practical and efficient nature of the proposed method. To validate the effectiveness of the proposed method, its predictions of the ultimate lateral strengths of different SWP are compared to test results of recent experimental investigations (AISI, 2004; Fulop and Dubina, 2004; Branston et al., 2006; Serrette et al., 1996, 2002). The comparison of predicted versus experimental results is presented in the last section of this chapter.

3.2. The Failure Modes of SWP

The failure of a SWP subjected to in-plane lateral loading at the ultimate strength state, occurs when the panel has no further strength to resist lateral forces. According to tests that have been carried out, such as by Gad et al. (1999), Branston et al. (2006), and Serrette et al. (2002), the predominant failure mode of SWP is associated with sheathing failure. It is observed that failure is often initiated at the sheathing-to-framing connections for common sheathing materials such as plywood, OSB, and GWB. The failure of the sheathing is evident due to rupture of the sheathing-to-framing connections and, as observed in some tests, the complete separation of the sheathing from the frame. However, when the thickness of the CFS studs is relatively small (e.g., thickness ≤ 0.84mm [33 mils]), the failure of the SWP can be initiated by the local buckling of the steel studs, even though the studs are braced by the sheathing. The failure of the steel studs can also occur when the sheathing is installed on both sides of the framework so as to double the sheathing thickness and thereby enhance the panel lateral strength. However, the resulting forces in the end studs are amplified, which can result in stud failure in compression, prior to failure of the sheathing. This mode of failure is explained in detail in Section 3.4.

Both failure modes discussed in the foregoing are accounted for in the proposed method for evaluating the lateral strength of SWP. The failure of the sheathing is identified by the failure associated with the sheathing-to-framing connections; the failure of steel studs is detected, when the axial force in the end post of the SWP exceeds the compressive strength of the end steel stud. The proposed method cannot be applied to SWP with light-gauge steel sheathing, since local buckling of the sheathing is not accounted for in this study.

3.3. The Lateral Strength of SWP Associated with Sheathing Failure

The lateral strength of a SWP, which is contributed to by the assembly of sheathing and steel framing studs, can be expressed as,

$$P_R = P_S + P_F \qquad \textbf{(3. 1)}$$

where P_S is the lateral strength associated with the sheathing. When the sheathing is provided on both sides of a shear wall panel, the lateral strength is given by,

$$P_S = \sum_{i=1}^{2} P_{S,i} \tag{3. 2}$$

where $P_{S,i}$ (i = 1, 2) are the lateral strengths of the sheathing installed on sides 1 and 2 of the panel, respectively (see Section 3.3.1). The lateral strength P_F associated with the steel framing studs is determined as,

$$P_F = K_F \Delta \tag{3. 3}$$

where K_F is the lateral stiffness associated with the framing studs, and Δ is the lateral deflection of the sheathing at impending failure at the ultimate lateral load level. Compared to the sheathing, the framing studs contribute little to the ultimate lateral strength of the SWP because their lateral stiffness is insignificant. Experimental results, such those published by the AISI (2004), provide evidence of the framing contribution to the SWP lateral strength. The test results show that the lateral strength of the SWP increase as the steel stud thickness increases (see Table 3.3). Therefore, for simplicity, K_F is taken as the elastic lateral stiffness of the framing studs, i.e.,

$$K_F = \sum_{studs} \frac{3E_F I_F}{h^3} \tag{3. 4}$$

where E_F and I_F are the Young's modulus and the moment of inertia of the framing studs, respectively, and h is the height of the panel.

Considering the compatibility of lateral deformation between sheathing and framing studs prior to the failure of the panel, the relationship between the sheathing strength and the lateral deformation of the panel is,

$$\Delta = \frac{P_S}{K_S} \tag{3. 5}$$

Substituting Eq. (3.5) into Eq. (3.3) yields,

$$P_F = \frac{K_F}{K_S} P_S \qquad \textbf{(3. 6)}$$

Then substituting Eq. (3.6) into Eq.(3.1), the lateral strength of the SWP is given by,

$$P_R = \left(1 + \frac{K_F}{K_S}\right) P_S \qquad \textbf{(3. 7)}$$

where P_S is the lateral strength of sheathing defined in Eq. (3.2), and K_S is the effective sheathing stiffness that can be calculated as,

$$K_S = \frac{G_S A_S}{1.2h} \alpha_V + \frac{3E_S I_S}{h^3} \alpha_B \qquad \textbf{(3. 8)}$$

where E_S and G_S are the Young's and shear modulus of the sheathing, respectively; h is the height of the SWP; α_V and α_B are sheathing lateral stiffness reduction coefficients for shear and bending deformation, respectively; and A_S and I_S are the cross-section area and moment of inertia of the sheathing, defined as,

$$A_S = t_S l, \qquad I_S = \frac{t_S l^3}{12} \qquad \textbf{(3. 9 a,b)}$$

in which t_S is the sheathing thickness, and l is the length of the SWP.

In addition to the material and cross-section properties of the sheathing, the lateral strength of the SWP is also highly affected by the characteristics and arrangement of the sheathing-to-framing connections. At its imminent state of failure, the lateral stiffness of the SWP is substantially less than its initial elastic stiffness. The degradation of the lateral stiffness is primarily contributed to by the failure of the sheathing-to-framing connections, as evidenced by experimental tests (Branston et al., 2006; Serrette et al., 2002). The sheathing stiffness reduction coefficients α_V and α_B, are introduced to account for failure effects of the connections that affect the sheathing lateral stiffness. Both reduction coefficients are calibrated from the test results reported by Branston et al. (2006), as described in Appendix B, and are evaluated as follows:

$$\alpha_V = \left(\frac{C_u}{3.3 \cdot n_C}\right)^{1.8} \cdot \left(\frac{6in}{s_C}\right) \qquad \textbf{(3. 10)}$$

$$\alpha_B = \left(\frac{6}{C_u}\right)^2 \cdot \left(\frac{6in}{s_C}\right)^{\frac{1.3 \cdot n_C}{C_u}} \quad \textbf{(3. 11)}$$

where s_C is the edge screw spacing in inches; n_C is the total number of screws used to fasten the sheathing to the steel framing; C_u is the ultimate strength factor, representing the number of effective screws of the SWP at its imminent state of failure (determined in Sections 3.3.1.1 and 3.3.1.2).

3.3.1. Lateral Strength of Sheathing

Consider the analogy between a SWP and an eccentrically loaded bolted steel connection. For both, the loads are applied eccentrically, and the strength reduction is primarily the result of the failure of connections initiated at locations which are far from the centre of rotation. In this study, an inelastic method for evaluating the strength of eccentrically loaded bolted connections (Brandt, 1982) is employed to evaluate the ultimate lateral strength of the sheathing. Brandt's method involves an iterative process to locate the instantaneous centre of inelastic rotation of a bolt group. As an extension of Brandt's method, the ultimate lateral strength of sheathing is evaluated as,

$$P_{S,i} = C_u V_r \, \eta \; ; \qquad (i = 1, 2) \quad \textbf{(3. 12)}$$

where V_r is the strength of a single sheathing-to-framing connection, as determined by the minimum value of the bearing resistance of the sheathing material, the shear resistance of the fastener, and the bearing resistance of the steel stud. The parameter C_u is the ultimate strength reduction factor related to the eccentrically applied load. The determination of C_u involves locating the so-called instantaneous centre of rotation of the fastener group (this is accomplished by using the iterative procedure in Section 3.3.1.1, or the simplified procedure in Section 3.3.1.2). The parameter η is a modification factor that accounts for the variation of the height-to-length ratio of the SWP, and is given by,

$$\eta = \sqrt{8.0 - \frac{h}{l}} - 1.45 \geq 0 \quad \textbf{(3. 13)}$$

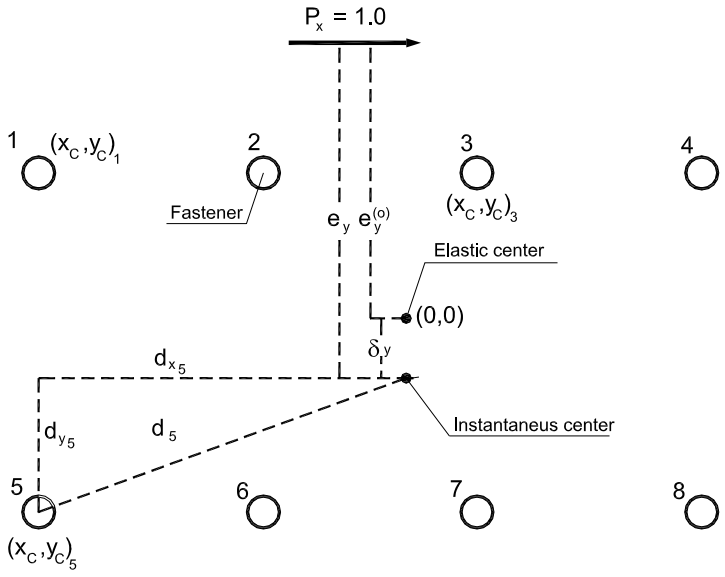

Figure 3.1. Fastener arrangement notation

3.3.1.1. Procedure for Evaluating the Ultimate Strength Reduction Factor Cu

Brandt's method of determining the ultimate strength reduction factor for eccentrically loaded bolted steel connections, involved an iterative process of locating the instantaneous centre of inelastic rotation of the bolt group. The process consists of locating the elastic centre of rotation (i.e., the centroid of the SWP), and then the distance between the elastic centre and the instantaneous centre is computed. By locating the instantaneous centre, the moments caused by the external loads and internal force in the screws are computed. Then, C_u is evaluated in addition to the unbalanced forces that cause the moments. Finally, the process is repeated until the equilibrium condition is reached to obtain C_u. In the following, Brandt's method is modified and extended to determine the ultimate strength reduction factor of sheathing.

For the eccentrically loaded fastener group shown in Figure 3.1, the *x, y* components of the distance from fastener *i* to the elastic centre of the fastener group are,

$$d_{xi} = x_{Ci}\,; \qquad d_{y_i}^{(0)} = y_{Ci} \tag{3. 14 a,b}$$

where x_{Ci}, y_{Ci} are the coordinates of the fasteners with respect to the elastic centre. In Eq. (3.14b) the superscript in parentheses denotes the iteration number. As the applied force P_x is in the x direction, it is noted that the component d_{xi} is invariant throughout the iterative process.

The polar moment of inertia of the fastener group, with respect to the elastic centre is,

$$J = \sum_{i=1}^{n_C} \left(x_{Ci}^2 + y_{Ci}^2 \right) \tag{3. 15}$$

Let P_x be a unit force applied on the location of the actual lateral force, which typically is on the top of the panel. The moment associated with P_x is,

$$M_0 = P_x e_y^{(0)} \tag{3. 16}$$

where $e_y^{(0)}$ is the initial eccentricity of P_x with respect to the elastic centre, and the superscript denotes the iteration number.

The iterative process of determining the instantaneous centre of rotation and the ultimate strength reduction factor C_u is as follows:

Step 1. Set the index of iteration $j = 0$, the tolerance of convergence $\varepsilon = 0.01$, the initial values of the unbalanced force $F_{gx}^{(0)} = P_x$, and the strength reduction factor $C_u^{(0)} = n_C$; Compute the polar moment of inertia of the fastener group, J, and the moment, M_0, based on Eqs. (3.15) and (3.16), respectively.

Step 2. Calculate the distance between the instantaneous centre of rotation and the elastic centre, and update the eccentricity of the applied unit force with respect to the instantaneous centre of rotation,

$$\delta_y^{(j)} = \left(F_{gx}^{(j)} / n_C \right) \left(J / M_0 \right) \tag{3. 17}$$

$$e_y^{(j+1)} = e_y^{(j)} + \delta_y^{(j)} \tag{3. 18}$$

Evaluate the moment associated with the applied unitary force,

$$M_p^{(j)} = P_x e_y^{(j+1)} \tag{3. 19}$$

Step 3. Update the distance between each fastener and the instantaneous centre of rotation, and compute the normalized deformation for all fasteners,

$$d_{y_i}^{(j+1)} = d_{y_i}^{(j)} + \delta_y^{(j)} \qquad (i = 1, 2, 3,\ldots n_C) \tag{3. 20}$$

$$d_i^{(j+1)} = \sqrt{\left(d_{x\,i}\right)^2 + \left(d_{y\,i}^{(j)}\right)^2} \qquad (i = 1, 2, 3,\ldots n_C) \tag{3. 21}$$

$$\Delta_{Ci}^{(j)} = \left(d_i^{(j+1)} / d_{\max}^{(j)}\right)\Delta_{C\max} \qquad (i = 1, 2, 3,\ldots n_C) \tag{3. 22}$$

where: d_{max} is the distance between the instantaneous centre of rotation and the furthest fastener; Δ_{max} is the maximum deformation of the sheathing-to-framing connection (taken herein as 10 mm (0.39 inch) for wood based sheathing material in accordance with tests carried out by Okasha (2004)).

Step 4. Calculate the normalized force in all the fasteners and the resulting moment with respect to the instantaneous centre of rotation,

$$\left(R_i / R_u\right)^{(j)} = \left(1 - e^{-10\Delta_{Ci}^{(j)}}\right)^{0.55} \qquad (i = 1, 2, 3,\ldots n_C) \tag{3. 23}$$

$$M^{(j)} = \sum_{i=1}^{n_C} \left(R_i / R_u\right)^{(j)} d_i^{(j+1)} \tag{3. 24}$$

Step 5. Compute the ultimate strength reduction factor,

$$C_u^{(j+1)} = \frac{M^{(j)}}{M_p^{(j)}} \tag{3. 25}$$

If $\dfrac{\left|C_u^{(j+1)} - C_u^{(j)}\right|}{C_u^{(j+1)}} \le \varepsilon,$ then the equilibrium condition is satisfied, i.e.,

$$C_u = C_u^{(j+1)} \tag{3. 26}$$

and the iterative process is terminated. Otherwise, go to Step 6.

Step 6. Compute the normalized ultimate fastener force,

$$R_u^{(j)} = \frac{M_p^{(j)}}{M^{(j)}} \qquad \textbf{(3. 27)}$$

and the normalized x components of the fastener forces,

$$R_{x_i}^{(j)} = \left(-d_{y_i}^{(j+1)} \Big/ d_i^{(j+1)}\right)\left(R_i / R_u\right)^{(j)} R_u^{(j)} \quad (i = 1, 2, 3, \ldots n_C) \qquad \textbf{(3. 28)}$$

The unbalanced force is then,

$$F_{gx}^{(j)} = P_x + \sum_{i=1}^{n_C} R_{x_i}^{(j)} \qquad \textbf{(3. 29)}$$

Return to Step 2.

As stated by Brandt (1982), and confirmed by this study, the iterative procedure for evaluating the ultimate strength reduction factor C_u converges after only a few iterations.

3.3.1.2. Simplified Evaluation of the Ultimate Strength Reduction Factor Cu

In design practice, it is desirable to avoid iterative processes even though they are simple to use. This study reveals that the ultimate strength reduction factor, C_u, converged at the second iteration for all of the cases presented in Section 3.7. Moreover, it is found that the difference between the values of C_u, obtained in the first and second iteration is often quite small. Thus, it is possible to further simplify the foregoing procedure by eliminating the iterative process without significantly affecting the accuracy of the ultimate strength reduction factor, C_u.

It is noted that in the iterative procedure, the deformations of the fasteners are linearly proportional to their distances from the instantaneous centre (Eq. 3.22). Having the deformations of the fasteners computed, the normalized forces in the fasteners are obtained from Eq. (3.23). According to Eq. (3.23), fasteners with larger deformation yield larger normalized forces. Instead of evaluating the normalized force for each fastener, the

simplified procedure adopted a normalized force of 0.93 (i.e., R/R_u = 0.93) for all the fasteners regardless of their distance from the instantaneous center. A value of 0.93 is calibrated from the results of the iterative procedure; that is, all the SWP presented in Branston et al. (2006) are analyzed using the iterative procedure and the average normalized force for all the SWP is 0.93. Since the purpose of iterating is to determine the forces in the fasteners, adopting a fixed value for the normalized forces eliminates the iterative procedure. For the iterative procedure, F_{gx} in Eq. (3.17) is replaced by P_x. The simplified procedure of evaluating the ultimate strength reduction factor C_u is as follows:

Step 1. Compute the polar moment of inertia of the fastener group J and the moment, M_0, based on Eqs. (3.15) and (3.16), respectively.

Step 2. Calculate the distance between the instantaneous centre of rotation and the elastic centre, and evaluate the eccentricity of the applied unitary force with respect to the instantaneous centre of rotation,

$$\delta_y = \left(P_x / n_C\right)\left(J / M_o\right) \quad \textbf{(3. 30)}$$

$$e_y = e_y^{(0)} + \delta_y \quad \textbf{(3. 31)}$$

Evaluate the moment associated with the applied unit force,

$$M_p = P_x e_y \quad \textbf{(3. 32)}$$

Step 3. Compute the distance between each fastener and the instantaneous centre of rotation,

$$d_{yi} = y_{Ci} + \delta_y \quad \textbf{(3. 33)}$$

$$d_i = \sqrt{\left(x_{Ci}\right)^2 + \left(d_{y_i}\right)^2} \quad \textbf{(3. 34)}$$

Calculate the moment associated with the fasteners,

$$M = 0.93\sum_{i=1}^{n_C} d_i \quad \textbf{(3. 35)}$$

Step 4. Compute the ultimate strength reduction factor,

$$C_u = \left| \frac{M}{M_p} \right| \tag{3. 36}$$

It is clear that the simplified procedure for evaluating the ultimate strength reduction factor C_u involves significantly less computational effort than that of the iterative procedure. The accuracy of the simplified procedure is demonstrated in Section 3.6. The maximum difference between the predicted lateral strengths of a SWP, found by using the iterative and simplified procedures, is only about 3% for the comparisons in Section 3.7.

3.4. The Lateral Strength of a SWP Associated with Frame Failure

In resisting the applied lateral load, the end framing studs of a SWP undergo either tension or compression, as they work to prevent over-turning of the panel, as shown in Figure 3.2. Typically the axial load in the studs are maximum at the end and zero at the centre of the SWP, thus the middle studs carry less load than the end studs. If a SWP is also subjected to gravity load, one end stud will experience larger compression force than the other end stud because the forces caused there by the lateral and gravity loads are additive, while they are subtractive at the other end. Generally, the failure of the steel framing for a SWP is associated with the failure of an end stud in compression, as observed in experimental tests (Roger et al., 2004; Serrette et al., 2002). As such, the lateral strength P_{fc}, of a SWP corresponds to the compressive strength of an end stud, and can be found from the equilibrium of the forces in Figure 3.2 to be,

$$P_{fc} = \frac{l}{h} P_n \tag{3. 37}$$

where l and h are the length and height of the SWP, respectively, and P_n is the nominal compressive strength of the end stud which, for this study, is evaluated in accordance with Chapter D of the North American Specification for the Design of Cold-formed Steel Structural Members, S136 (2001). As recommended by Telue and Mahendran (2001) through their experimental investigation, the effective length factors associated with the end stud are taken as K_{ex}=0.75, and K_{ey}=K_{et}=0.10 for SWP with sheathing installed on

its two sides, and K_{ex}=0.75, K_{ey}=0.10, and K_{et}=0.20 for SWP with sheathing installed on one side. Where $K_e = h / KL$, where K is the effective length factor ($K=1$ is assumed for the studs), and L is the unbraced length of the SWP. In the case where the lateral strength of a SWP, given by Eq. (3.37), is less than the strength value P_R computed by Eq. (3.1), the lateral strength of the SWP is taken as,

$$P_R = P_{fc} \tag{3. 38}$$

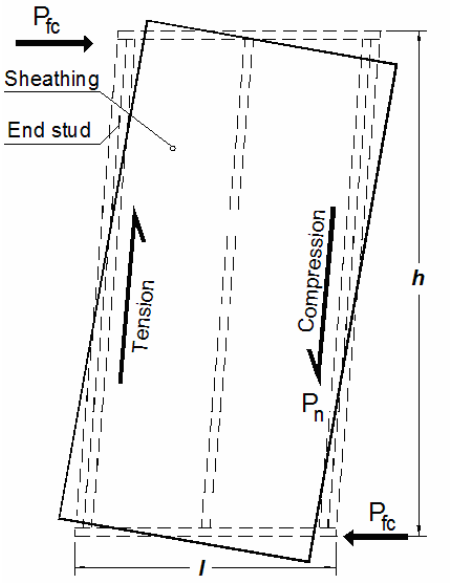

Figure 3.2. Panel rotation and force distribution

3.5. Estimation of the Lateral Displacement of a SWP

Having calculated the lateral strength of a SWP, the lateral displacement of the panel at the ultimate lateral load level can be conveniently evaluated as

$$\Delta = \frac{P_R}{K_F + K_S} \tag{3. 39}$$

where P_R is the lateral strength of the SWP, and K_F and K_S are the lateral stiffnesses defined by Eqs. (3.4) and (3.8) for the steel framing and sheathing, respectively.

3.6. Illustrative Example

A step-by-step example for evaluating the lateral strength and deformation of the SWP in Figure 3.3 is presented in the following. For purposes of manual evaluation, the simplified procedure, developed in Section 3.3.1.2, is employed to demonstrate the practical and efficient nature of the proposed method. The material properties and construction details of the SWP are adopted from an experimental study, conducted by Branston et al. (2006), and the here results are compared with those of the same study.

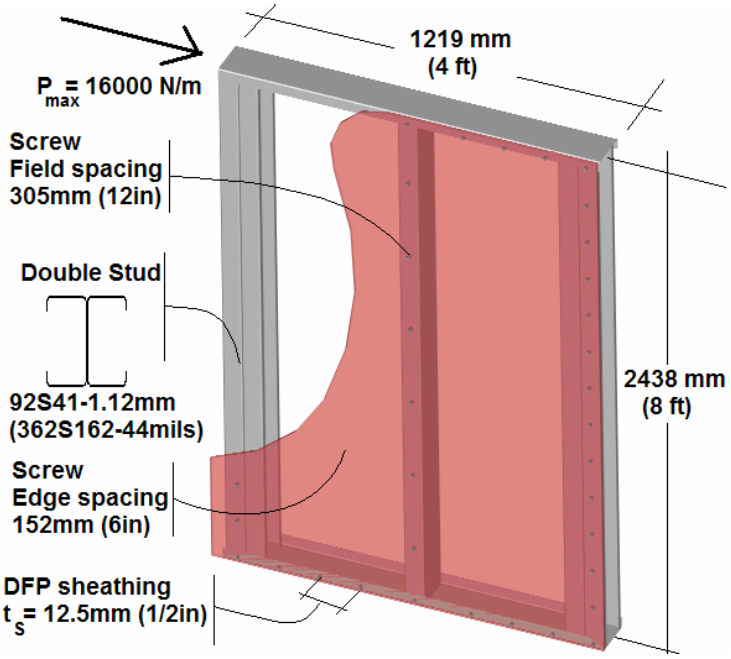

Figure 3.3. Shear wall panel tested by Branston et al. (2006)

For the SWP in Figure 3.3, the height and length of the panel are h = 2438 mm and l= 1219 mm, respectively, and the sheathing is present on only one side of the frame. The characteristics and material properties of the steel framing studs are:

Yield and tensile strength: $F_{y\text{-}steel}$ = 230 MPa and $F_{u\text{-}steel}$ = 344 MPa

Young's modulus: E_F = 203000 MPa

End steel stud shape: Two C-shape 362S162-44mils sections connected back-to-back

End steel stud thickness: t_F = 1.12 mm

Moment of inertia of the double end-stud: $I_F = 1.816\times10^5$ mm^4

Moment of inertia of the intermediate stud: $I_F = 5.124\times10^4$ mm^4

The characteristics and material properties of the Douglas Fir Plywood sheathing are CANPLY (2003):

The thickness of the sheathing: $t_S = 12.5$ mm

The bearing strength of the sheathing: $F_{u\text{-}sheathing} = 4.5$ MPa

Young's and shear modulus of the sheathing: $E_S = 10445$ MPa and $G_S = 825$ MPa

The characteristics of the screw fasteners are:

No. 8 screw fasteners and screw diameter: $d_C = 4.064$ mm

Screw spacing on the sheathing perimeter: $s_C = 152$mm

Total number of screws on the sheathing: $n_C = 50$

The evaluation of the lateral strength of the SWP, corresponding to failure of the sheathing, is carried out as follows:

Step 1. Compute the polar moment of inertia of the fastener group, J, and the moment, M_0, using Eqs. (3.15) and (3.16), respectively,

$$J = \sum_{i=1}^{n_C} \left(x_{Ci}^2 + y_{Ci}^2 \right) = 5.137 \times 10^7 \text{ mm}^2$$

$$M_o = P_x e_y^{(0)} = 1 \times 1219 = 1219 \text{ mm}$$

Step 2. Compute the distance between the instantaneous centre of rotation and the elastic centre, δ_y, and the eccentricity of the applied unit force P_x. Both shown in Figure 3.1 with respect to the instantaneous centre of rotation, e_y, using Eqs. (3.30) and (3.31), respectively,

$$\delta_y = \frac{P_x J}{n_C M_o} = \frac{1 \times 5.137 \times 10^7}{50 \times 1219} = 842.82 \text{ mm}$$

$$e_y = e_y^{(0)} + \delta_y = 1219 + 842.82 = 2061.82 \text{ mm}$$

Then compute the moment associated with the applied unit force using Eq. (3.32),

$$M_p = P_x e_y = 1 \times 2061.82 = 2061.82 \text{ mm}$$

Step 3. Compute the distance between each fastener and the instantaneous centre of rotation using Eqs. (3.33) and (3.34). Compute the moment associated with the fasteners using Eq. (3.35),

$$M = 0.93\sum_{i=1}^{n_C} d_i = 0.93\sum_{i=1}^{50} d_i = 53992 \text{ mm}$$

Step 4. Compute the strength reduction factor using Eq. (3.36),

$$C_u = \frac{M}{M_p} = \frac{53992}{2061.82} = 26.186$$

Step 5. Compute the lateral strength of a single sheathing-to-framing connection V_r to determine the lateral strength of the sheathing, as expressed in Eq. (3.12). The parameter V_r is the minimum strength of a sheathing-to-framing connection, accounting for: the bearing strength of the sheathing, bearing strength of the framing, shear strength of the screws, and screw pullout.

Bearing strength of the sheathing and framing (S136, 2001):

$$B_{r-sheathing} = 3.0 \cdot t_S \cdot d_C \cdot F_{u-sheathing} = 3.0 \times 12.5 \times 4.064 \times 4.5 = 685.8N$$

$$B_{r-steel} = 3.0 \cdot t_F \cdot d_C \cdot F_u = 3 \times 1.12 \times 4.064 \times 344 = 4687N$$

Shear and pullout strength of the screws, based on Steel Stud Manufacturers Association (SSMA, 2001), $V_{r-Sscrew} = 3256N$

$$V_{r-Pscrew} = 1255N$$

$$V_r = \min\left\{B_{r-sheathing}, B_{r-steel}, V_{r-Sscrew}, V_{r-Pcrew}\right\} = 685.8N$$

Step 6. Compute the lateral strength of the sheathing using Eqs. (3.13) and (3.12),

$$\eta = \sqrt{8 - \frac{h}{l}} - 1.45 = \sqrt{8 - \frac{2438}{1219}} - 1.45 = 1.0$$

$$P_S = C_u V_r \eta = 26.186 \times 685.8 \times 1.0 = 17958N$$

Step 7. Compute the sheathing and framing lateral stiffness:

Sheathing stiffness reduction factors using Eqs. (3.10) and (3.11),

$$\alpha_V = \left(\frac{C_u}{3.3 \cdot n_f}\right)^{1.8} \cdot \left(\frac{6in}{s_C}\right) = \left(\frac{26.186}{3.3 \cdot 50}\right)^{1.8} \cdot \left(\frac{6in}{6in}\right) = 0.036$$

$$\alpha_B = \left(\frac{6}{C_u}\right)^2 \cdot \left(\frac{6in}{s_C}\right)^{\frac{1.3 \cdot n_f}{C_u}} = \left(\frac{6}{26.186}\right)^2 \cdot \left(\frac{6in}{6in}\right)^{\frac{1.3 \cdot 50}{26.186}} = 0.053$$

then, compute the cross section area, the moment of inertia, and the lateral stiffness of the sheathing based on Eqs. (3.9 a,b) and (3.8), respectively.

$$A_S = t_S l = 12.5 \times 1219 = 15238 \text{ mm}^2$$

$$I_S = \frac{t_S l^3}{12} = \frac{12.5 \times 1219^3}{12} = 1.887 \times 10^9 \text{ mm}^4$$

$$K_S = \frac{G_S A_S}{1.2h}\alpha_V + \frac{3E_S I_S}{h^3}\alpha_B = \frac{825 \times 15238}{1.2 \times 2438}0.036 + \frac{3 \times 10445 \times 1.887 \times 10^9}{2438^3}0.053$$

$$= 370.95 \text{ N/mm}$$

Upon noting from Figure 3.3 that there are two end studs with double C- sections connected back-to-back and one intermediate stud with single C-shape section, compute the frame stiffness using Eq. (3.4),

$$K_F = \sum_{studs} \frac{3E_F I_F}{h^3} = 2\left(\frac{3 \times 203000 \times 1.816 \times 10^5}{2438^3}\right) + \left(\frac{3 \times 203000 \times 5.124 \times 10^4}{2438^3}\right)$$

$$= 17.42 \text{ N/mm}$$

Step 8. Finally, compute the lateral strength of the SWP corresponding to sheathing failure using Eq. (3.7),

$$P_R = \left(1 + \frac{K_f}{K_S}\right)P_S = \left(1 + \frac{17.42}{370.95}\right)17958 = 18801 \text{ N}$$

To further evaluate the lateral strength of the SWP corresponding to frame failure, the compressive strength of the steel end studs must be determined in advance. The end studs are formed with two C-shape 362S162-44 steel studs connected back-to-back. Based on the recommendation of Telue and Mahendran (2001), the effective length factors of the studs are taken as $K_x = 0.75$, $L_y = 0.10$, and $L_t = 0.20$. The unrestrained length of the studs for the x and y directions and torsion are $L_x = L_y = L_t = 2438$mm, respectively. Based on CSA S136-01 (2001), the nominal compressive strength of the end studs is: $P_n = 71.166$ kN. Using Eq. (3.37), the lateral strength of the SWP corresponding to frame failure is then computed as,

$$P_{fc} = \frac{l}{h}P_n = \frac{1219}{2438}71166 = 35583 \text{ N}$$

As $P_{fc} = 35583 > 18801$ N (see Step 8), sheathing failure defines the lateral strength of the SWP; i.e., $P_R = 18801$ N.

The lateral displacement associated with sheathing failure computed using Eq. (3.39) as,

$$\Delta = \frac{P_R}{K_F + K_S} = \frac{18801}{17.42 + 375.90} = 48.4mm$$

Compared to the computed results found in the foregoing for the SWP, the experimental results reported by Branston et al. (2006) for the lateral strength by unit of length and displacement of the same panel are 16000 N/m and 54.8 mm, respectively; therefore, the calculated-to- test ratios for the lateral strength and displacement of the SWP are:

$$\text{Strength ratio} = \frac{18801N}{16000N/m \times 1.219m} = 0.96, \quad \text{Displacement ratio} = \frac{48.4}{54.8} = 0.88$$

3.7. Comparison between Analytical and Experimental Results

Experimental results reported from AISI (2004), Fulop and Dubina (2004), Branston et al. (2006), and Serrette et al. (1996, 2002) are used to validate the accuracy of the proposed analytical method of evaluating the ultimate lateral strength of a SWP. The experimental results for strength and displacement, obtained by all the researches referenced in this section, are at the ultimate limit state. Since not all properties are reported in the foregoing literature, the material properties this study adopted in the evaluation may not be identical to those of the tested materials. The geometric gross properties of the steel studs are computed based on the cross-section dimensions reported in the literature. Unless otherwise specified in individual cases, the yield strength and Young's modulus values used in the calculations for steel are 230 MPa and 203000 MPa, respectively. Unless otherwise specified, the following material properties for sheathing material are employed to evaluate the ultimate lateral strength of the SWP: the shear modulus of elasticity for OSB, DFP and CSP = 925MPa, 825MPa, and 497MPa (Okasha, 2004), respectively; the modulus of elasticity for OSB = 9917MPa (OSB, 1995), while that for DFP and CSP = 10445MPa and 7376MPa (CANPLY, 2003), respectively; the elastic and shear moduli for GWB = 1290MPa (GA-235, 2001) and 561MPa, respectively. The connection strength corresponding to the bearing strength of GWB is B_r=228 N (51.25 lb), which is the lowest experimental value tabulated by Lee (1999).

For all of the comparisons made in the following, the SWP lateral strengths are predicted using both the Iterative Procedure (IP) and the Simplified Procedure (SP) so that the differences between their predictions can be identified. However, the strengths computed using the simplified procedure are alone used to calculate the ratios of the predicted-to-test values since it is the recommended procedure. Furthermore, the lateral displacements from the experimental tests are compared to the lateral displacements predicted by the SP as illustrated in the example in Section 3.6.

Shown in Table 3.1 and Table 3.2 are the comparisons between predicted and test results for lateral strengths and lateral displacements. The experimental results listed on Tables 3.1 and 3.2 were obtained from monotonic testing. Experimental results for cyclic testing are not listed in these tables because they were not available at the time of preparation of this chapter. Prof. Rogers provided the author experimental results derived from the first part of his testing schedule, which was for monotonic testing. The three different sheathing materials investigated were OSB, DFP and CSP with thicknesses of 11 mm, 12.5 mm, and 12.5 mm, respectively. The C-shape cold-formed steel studs were 92S41-1.12 mm (362S162-44mils), spaced 610 mm (24 in) on centre. Double C-shape back-to-back studs were placed at the ends of the panel and the end studs were attached with S/HD10 hold-downs to the floor. The sheathing was attached on one side of the panel using No. 8 (diameter = 4.06 mm) screws at every 305 mm (12 in) in the field of the panel (i.e., location other than the edge). Three edge screw spacings of 76 mm (3 in), 102 mm (4 in) and 152 mm (6 in) were investigated for SWP lengths of 1219 mm (4 ft) and 2438 mm (8 ft), as tabulated in Tables 3.1 and 3.2, respectively. Two edge screw spacings of 102 mm (4 in) and 152 mm (6 in) were investigated for SWP length of 609 mm (2 ft), as listed in Table 3.2.

From Table 3.1 and Table 3.2, it can be seen that the maximum difference between the test results and predicted results for the lateral strength of the SWP is 10%, whereas the maximum difference between the test and predicted results for the SWP lateral displacements is 21%. It is noteworthy that the predicted SWP lateral strengths are governed by sheathing failure, except for the panels with DFP sheathing and screw

spacing of 76 mm listed in Table 3.1. The SWP lateral strengths predicted by both the iterative and simplified procedure indicate that stud failure governs, which is confirmed by the test results.

Table 3.1 Comparison between predicted and test (Branston et al., 2006) results for lateral strengths and displacements

Steel stud 92S41-1.12mm. Screw size: No. 8. Field screw spacing: 305mm Wall length and height: **1219mm, 2438mm.** Sheathing length and height: **1219mm, 2438mm**										
Sheathing material and thickness	Test ID (Branston et al., 2006)	Edge screw spacing mm	Lateral strength, kN/m					Lateral displacement, mm		
			Test Branston	Predicted[2]			Ratio Test / Pred[3]	Test	SP	Ratio Test / Pred[3]
				Sheathing failure		Stud failure				
				IP[1]	SP[1]					
OSB 11 mm One side	21-A,B,C	152	13.20	12.26	12.24	29.19	**1.08**	41.1	42.1	**0.98**
	23-A,B,C	102	19.30	18.06	18.01		**1.07**	39.5	46.2	**0.85**
	25-A,B,C	76	23.50	23.83	23.76		**0.99**	40.7	49.3	**0.83**
DFP 12.5mm One side	11-A,B,C	152	16.00	15.45	15.42		**1.04**	54.8	48.4	**1.13**
	5-A,B,C,D	101	23.80	22.78	22.72		**1.05**	60.6	53.6	**1.13**
	13-A,B,C	76	29.70	30.10	30.00		**1.02**	58.2	57.5	**1.01**
CSP 12.5mm One side	7-A,B,C	152	12.70	12.49	12.46		**1.02**	50.7	57.8	**0.88**
	1-A,B,C	102	16.60	18.32	18.27		**0.91**	60.6	64.5	**0.94**
	9-A,B,C	76	25.10	24.13	24.05		**1.04**	61.0	69.7	**0.88**
Average							**1.02**			**0.96**
Standard deviation							**0.05**			**0.11**
Coefficient of variation							**0.05**			**0.11**

[1] IP = Iterative procedure, SP = Simplified Procedure

[2] Predicted SWP strengths are evaluated based on sheathing and stud failures

[3] The "Pred" is the smaller one of the predicted strengths, based on the sheathing failure, using SP, and stud failure

Table 3.2. Comparison between predicted and test (Branston et al., 2006) results for lateral strengths and displacements

Steel stud 92S41-1.12mm. Screw size: No. 8, field screw spacing: 305mm. Sheathing on one side										
Sheathing material and thickness	Test ID (Branston et al., 2006)	Edge screw spacing mm	Lateral strength, kN/m					Lateral displacement, mm		
			Test	Predicted			Ratio Test / Pred	Test	SP	Ratio Test / Pred
				Sheathing failure		Stud failure				
				IP	SP					
Wall length and height: **609mm, 2438mm.** Sheathing length and height: **609mm, 2438mm**										
OSB 11 mm	19-A,B,C	152	12.50	10.95	11.09	29.19	**1.13**	78.4	56.0	**1.40**
	27-A,B,C	102	18.40	15.48	15.68		**1.17**	78.0	56.3	**1.39**
CSP 12.5mm	15-A,B,C	152	12.20	11.63	11.50		**1.06**	103.3	80.3	**1.29**
	17-A,B,C	102	18.00	16.17	16.10		**1.12**	107.0	81.2	**1.32**
Wall length and height: **2438mm, 2438mm.** Sheathing length and height: (2) **1219mm, 2438mm**										
CSP 12.5mm	29-A,B,C	152	13.60	13.35	13.22	29.19	**1.03**	50.5	50.9	**0.99**
	31ABCDEF	102	20.50	18.96	18.71		**1.10**	55.6	55.6	**1.00**
	33-A,B,C	76	26.30	24.55	24.19		**1.09**	64.1	60.0	**1.07**
Average							**1.10**			**1.21**
Standard deviation							**0.05**			**0.18**
Coefficient of variation							**0.05**			**0.15**

Table 3.3 presents a comparison between the predicted lateral strength of SWP with OSB sheathing to that published in the Standard for Cold-Formed Steel Framing-Lateral Design, (AISI, 2004). Table 3.3 lists the lateral strengths provided by the AISI (2004) for seismic design. The length and height of the SWP are 1219 mm (4 ft) and 2438 mm (8 ft), respectively. The steel stud size is 89S41 (350S162), and the four different stud thicknesses that are described in the AISI (2004) standard are 0.838 mm (33 mils), 1.092 mm (43 mils), 1.372 mm (54 mils), and 1.727 mm (68 mils). Double studs are used for the end studs, and information of the hold-downs is not provided. OSB sheathing was attached on one side of the panel using No. 8 or No. 10 screws at every 305 mm (12 in) in the field. The four edge screw spacings used are 51 mm (2 in), 76 mm (3 in), 102 mm (4 in), and 152 mm (6 in). Table 3.3 indicates that the lateral strengths of all SWP are

governed by sheathing failure, and that there is a good correlation between predicted and test results for the SWP lateral strength. However, Table 3.3 shows a larger standard deviation than Tables 3.1 and 3.2, which may result from the difference in the material properties, assumed for the OSB in the predictions and the properties used in the testing.

Table 3.3. Comparison between predicted and test (AISI, 2004) results for lateral strengths

OSB sheathing: 11.1mm on one side. Stud designation: 89S41mm (350S162). Wall length and height: 1219mm, 2438mm. Sheathing length and height: 1219mm, 2438mm							
Screw size	Stud thick. mm (mils)	Edge screw spacing mm	Lateral strength, kN/m				
			AISI (2004)	Predicted			Ratio AISI / Pred
				Sheathing failure		Stud failure	
				IP	SP		
No. 8 (4.06 mm)	0.838 (33)	152.4	10.22	12.15	12.12	21.17	**0.84**
		101.6	13.35	17.93	17.88		**0.75**
	1.092 (43)	152.4	12.04	12.28	12.25	29.88	**0.98**
		101.6	18.02	18.07	18.02		**1.00**
		76.2	22.55	23.85	23.77		**0.95**
		50.8	30.06	35.37	35.26		**0.85**
	1.372 (54)	152.4	13.72	12.41	12.38	39.59	**1.11**
		101.6	20.58	18.22	18.17		**1.13**
		76.2	25.69	24.00	23.93		**1.07**
		50.8	34.30	35.54	35.43		**0.97**
No.10 (4.83 mm)	1.727 (68)	152.4	17.98	14.91	14.88	52.30	**1.21**
		101.6	26.97	21.82	21.76		**1.24**
		76.2	33.71	28.70	28.61		**1.18**
		50.8	44.95	42.41	42.27		**1.06**
Average							**1.02**
Standard deviation							**0.15**
Coefficient of variation							**0.14**

Shown in Table 3.4 are the comparisons between predicted and test results for lateral strengths and displacements, conducted by Serrette et al. (2002). The SWP dimensions were 2438 mm (8 ft) by 2438 mm (8 ft). OSB sheathing was fastened on one side or both sides of the panel using No. 8 or No. 10 screws. The screw spacing was 51 mm (2 in) on the edge and 305 mm (12 in) in the field of the sheathing. The framing steel studs investigated in the two tests were 350S162 (89S41) with thicknesses of 1.37mm (54 mils) and 1.73mm (68 mils), and yield strength of 407MPa (59 ksi) and 386MP*a* (56 ksi), respectively. The studs were spaced at 610 mm (24 in) on centre, and double studs were placed at the ends of the SWP; information of the hold-downs is not provided. The ultimate test lateral strengths shown in Table 3.4 are the average values from two specimens, tested under reversed cyclic loading protocol (SEAOC, 1997). For the two cases, where OSB sheathing is applied on only one side of the panel, the SWP lateral strength is governed by sheathing failure; when the OSB sheathing is installed on both sides of the panel, the strength is governed by stud failure.

Table 3.4. Comparison between predicted and test (Serrette et al., 2002) results for lateral strengths

SWP description Walls length and height: 2438mm, 2438mm. Sheathing length and height: (2) 1219mm, 2438mm	Test ID	Screw Size No.	Stud thick. mm (mils)	Lateral strength, kN/m				
				Test	Predicted			Ratio Test / Pred
					Sheathing failure		Stud failure	
					IP	SP		
OSB sheathing on **one side**: 11mm. Steel stud: 89S41 Screw spacing (mm) Edge: 51; Field: 305	1-2	8	1.37 (54)	34.38	35.68	34.98	57.83	**1.02**
	3-4	10	1.73 (68)	44.96	42.44	41.61	74.21	**0.93**
OSB sheathing on **both sides**: 11mm. Steel stud: 89S41. Screw spacing (mm) Edge: 51; Field: 305	6-7	8	1.37 (54)	60.96	70.91	69.51	60.49	**0.99**
	8-9	10	1.73 (68)	76.53	84.24	82.58	77.39	**1.08**
Average								**1.00**
Standard deviation								**0.06**
Coefficient of variation								**0.06**

Shown in Table 3.5 are the comparisons between predicted and test results for lateral strength and displacement, conducted by Fulop and Dubina (2004). In this case OSB sheathing was presented on one side of the panel, and the steel studs were spaced 610 mm (24 in) on centre. Information regarding the type of hold-downs employed to attach the SWP to the floor is not provided. Differing from the foregoing experimental investigations, the dimensions of the SWP panel were 3600 mm (≈12 ft) in length and 2440 mm (8 ft) in height. The lateral strength listed in Table 3.5 for the test was obtained from only one specimen.

Table 3.5. Comparison between predicted and test (Fulop and Dubina, 2004) results for lateral strengths and displacements

SWP description	Screw Dia. mm	Lateral strength, kN/m					Lateral displacement, mm		
		Test Fulop and Dubina (2004)	Predicted			Ratio Test/Pred	Test	SP	Ratio Test/Pred
			Sheathing failure		Stud failure				
			IP	SP					
OSB sheathing: 10mm Steel stud: 150S41-1.5mm Screw spacing (mm) Edge: 102; Field: 305 Wall length and height: 3600mm, 2440mm. Sheathing length and height: (3) 1200mm, 2440mm	4.2	21.88	20.16	19.53	47.66	**1.12**	42.85	44.16	**0.97**

Shown in Table 3.6 are the comparisons between predicted and test results for lateral strengths and displacements, conducted by Serrette et al. (1996). The SWP length and height were 2438 mm (8 ft) and 2438 mm (8 ft), respectively. The GWB sheathing was fastened on both sides of the panel with No. 6 screws. The screw spacing was 152 mm (6 in) on the edge and 305 mm (12 in) in the field of the panel. The steel studs were 150S32 (600S125) with thickness of 0.88 mm (33 mils), and information of the hold-downs employed is not provided. The studs were spaced 610 mm (24 in) on centre, and the

sheathing was attached to the studs using No. 6 screws. The lateral strength shown in Table 3.6 for the test was the average value for four specimens.

Table 3.6. Comparison between predicted and test (Serrette et al., 1996) results for lateral strengths and displacements

SWP description	Screw No.	Lateral strength, kN/m					Lateral displacement, mm		
		Test	Predicted			Ratio[1] Test / Pred	Test	SP	Ratio Test / Pred
			Sheathing failure		Stud failure				
			IP	SP					
GWB sheathing: 12.7mm Steel stud: 150S32-0.88mm Screw spacing (mm) Edge: 152; Field: 305 Wall length and height: 2438mm, 2438mm. Sheathing length and height: (2) 1219mm, 2438mm	6	10.93	11.15	10.97	23.46	**1.00**	40.00	37.1	**0.93**

[1] The "Pred" is the smaller one of the predicted strengths based on sheathing (SP) and stud failures

Recently, CFS steel laminates have been employed as sheathing for SWP. Although CFS laminates are thin plates that are prone to local buckling, they can be used efficiently when bonded to thicker plates of other materials, such as GWB. For example, there is a marketplace double layer board called Sureboard (2006), which is composed of a 0.69 mm (27 mils) thick CFS steel sheathing bonded to a 12.7 mm (0.5 in) thick GWB.

Table 3.7 presents a comparison of experimentally determined SWP lateral strengths of Sureboard, obtained by the ICC Evaluation Service (ER-5762, 2003), with corresponding strengths predicted by this study. The comparisons are presented for steel studs of three different thicknesses, i.e., 33 mils, 43 mils, and 54 mils. In all comparisons the sheathing is attached to the framing with No. 6 screws with different spacing at the edge of the panel (i.e., 152 mm, 102 mm, 76 mm, and 51 mm). Information regarding the type of hold-downs employed to attach the SWP to the floor is not provided. Unlike all of the previous comparisons where failure of a sheathing-to-framing connection was governed by the bearing capacity of the sheathing material, Sureboard failure is governed by screw

pullout. This was determined comparing the strengths of a sheathing-to-framing connection for failure of the sheathing, stud, and screw as described in the example of Section 3.6.

A considerable discrepancy can be observed in Table 3.7 among of several of the predictions made by this study and those reported, by ER-5762 (2003). A factor affecting the precision of the prediction calculations is the value adopted for the strength of the sheathing-to-framing connection, V_r. The same value was used for all predictions, even though studs with three different thicknesses are used. The strength of the sheathing-to-framing connections is governed by the thickness of the sheathing steel, which is smaller than the thickness of the studs. Even so, the thickness of the studs can affect the strength of the connections. Therefore, accurate information, regarding the strength of sheathing-to-framing connections for Sureboard, is needed to yield accurate estimations of the lateral strength of SWP with Sureboard.

Table 3.7. Comparison between predicted and test (ER-5762, 2003) results for lateral strengths and displacements

SWP description	Edge screw spacing mm	Lateral strength, kN/m					Lateral displacement, mm		
		Test	Predicted			Ratio Test/Pred	Test	SP	Ratio Test/Pred
Sureboard Series 200, Steel thick. 0.69 mm GWB 12.7 mm (1/2 in)			Sheathing failure		Stud failure				
			IP	SP					
Stud thick. 0.84 mm (33mils) @ 610 mm oc.	152	15.83	14.56	14.53	36.44	**1.09**	13.97	16.97	**0.82**
	102	22.55	21.62	21.56		**1.05**	17.78	17.53	**1.01**
	76	25.25	28.68	28.59		**0.88**	17.78	17.72	**1.00**
	51	27.95	42.79	42.65		**0.77**	17.78	18.16	**0.98**
Stud thick. 1.09 mm (43mils) @ 610 mm oc.	152	20.50	14.62	14.58	55.70	**1.41**	20.83	17.02	**1.22**
	102	28.09	21.68	21.62		**1.30**	24.64	17.53	**1.41**
	76	31.30	28.74	28.65		**1.09**	24.64	17.78	**1.39**
	51	34.44	42.86	42.72		**0.81**	21.08	18.16	**1.16**
Stud thick. 1.37 mm (43mils) @ 610 mm oc.	76	42.25	28.8	28.76	73.31	**1.47**	25.65	17.78	**1.44**
	51	50.49	42.92	42.78		**1.18**	31.5	18.16	**1.73**
Average						**1.10**			**1.22**

Standard deviation	**0.24**		**0.28**
Coefficient of variation	**0.22**		**0.23**

Chapter 4

Simplified Finite Element Analysis (SFEA) for CFS Buildings

4.1. Introduction

Typically, CFS buildings are built with structural SWP, load-bearing and non-load bearing wall panels, floor panels, and roof panels SWP are built with CFS studs and tracks, covered with structural sheathing attached with screws on one or two sides, as shown in Figure 3.3. Wall panels are built similarly, but without structural sheathing. The floor panels can be built in three ways: flat slabs, flat slabs supported by CFS joists, or panels supported by CFS joists. The slabs can be constructed of concrete, and the panels can be constructed of CFS, structural steel or wood. Roof panels are built in the same fashion as the floor panels, though steel and wood are more commonly used than concrete.

In engineering practice, typically the analysis of CFS buildings is conducted using Conventional Finite Element Analysis (CFEA). In this approach, the shear wall, wall, floor and roof panels are modeled using frame elements for the studs, tracks, and joists, and shell elements for the sheathing and slabs. Shown in Figure 4.1, is a typical model of a three-storey CFS building. Although CFEA is effective for analyzing CFS buildings, generating and analyzing the model is time consuming due to the large number of elements. Reviewing the results from CFEA is also time consuming, because all the studs in the building need to be reviewed in order to identify the studs with larger axial forces.

Presented in this Chapter is the proposed methodology to carry out a SFEA of CFS buildings. The objective of the development of the methodology is to provide a simple analysis procedure having acceptable accuracy for the PBD assessment of CFS buildings.

Specifically, the SFEA method is devised to reduce the number of elements in the model, thus the model can be generated and analyzed in less time. Also, reviewing the results becomes simpler, because the output can be set up to print out the lateral force in each SWP along with the forces in the most critical studs. Although the advantages may not be significant for a single linear analysis, for the pushover analysis of CFS buildings the advantages become significant, because usually the analysis must be carried out many times, depending on the number of applied loading increments.

Basically, the SFEA of CFS buildings consists of two aspects: 1) transforming the SWP, wall panels, floor panels, and roof panels into flat shell elements with equivalent material and geometric properties; 2) modeling each panel with an equivalent (e.g., sixteen-node) shell element in the finite element analysis. Shown in Figure 4.1 is the model of the building that is analyzed using CFEA, in which the SWP are modeled with shell and frame elements. Also depicted in Figure 4.1 are the equivalent shell elements, represented by the large dark rectangles that are used for the SFEA model. Thus, the relative difference in size of the elements that would be used for CFEA and SFEA for this building is evident.

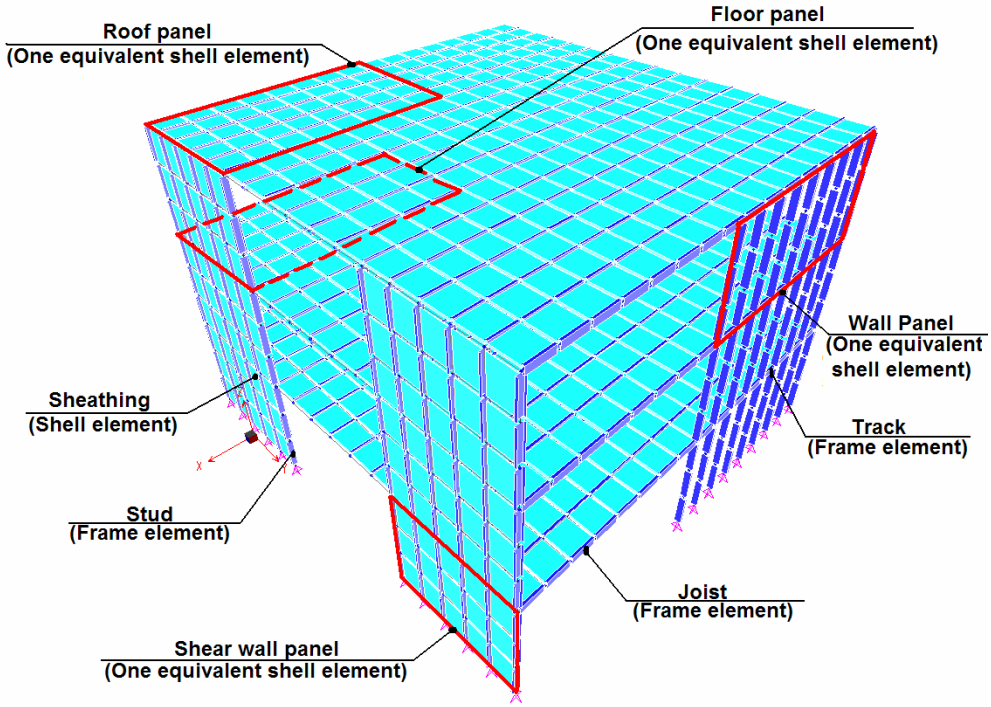

Figure 4.1 Modeling of a CFS building using finite element analysis

In Section 4.2 the method for transforming the panels into shell elements of equivalent material and geometric properties is described. A nonlinear finite element formulation is presented in Section 4.3. After the SFEA of a CFS building is conducted, the internal forces in the studs are estimated using the procedure in Section 4.4. Next, nine SWP are analyzed by SFEA and CFEA, and the results are compared and discussed in Section 4.5. To account for the SWP material nonlinearities in the pushover analysis, a stiffness degradation model is developed in Section 4.6. Finally, in Section 4.7 several SWP are analyzed by SFEA, and the results are compared to those from experimental testing.

4.2. Modeling of SWP with Equivalent Shell Elements

Panels are generally complex to analyze because they are geometric orthotropic elements having different cross section geometry in their orthogonal directions. To simplify the analysis, however, this study considers panels as natural orthotropic elements having the same geometry but different material properties in their orthogonal directions. Typically, common finite element formulations allow natural orthotropic elements but do not accept geometric orthotropic elements. Figure 4.2 shows the cross section of a panel and its equivalent shell cross section, where: s_F is the spacing between studs, s_C is the distance between screws on the edge of the panel, and c_1 and c_2 are the distances from the centre of the studs to the mid-plane of the sheathing on side 1 and 2, respectively. The parameters E_F, A_F, and I_F denote the modulus of elasticity, cross sectional area, and moment of inertia about the strong bending axis of the studs, respectively, while l is the length of the panel and equivalent shell element, and t_{S1} and t_{S2} are thicknesses of the sheathing on side 1 and side 2, respectively.

Troitsky (1976) developed equations to determine the equivalent rigidity of orthotropic ribbed plates in bending. In this study the Troitsky equations are extended to account for the axial rigidity of the panel in the direction along the longitudinal axis of the studs (i.e., y direction). The equivalent thickness and modulus of elasticity in the y direction of a shell element are determined by equating and solving the axial and flexural rigidities of a panel and an orthotropic element. Afterwards, the equivalent modulus of elasticity in the

x direction is determined by equating and solving the bending rigidity of a panel and a orthotropic shell .

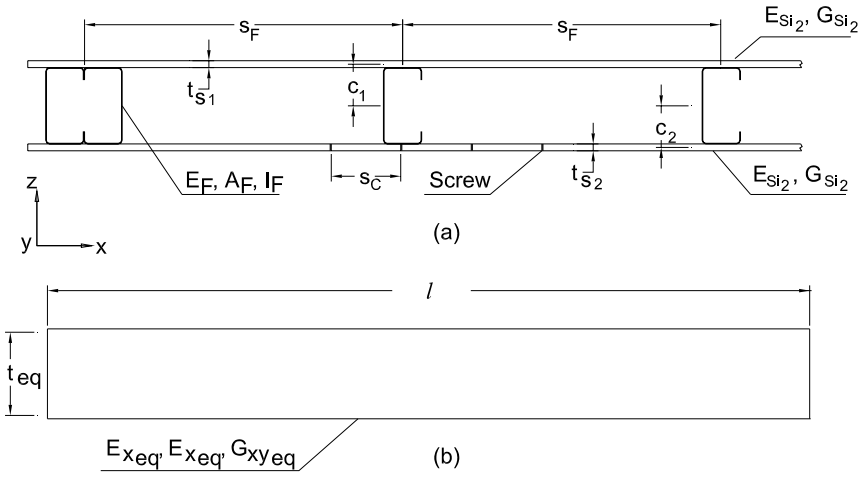

Figure 4.2. a) Panel cross-section, and b) equivalent shell

The general equations for the axial and flexural rigidities of an orthotropic plate or shell are given by,

$$T = \frac{E_i \cdot A_i}{1-\nu_x \nu_y}, \qquad D = \frac{E_i \cdot I_i}{1-\nu_x \nu_y} \tag{4. 1 a,b}$$

where T, and D, are the axial and flexural rigidities of an orthotropic flat element; A_i, I_i, and v_i are the cross sectional area, moment of inertia of the orthotropic element, and Poisson ratio, respectively. The index i denotes the direction (e.g., x or y) in which the properties are measured. Substituting the properties of a panel into Eqs. (4.1 a,b) and dividing through by the length l, the axial and flexural rigidities per unit of length are expressed as follows.

$$T_y^{(q)} = \frac{E_{y1}^{(q)} \cdot t_{S1}^{(q)}}{1-\nu_{x1}\nu_{y1}} + \frac{E_{y2}^{(q)} \cdot t_{S2}^{(q)}}{1-\nu_{x2}\nu_{y2}} + \frac{E_F A_F n_F}{l} \tag{4. 2}$$

$$D_y^{(q)} = \frac{E_{y1}^{(q)}}{1-\nu_{x1}\nu_{y1}}\left(\frac{t_{S1}^3}{12} + t_{S1} \cdot c_1^2\right) + \frac{E_{y2}^{(q)}}{1-\nu_{x1}\nu_{y1}}\left(\frac{t_{S2}^3}{12} + t_{S2} \cdot c_2^2\right) + \frac{E_F I_F n_F}{l} \tag{4. 3}$$

$$E_{y1}^{(q)} = \lambda^{(q)} E_{Sy1} \qquad E_{y2}^{(q)} = \lambda^{(q)} E_{Sy2} \tag{4. 4 a,b}$$

where: E_{Sy} is the sheathing modulus of elasticity in the y direction; t_s is the thickness; λ is the stiffness degradation coefficient, computed from Eq. (4.52); subscripts 1 and 2 represent the side of the panel in which the properties are measured; v_x and v_y are the sheathing Poisson ratios in the x and y directions; n_F is the number of studs in the panel; and q is a load increment index associated with the nonlinear analysis.

Substituting the properties of the equivalent shell into Eqs. (4.1 a,b), and dividing through by l, the axial and flexural rigidities per unit length are expressed as follows.

$$T_{yeq}^{(q)} = \frac{E_{yeq}^{(q)} \cdot t_{eq}^{(q)}}{1 - \nu_{xeq}\nu_{yeq}}, \qquad D_{yeq}^{(q)} = \frac{E_{yeq}^{(q)} \cdot t_{eq}^{3\,(q)}}{12\left(1 - \nu_{xeq}\nu_{yeq}\right)} \qquad \textbf{(4. 5 a,b)}$$

where: E_{yeq} and t_{eq} are the modulus of elasticity and thickness of the equivalent shell, respectively; v_{xeq} and v_{yeq} are the equivalent shell Poisson ratios in the x and y directions, respectively.

By equating $T_y^{(q)}$ and $T_{yeq}^{(q)}$, the following equation is obtained,

$$\frac{E_{yeq}^{(q)} \cdot t_{yeq}^{(q)}}{1 - \nu_{xeq}\nu_{yeq}} = \frac{E_{y1}^{(q)} \cdot t_{S1}}{1 - \nu_{x1}\nu_{y1}} + \frac{E_{y2}^{(q)} \cdot t_{S2}}{1 - \nu_{x2}\nu_{y2}} + \frac{E_F A_F n_F}{l} \qquad \textbf{(4. 6)}$$

By equating $D_y^{(q)}$ and $D_{yeq}^{(q)}$, the following equation is obtained,

$$\frac{E_{yeq}^{(q)} \cdot t_{eq}^{3\,(q)}}{12\left(1 - \nu_{xeq}\nu_{yeq}\right)} = \frac{E_{y1}^{(q)}}{1 - \nu_{x1}\nu_{y1}}\left(\frac{t_{S1}^3}{12} + t_{S1} \cdot c_1^2\right) + \frac{E_{y2}^{(q)}}{1 - \nu_{x1}\nu_{y1}}\left(\frac{t_{S2}^3}{12} + t_{S2} \cdot c_2^2\right) + \frac{E_F I_F n_F}{l} \qquad \textbf{(4. 7)}$$

By solving Eqs. (4.6) and (4.7), the equivalent modulus of elasticity in the y direction and thickness of the equivalent shell element, at load increment q, are expressed as

$$E_{yeq}^{(q)} = \frac{\left(\alpha_1^{(q)} + \alpha_2\right)^2 \left(1 - \nu_{xeq}\nu_{yeq}\right)}{l \cdot \left(1 - \nu_{x2}\nu_{y2}\right)\left(1 - \nu_{x1}\nu_{y1}\right)\left[\left(\alpha_1^{(q)} + \alpha_2\right)\left(\alpha_3^{(q)} + \alpha_4^{(q)} + \alpha_5^{(q)}\right)\right]^{1/2}} \qquad \textbf{(4. 8)}$$

$$t_{eq}^{(q)} = \frac{\left[\left(\alpha_1^{(q)} + \alpha_2\right)\left(\alpha_3^{(q)} + \alpha_4^{(q)} + \alpha_5^{(q)}\right)\right]^{1/2}}{\left(\alpha_1^{(q)} + \alpha_2\right)} \qquad \textbf{(4. 9)}$$

where

$$\alpha_1^{(q)} = E_F \cdot A_F \cdot n_F + l \cdot \left[{}_q E_{y1} \cdot t_{S1} \left(1 - \nu_{x2}\nu_{y_2}\right) + {}_q E_{y2} \cdot t_{S2} \left(1 - \nu_{x1}\nu_{y_1}\right) \right]$$

$$\alpha_2 = -E_F \cdot A_F \cdot n_F \cdot \left[\nu_{x2}\nu_{y_2} \left(1 - \nu_{x1}\nu_{y_1}\right) + \nu_{x1}\nu_{y_1} \right]$$

$$\alpha_3^{(q)} = 12 \cdot l \cdot {}_q E_{y1} \cdot t_{S1} \cdot c_1^2 \left(1 - \nu_{x2}\nu_{y_2}\right) - 12 \cdot E_F \cdot I_F \cdot n_F \left(\nu_{x2}\nu_{y_2} + \nu_{x1}\nu_y\right)$$

$$\alpha_4^{(q)} = l \cdot {}_q E_{y2} \cdot t_{S2} \cdot \left(t_{S2}^3 \cdot \left(1 - \nu_{x1}\nu_y\right) + 12 \cdot c_1^2 \right) - l \cdot {}_q E_{y1} \cdot t_{S1}^3 \cdot \nu_{x2}\nu_{y_2}$$

$$\alpha_5^{(q)} = l \cdot {}_q E_{y1} \cdot t_{S1}^3 + 12 \cdot E_F \cdot I_F \cdot n_F \left(1 + \nu_{x2}\nu_{y_2}\nu_{x1}\nu_y\right) - 12 \cdot l \cdot {}_q E_{y2} \cdot t_{S2} \cdot c_2^2 \cdot \nu_{x1}\nu_{y_1}$$

It is noted that all the right terms in Eq. (4.9) are contained in Eq. (4.8), thus the terms in Eq. (4.8) are replaced by $t_{eq}^{(q)}$, such that,

$$E_{yeq}^{(q)} = \frac{\left(\alpha_1^{(q)} + \alpha_2\right)\left(1 - \nu_{xeq}\nu_{yeq}\right)}{t_{eq}^{(q)} \cdot l \cdot \left(1 - \nu_{x2}\nu_{y_2}\right)\left(1 - \nu_{x1}\nu_{y_1}\right)} \qquad \textbf{(4. 10)}$$

The flexural rigidity of the panel in the *x* direction at load increment *q* is given by,

$$D_x^{(q)} = \frac{E_{x1}^{(q)}}{1 - \nu_{x1}\nu_{y1}} \left(\frac{t_{S1}^3}{12} + t_{S1} \cdot c_1^2 \right) + \frac{E_{x2}^{(q)}}{1 - \nu_{x2}\nu_{y2}} \left(\frac{t_{S2}^3}{12} + t_{S2} \cdot c_2^2 \right) \qquad \textbf{(4. 11)}$$

$$E_{x1}^{(q)} = \lambda^{(q)} E_{Sx1}^{(q)}, \qquad E_{x2}^{(q)} = \lambda^{(q)} E_{Sx2}^{(q)} \qquad \textbf{(4. 12 a,b)}$$

where E_{Sx} is the sheathing Young's modulus in the *x* direction. The flexural rigidity of the equivalent shell in the *x* direction is given by,

$$D_{xeq}^{(q)} = \frac{E_{xeq}^{(q)} \cdot t_{eq}^{3\,(q)}}{12\left(1 - \nu_{xeq}\nu_{yeq}\right)} \qquad \textbf{(4. 13)}$$

By equating and solving $D_x^{(q)}$ and $D_{xeq}^{(q)}$, the modulus of elasticity of the equivalent shell element in the *x* direction is given by,

$$E_{xeq}^{(q)} = \left(\frac{E_{x1}^{(q)}}{1 - \nu_{x1}\nu_{y1}} \left(\frac{t_{S1}^3}{12} + t_{S1} \cdot c_1^2 \right) + \frac{E_2^{(q)}}{1 - \nu_{x2}\nu_{y2}} \left(\frac{t_{S2}^3}{12} + t_{S2} \cdot c_2^2 \right) \right) \cdot \frac{12\left(1 - \nu_x\nu_y\right)}{t_{eq}^{3\,(q)}} \qquad \textbf{(4. 14)}$$

and the shear rigidity of the panel in its plane (i.e., *x*-*y* plane) is given by,

$$D_{xy}^{(q)} = G_{xy1}^{(q)} \cdot l \cdot t_{S1} + G_{xy2}^{(q)} \cdot l \cdot t_{S2} \quad \textbf{(4. 15)}$$

$$G_{xy}^{(q)} = \lambda^{(q)} \cdot G_S \quad \textbf{(4. 16)}$$

where G_S denotes the shear modulus of elasticity of the sheathing. The shear rigidity of the equivalent shell is given by,

$$D_{xyeq}^{(q)} = G_{xyeq}^{(q)} \left(l \cdot t_{eq}^{(q)} \right) \quad \textbf{(4. 17)}$$

By equating the equivalent shell and the panel rigidity, $D_{xy}^{(q)}$ and $D_{xyeq}^{(q)}$, and solving for the equivalent shear modulus of elasticity,

$$G_{xyeq}^{(q)} = \frac{G_{xy1}^{(q)} \cdot t_{S1} + G_{xy2}^{(q)} \cdot t_{S2}}{t_{eq}^{(q)}} \quad \textbf{(4. 18)}$$

For panels with different types of sheathing on the two sides, the Poisson ratios for the equivalent shell in the *x* and *y* directions are given by,

$$\nu_{xeq} = \frac{\nu_{x2}\nu_{x1}\left(E_{Sx1} \cdot t_{S1} + E_{Sx2} \cdot t_{S2}\right)}{\nu_{x2} \cdot E_{Sx1} \cdot t_{S1} + \nu_{x1} \cdot E_{Sx2} \cdot t_{S2}}, \quad \nu_{yeq} = \frac{\nu_{y2}\nu_{y1}\left(E_{Sy1} \cdot t_{S1} + E_{Sy2} \cdot t_{S2}\right)}{\nu_{y2} \cdot E_{Sy1} \cdot t_{S1} + \nu_{y1} \cdot E_{Sy2} \cdot t_{S2}} \quad \textbf{(4. 19 a,b)}$$

For panels with sheathing on only one side, or the same type of sheathing on both sides, the Poisson ratios for the equivalent shell are given by,

$$\nu_{xeq} = \nu_{x1} \qquad \nu_{yeq} = \nu_{y1} \quad \textbf{(4. 20 a,b)}$$

These equivalent Poisson ratio equations were obtained by assuming that the deformations in the *x* and *y* directions of the panel and equivalent shell are the same. Furthermore, it is assumed that compatibility of deformations exists between the sheathing on either side of the panel.

4.3. Nonlinear Finite Element Formulation

The shell element used in this study to model the panels in a CFS building is an isoparametric element, which typically has between four and sixteen nodes. The sixteen-node shell element, in Figure 4.3, is selected to model the CFS equivalent shell elements.

The reason for this is that this element has the ability to provide more accurate results than elements of fewer nodes, when a typical CFS panel is modeled with one shell element. Each node of the sixteen-node shell element has five degrees of freedom (i.e., three translations along the *x*, *y*, and *z* axes, and two rotations about the *x* and *y* axes), which is adequate to simulate CFS panels used in construction practice.

An updated Lagrangian formulation is adopted to develop the element stiffness matrix of the sixteen-node shell element, where the values of all parameters, static and kinematic, are computed in accordance with the latest deformed configuration of the element. The procedure to achieve the elastic and geometric stiffness matrices for the sixteen-node shell element is presented in the following (Bathe and Bolourchi, 1982).

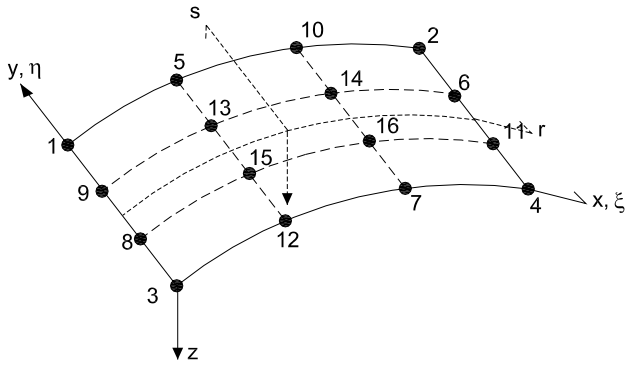

Figure 4.3. Sixteen-node shell element

The shape functions of a shell element are obtained by means of the following Lagrange interpolation equation:

$$N_k = \frac{(x_1-\alpha)(x_2-\alpha)\cdots(x_{nd}-\alpha)}{(x_1-x_j)(x_2-x_j)(x_{nd}-x_j)} \quad for\ nd \neq j \qquad \textbf{(4. 21)}$$

where N_k is a cubic shape function for node *k*, where *x* is the natural coordinate of the node *k* measured in the direction α (i.e., *s* or *r*, as shown in Figure 4.3), and *nd* is the number of nodes in the direction α (i.e., *nd*=4 for the sixteen-node shell element in the *s* and *r* directions). The natural coordinates *s* or *r,* represent the "normalized" dimensions of the shell element, since the length of each side of the shell element is always 2. For instance, the coordinates of node 1 in the *r* and s directions are -1 and 1, respectively; the

coordinates of node16 in the *r* and *s* directions are 1/3 and -1/3, respectively. The index *j* represents the node under consideration (j=1,2,3 or 4). From Eq. (4.21), the following expressions for the cubic shape functions for each node of the shell element are,

$$N_1 = -\frac{1}{256}(1+s)(1+3s)(-1+3s)(1+3r)(-1+3r)(-1+r) \quad \textbf{(4. 22 a)}$$

$$N_2 = \frac{1}{256}(1+s)(1+3s)(-1+3s)(1+3r)(-1+3r)(1+r) \quad \textbf{(4. 22 b)}$$

$$N_3 = \frac{1}{256}(1+3s)(-1+3s)(-1+s)(1+3r)(-1+3r)(-1+r) \quad \textbf{(4. 22 c)}$$

$$N_4 = \frac{-1}{256}(1+3s)(-1+3s)(-1+s)(1+3r)(-1+3r)(1+r) \quad \textbf{(4. 22 d)}$$

$$N_5 = \frac{9}{256}(-1+3s)(1+3s)(1+s)(1+r)(-1+3r)(-1+r) \quad \textbf{(4. 22 e)}$$

$$N_6 = \frac{-9}{256}(1+s)(1+3s)(-1+s)(1+3r)(-1+3r)(1+r) \quad \textbf{(4. 22 f)}$$

$$N_7 = \frac{9}{256}(1+3s)(-1+3s)(-1+s)(1+r)(1+3r)(-1+r) \quad \textbf{(4. 22 g)}$$

$$N_8 = \frac{-9}{256}(1+s)(-1+3s)(-1+s)(1+3r)(-1+3r)(-1+r) \quad \textbf{(4. 22 h)}$$

$$N_9 = \frac{9}{256}(1+s)(1+3s)(-1+s)(1+3r)(-1+3r)(-1+r) \quad \textbf{(4. 22 i)}$$

$$N_{10} = \frac{-9}{256}(1+s)(1+3s)(-1+3s)(1+r)(1+3r)(-1+r) \quad \textbf{(4. 22 j)}$$

$$N_{11} = \frac{9}{256}(1+s)(-1+3s)(-1+s)(1+3r)(-1+3r)(1+r) \quad \textbf{(4. 22 k)}$$

$$N_{12} = \frac{-9}{256}(1+3s)(-1+3s)(-1+s)(1+r)(-1+3r)(-1+r) \quad \textbf{(4. 22 l)}$$

$$N_{13} = \frac{-81}{256}(1+s)(1+3s)(-1+s)(1+r)(-1+3r)(-1+r) \quad \textbf{(4. 22 m)}$$

$$N_{14} = \frac{81}{256}(1+s)(1+3s)(-1+s)(1+r)(1+3r)(-1+r) \quad \textbf{(4. 22 n)}$$

$$N_{15} = \frac{81}{256}(1+s)(-1+3s)(-1+s)(1+r)(-1+3r)(-1+r) \quad \textbf{(4. 22 o)}$$

$$N_{16} = \frac{-81}{256}(1+s)(-1+3s)(-1+s)(1+r)(1+3r)(-1+r) \qquad \textbf{(4. 22 p)}$$

The coordinates at any point within the element at load increment q are mathematically expressed as,

$$x^{(q)} = \sum_{k=1}^{n} N_k x_k^{(q)} + \frac{t}{2}\sum_{k=1}^{n} t_{eq\,k}^{(q)} N_k V_{nx\,k}^{(q)} \qquad \textbf{(4. 23)}$$

$$y^{(q)} = \sum_{k=1}^{n} N_k y_k^{(q)} + \frac{t}{2}\sum_{k=1}^{n} t_{eq\,k}^{(q)} N_k V_{ny\,k}^{(q)} \qquad \textbf{(4. 24)}$$

$$z^{(q)} = \sum_{k=1}^{n} N_k z_k^{(q)} + \frac{t}{2}\sum_{k=1}^{n} t_{eq\,k}^{(q)} N_k V_{nz\,k}^{(q)} \qquad \textbf{(4. 25)}$$

where $t_{eq}^{(q)}$ is the equivalent shell thickness, and $x_k^{(q)}$, $y_k^{(q)}$, $z_k^{(q)}$ are the Cartesian coordinates of node k. The parameters N_k (k=1,..,n) are the shape functions, defined in (4.22), as functions of r and s. The parameter V_n is a unit vector normal to the shell surface, and the x, y, and z subscripts represent the vector components. In the same manner, the equations to find the displacements at any point within the shell element are given by,

$$u^{(q)} = \sum_{k=1}^{n} N_k x_k^{(q)} + \frac{t}{2}\sum_{k=1}^{n} t_{eq\,k}^{(q)} N_k V_{nx\,k}^{(q)} \qquad \textbf{(4. 26)}$$

$$v^{(q)} = \sum_{k=1}^{n} N_k y_k^{(q)} + \frac{t}{2}\sum_{k=1}^{n} t_{eq\,k}^{(q)} N_k V_{ny\,k}^{(q)} \qquad \textbf{(4. 27)}$$

$$w^{(q)} = \sum_{k=1}^{n} N_k z_k^{(q)} + \frac{t}{2}\sum_{k=1}^{n} t_{eq\,k}^{(q)} N_k V_{nz\,k}^{(q)} \qquad \textbf{(4. 28)}$$

where $V_{ni\,k} = V_{ni\,k}^{(q)} - V_{ni\,k}^{(q-1)}$ is a vector normal to the shell element surface that stores the increments of the direction cosines in the $i = x$, y or z direction. The elements of $V_{ni\,k}$ are expressed as a function of the rotations at node k. However, a convenient way to determine V_{ni} is by defining two initial orthogonal unit vectors $V_{1k}^{(1)}$ and $V_{2k}^{(1)}$ for the initial load increment, as depicted in Figure 4.4, given by,

$$V_{1k}^{(1)} = \frac{e_2 \times V_{nk}^{(1)}}{\left\| e_2 \times V_{nk}^{(1)} \right\|_2} \qquad \textbf{(4. 29)}$$

where e_2 is a unit vector in the direction of the local y axis of the shell element. The corresponding vector $V_{2k}^{(1)}$ is then,

$$V_{2k}^{(1)} = V_{nk}^{(1)} \times V_{1k}^{(1)} \qquad \textbf{(4. 30)}$$

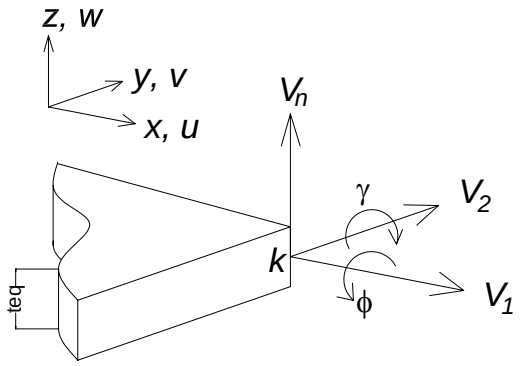

Figure 4.4. Vectors at node *k*

As shown in Figure 4.4, let ϕ_k and γ_k be the rotations of the normal vector $V_{nk}^{(q)}$ around the vectors $V_{1k}^{(q)}$ and $V_{2k}^{(q)}$, respectively, measured in the configuration corresponding to load increment q. Thus, for small rotations, V_n is given by,

$$V_{nk} = -V_{2k}^{(q)}\phi_k + V_{1k}^{(q)}\gamma_k \qquad \textbf{(4. 31)}$$

Since the formulation presented in this section is intended for large deformations, V_n must be evaluated as,

$$V_{nk} = V_{nk}^{(q-1)} + \int_{\phi,\gamma_k} V_{2k}^{(q-1)} d\phi_k + V_{1k}^{(q-1)} d\gamma_k \qquad \textbf{(4. 32)}$$

where the node rotations ϕ and γ are obtained from the previous analysis results. For the first iteration, note that the rotations are equal to zero. The integration in Eq. (4.32) can

be performed using multiple steps as for the Euler method (Bathe and Bolourchi, 1982). Also the integration can be performed in one step by using an orthogonal transformation matrix of finite rotations (Argyris, 1982) having the following form,

$$V_{nk}^{(q)} = T_{\varphi} V_{nk}^{(q-1)} \tag{4. 33}$$

where the orthogonal transformation matrix is,

$$T_{\varphi} = I_3 + \frac{\sin(\varphi)}{\varphi} S + \frac{1}{2}\left(\frac{\sin(\varphi/2)}{\varphi/2}\right)^2 S^2 \tag{4. 34}$$

in which,

$$\varphi = \sqrt{\phi_k^2 + \gamma_k^2}\,, \qquad S = \begin{bmatrix} 0 & 0 & \gamma_k \\ 0 & 0 & -\phi_k \\ -\gamma_k & \phi_k & 0 \end{bmatrix}$$

Having the equations to evaluate the displacement components at any point in the shell element (i.e., (4.26) to (4.28)), the displacement derivatives, in terms of natural coordinates, are expressed in Cartesian coordinates as,

$$\begin{Bmatrix} u_{,x} \\ u_{,y} \\ u_{,z} \\ v_{,x} \\ \vdots \\ w_{,x} \end{Bmatrix} = \begin{bmatrix} J_m^{-1} & 0 & 0 \\ 0 & J_m^{-1} & 0 \\ 0 & 0 & J_m^{-1} \end{bmatrix} \begin{Bmatrix} u_{,r} \\ u_{,s} \\ u_{,t} \\ v_{,r} \\ \vdots \\ w_{,r} \end{Bmatrix} \tag{4. 35}$$

where the comma denotes derivation, and the Jacobian matrix J_m is defined as,

$$J_m = \begin{bmatrix} \frac{\partial x}{\partial r} & \frac{\partial y}{\partial r} & \frac{\partial z}{\partial r} \\ \frac{\partial x}{\partial s} & \frac{\partial y}{\partial s} & \frac{\partial z}{\partial s} \\ \frac{\partial x}{\partial t} & \frac{\partial y}{\partial t} & \frac{\partial z}{\partial t} \end{bmatrix} \tag{4. 36}$$

Using the displacement derivatives of Eq. (4.35), the linear strain-displacement matrix is,

$$B_L^{(q)} = \begin{bmatrix} h_{k,1}^{(q)} & 0 & 0 & g_{11}^{k\,(q)} G_1^{k(q)} & g_{21}^{k\,(q)} G_1^{k(q)} \\ 0 & h_{k,2}^{(q)} & 0 & g_{12}^{k\,(q)} G_2^{k(q)} & g_{22}^{k\,(q)} G_2^{k(q)} \\ 0 & 0 & h_{k,3}^{(q)} & g_{13}^{k\,(q)} G_3^{k(q)} & g_{23}^{k\,(q)} G_3^{k(q)} \\ h_{k,2}^{(q)} & h_{k,1}^{(q)} & 0 & \left(g_{11}^{k\,(q)} G_2^{k(q)} + g_{12}^{k\,(q)} G_1^{k(q)}\right) & \left(g_{21}^{k\,(q)} G_2^{k(q)} + g_{22}^{k\,(q)} G_1^{k(q)}\right) \\ h_{k,3}^{(q)} & 0 & h_{k,1}^{(q)} & \left(g_{11}^{k\,(q)} G_3^{k(q)} + g_{13}^{k\,(q)} G_1^{k(q)}\right) & \left(g_{21}^{k\,(q)} G_3^{k(q)} + g_{23}^{k\,(q)} G_1^{k(q)}\right) \\ 0 & h_{k,3}^{(q)} & h_{k,2}^{(q)} & \left(g_{12}^{k\,(q)} G_3^{k(q)} + g_{13}^{k\,(q)} G_2^{k(q)}\right) & \left(g_{22}^{k\,(q)} G_3^{k(q)} + g_{23}^{k\,(q)} G_2^{k(q)}\right) \end{bmatrix} \quad \textbf{(4. 37)}$$

where

$$h_{k,1}^{(q)} = J_{m\,i1}^{-1(q)} h_{k,r} + J_{m\,i2}^{-1(q)} h_{k,s} \qquad G_i^{k(q)} = t\left(J_{m\,i1}^{-1(q)} h_{k,r} + J_{m\,i2}^{-1(q)} h_{k,s}\right) + J_{m\,i3}^{-1(q)} h_k$$

$$g_{1i}^{k(q)} = -\frac{1}{2} t_{eq} V_{2i}^{k(q)} \qquad g_{2i}^{k\,(q)} = \frac{1}{2} t_{eq} V_{1i}^{k(q)}$$

The nonlinear strain-displacement matrix is,

$$B_{NL}^{(q)} = \begin{bmatrix} h_{k,1}^{(q)} & 0 & 0 & g_{11}^{k\,(q)} G_1^{k(q)} & g_{21}^{k\,(q)} G_1^{k(q)} \\ 0 & h_{k,1}^{(q)} & 0 & g_{12}^{k\,(q)} G_1^{k(q)} & g_{22}^{k\,(q)} G_1^{k(q)} \\ 0 & 0 & h_{k,1}^{(q)} & g_{13}^{k\,(q)} G_1^{k(q)} & g_{23}^{k\,(q)} G_1^{k(q)} \\ h_{k,2}^{(q)} & 0 & 0 & g_{11}^{k\,(q)} G_2^{k(q)} & g_{21}^{k\,(q)} G_2^{k(q)} \\ 0 & h_{k,2}^{(q)} & 0 & g_{12}^{k\,(q)} G_2^{k(q)} & g_{22}^{k\,(q)} G_2^{k(q)} \\ 0 & 0 & h_{k,2}^{(q)} & g_{13}^{k\,(q)} G_2^{k(q)} & g_{23}^{k\,(q)} G_2^{k(q)} \\ h_{k,3}^{(q)} & 0 & 0 & g_{11}^{k\,(q)} G_3^{k(q)} & g_{21}^{k\,(q)} G_3^{k(q)} \\ 0 & h_{k,3}^{(q)} & 0 & g_{11}^{k\,(q)} G_3^{k(q)} & g_{22}^{k\,(q)} G_3^{k(q)} \\ 0 & 0 & h_{k,3}^{(q)} & g_{11}^{k\,(q)} G_3^{k(q)} & g_{23}^{k\,(q)} G_3^{k(q)} \end{bmatrix} \quad \textbf{(4. 38)}$$

The Cauchy stress matrix is,

$$\tau^{(q)} = \begin{bmatrix} \tau_{11}^{\ (q)} I_3 & & Sym. \\ \tau_{12}^{\ (q)} I_3 & \tau_{22}^{\ (q)} I_3 & \\ \tau_{13}^{\ (q)} I_3 & \tau_{31}^{\ (q)} I_3 & \tau_{33}^{\ (q)} I_3 \end{bmatrix} \quad \textbf{(4. 39)}$$

where I_3 is a 3x3 identity matrix.

The Cauchy stress vector is,

$$\tau^{T(q)} = \left[\tau_{11}^{(q)} \quad \tau_{22}^{(q)} \quad \tau_{33}^{(q)} \quad \tau_{12}^{(q)} \quad \tau_{13}^{(q)} \quad \tau_{23}^{(q)}\right] \tag{4. 40}$$

Lastly, the element linear and nonlinear stiffness matrices are expressed as

$$k_L^{(q)} = \int_V B_L^{(q)T} C^{(q)} B_L^{(q)} dV^{(q)} \tag{4. 41}$$

$$k_{NL}^{(q)} = \int_V B_{NL}^{(q)T} \tau^{(q)} B_{NL}^{(q)} dV^{(q)} \tag{4. 42}$$

where C is the constitutive matrix at load increment q, expressed as follows,

$$C^{(q)} = \begin{bmatrix} E_{xeq}^{(q)} & \nu_{xy} E_{xeq}^{(q)} & 0 & 0 & 0 & 0 \\ \nu_{yx} E_{yeq}^{(q)} & E_{yeq}^{(q)} & 0 & 0 & 0 & 0 \\ 0 & 0 & 0 & 0 & 0 & 0 \\ 0 & 0 & 0 & G_{xyeq}^{(q)} & 0 & 0 \\ 0 & 0 & 0 & 0 & \frac{5}{6} G_{xyeq}^{(q)} & 0 \\ 0 & 0 & 0 & 0 & 0 & \frac{5}{6} G_{xyeq}^{(q)} \end{bmatrix} \tag{4. 43}$$

where E_{xeq}, E_{yeq}, G_{xyeq} are computed from Eqs. (4.8), (4.14), and (4.18), respectively. The modulus of elasticity in the z direction is not considered, because the stresses in this direction are negligible for plates and shells. The shear modulus of elasticity in the planes x-z and y-z are affected by a factor of 5/6 to account for the parabolic variation of the transverse shear strain through the thickness of the shell element (Cook, Malkus and Plesha, 1989).

Equations (4.41) and (4.42) are integrated over the volume of the shell element. The integration can be carried out using Gauss-Legendre sampling points, where the weighting values are known. The number of sampling points depends on the type of element; for a sixteen-node element, a 4x4x2 integration is recommended in order to achieve a good approximation (i.e., the numerical integration is performed by using 32 sampling points). A detailed description of the nonlinear finite element analysis formulation is provided by Bathe and Bolourchi (1982), and Bathe (1996).

The structural elastic stiffness matrix of a building, at load increment q, is expressed as,

$$K_L^{(q)} = \sum_{n_e} k_L^{(q)} \tag{4. 44}$$

where n_e is the number of shell elements in the model of the building. The structural geometric nonlinear stiffness matrix of a building, at load increment q, is expressed as,

$$K_{NL}^{(q)} = \sum_{n_e} k_{NL}^{(q)} \tag{4. 45}$$

Finally, the equilibrium conditions in terms of incremental displacements Δu for the structure are represented by,

$$\left(K_L^{(q)} + K_{NL}^{(q)}\right) \cdot \Delta U^{(i)} = R^{(q+1)} - \left(\mathrm{F}^{(q+1)}\right)^{(i-1)} \tag{4. 46}$$

where $R^{(q+1)}$ is the vector of externally incremental applied loads on the building, $R^{(q+1)}$ - $F^{(q+1)}$ represents the unbalanced forces in the building. i is the equilibrium iteration index associated with the solution using iterative methods, such as the Newton-Raphson method (Bathe, 1996). Note that iterative methods perform equilibrium iterations to reduce or eliminate the unbalance force within each load increment. Thus, the solution of Eq. (4.46) is reached when the vector of internal forces $F^{(q+1)}$ is equal to the vector of external forces R. The vector of internal forces is evaluated as,

$$\left(F^{(q+1)}\right)^{(i-1)} = \int_{\left(V^{(q+1)}\right)^{(i-1)}} \left(B_L^{(q+1)^T}\right)^{(i-1)} \left(\hat{\tau}^{(q+1)}\right)^{(i-1)} \left(dV^{(q+1)}\right)^{(i-1)} \tag{4. 47}$$

If a single-step incremental load method is used to solve the nonlinear equilibrium Eq. (4.46), no equilibrium iterations are performed. Thus, the internal force vector $F^{(q+1)}$ is removed from Eq. (4.46), and the equilibrium equation reduces to the following expression,

$$\left(K_L^{(q)} + K_{NL}^{(q)}\right) \cdot \Delta U = R^{(q+1)} \tag{4. 48}$$

Once the incremental displacements ΔU are obtained from the solution of Eq. (4.46) or Eq. (4.48), the accumulated nodal displacements of the building are expressed as,

$$\left(U^{(q)}\right)^{(i)} = \left(U^{(q-1)}\right)^{(i-1)} + \Delta U^{(i-1)} \quad \text{and} \quad U^{(q)} = U^{(q-1)} + \Delta U \qquad \textbf{(4. 49 a,b)}$$

for iterative and single-step methods, respectively.

Knowing the nodal displacements of the building, the internal forces in the members are computed using the strain-displacement matrices for the shell elements. The equations, for estimating the axial force and bending moment in the studs, are presented in the next section.

4.4. Estimating the Internal Forces in the Studs from the Equivalent Shell

Transforming SWP into equivalent shell elements simplifies the analysis process for CFS buildings, because the designer can model a complete SWP using one equivalent shell element that includes the sheathing and studs. As a result, the studs are not explicitly included in the model of the SWP as frame elements. However, the internal forces in the studs still need to be identified in order to review the gravity design, when PBD is being carried out, or the capacity of the studs is evaluated.

The internal stresses at any point of the SWP can be computed through the strain-displacement matrices using the nodal displacements from the structural analysis. The procedure to estimate the axial forces in the studs is described in the following. First, the locations of the studs within the equivalent shell elements need to be identified. Then the axial stresses in the direction of the studs, σ_{my}, are computed in the mid-plane of the shell element, at several points along each stud within the equivalent shell element. In this study, the axial stresses are computed at three points along the studs; that is, in the bottom, the middle, and the top section of the stud element. The stresses could be computed at more points, but the accuracy would not be improved much, because typically the maximum forces and moments are registered at these three locations. In terms of the finite element analysis, identifying a specific point within a shell element consists of determining the Cartesian coordinates of the selected point and then its natural coordinates (i.e., r, and s). Finally, having the stresses at the selected points of each stud,

the largest stress is used to determine the maximum axial force in the stud. The axial force in the stud is estimated with the expression

$$P_F = t_{eq}\sigma_{my} w_{SF} \quad \textbf{(4. 50)}$$

where t_{eq} is the thickness of the equivalent shell, and σ_{my} is the maximum stress in the y direction at the mid-plane of the shell element at the bottom, middle, or top of the stud. The parameter w_{SF} is equal to $s_F/2$ for the end-studs and s_F for intermediate studs, where s_F is the distance between studs on centre. The internal bending moments in each stud, computed from the equivalent shell element, are given by the following equation,

$$M_x = w_{SF} \int_{-\frac{t_{eq}}{2}}^{\frac{t_{eq}}{2}} z_i \cdot \sigma_y \cdot dz \quad \textbf{(4. 51)}$$

where σ_y is the stress through the thickness of the equivalent shell element in the y direction, at distance z from the mid-plane. The internal moments in each stud are also computed at the bottom, middle and top section, so that the maximum moment for the stud can be identified.

Although the material and geometric properties of the shell elements are set equivalent to the properties of the SWP, their structural forms are different. The SWP consist of studs and sheathing, similar to a ribbed plate, whereas the shell elements are flat plates with a uniform thickness. Therefore, a variation in the prediction of the forces in the studs is expected.

The accuracy of the axial force evaluation, based on the shell elements, which may not be as good as that for the lateral displacements and forces, is affected by the following factors. First, the vertical stiffness of a SWP is not uniform along its cross section, because the stiffness is greater in the locations where the studs are placed and smaller at the locations without studs; for the equivalent shell elements the vertical stiffness is evenly distributed along its cross section. Second, SWP are subjected to forces that are transmitted to the studs from the joists, where the distance between studs is typically small (e.g., 406 mm, 609 mm). For the equivalent shell elements, the loads are

concentrated forces on the top four nodes that are typically evenly spaced at one-third of the length of the equivalent shell element. Thus, depending on the aspect ratio of the equivalent shell element the distance between nodes may be larger than the studs spacing. This discrepancy can adversely affect the accuracy in the prediction of the axial forces. Third, in this study, the stress used for estimating the axial forces is computed at three discrete points along the height of the equivalent shell elements, in the locations of the studs. Consequently, if any of these selected points coincide with an area of stress concentration, the axial force results may be inaccurate. The stresses at any location within an equivalent shell element are computed using the shape functions, even though the points may not coincide with the nodes of the equivalent shell element.

4.5. Comparison of Results for SWP with SFEA and CFEA.

To demonstrate the effectiveness of SFEA for SWP, a comparison of results for nine SWP with different lengths is carried out using SFEA and CFEA. Although CFEA is a numerical approach for which the solution may not be exact, CFEA can provide accurate results for most engineering problems. The accuracy of CFEA depends primarily on the type, size, and number of elements used to model a structure. Even though CFEA is an approximate approach, its precision is appropriate for most civil engineering problems. Therefore, in this study CFEA is used as a benchmark for comparing the results from SFEA.

The SFEA is carried out using a computer program described in Section 5.6, whereas the CFEA is carried out using SAP2000 (2006) which is a commercial software widely used in structural engineering practice. Nine SWP are analyzed with different lengths: 609 mm (2 ft), 1219 mm (4 ft), 2438 mm (8 ft), 3657 mm (12 ft), 4876 mm (16 ft), 6095 mm (20 ft), 7314 mm (24 ft), 8533 mm (28 ft), and 9752 mm (32 ft). The height of all the SWP is 2438 mm (8 ft) and, therefore, the corresponding aspect ratios (i.e., height-to-length ratio) of the foregoing SWP are 0.25, 0.5, 1.0, 1.5, 2.0, 2.5, 3.0, 3.5, and 4.0, respectively. All of the SWP are built with the same details and material properties: oriented strand board (OSB) sheathing on one side, C-section studs and tracks 152C51– 1.18 mm (600S200-43

mils) with no lip, spaced at 406 mm (16 in) on centre, and with one end-stud. The C-section profiles used for the top tracks are the same as those of the studs.

For the SFEA, one shell element and three frame elements are used to model each SWP. The top track is modeled with three frame elements, since the shell elements have four nodes on the top, but the bottom tracks are not included in the model because the bottom nodes are fixed (i.e., the SWP is a cantilever). For the CFEA, the studs are modeled with frame elements 203 mm in length, and the sheathing is modeled using square four-node shell elements with a 203 mm side length. Thus, as the length of the SWP is increased, the number of shell elements in the CFEA model increases as well, while the number of shell elements for the SFEA remains the same. Shown in Figure 4.5 are both the simplified and conventional analysis models. Given in Table 4.1 is the number of shell and frame elements employed in each model (note the substantially smaller number of shell elements in the SFEA model). The nodal loads for both models are calculated, based on a uniformly distributed load on the top track of 17.23 kN/m, and are applied at the top four nodes in the x and y directions, as depicted in Figure 4.5. Also, a 1.00 kN/m^2 load is applied on the face of the SWP to simulate wind loads.

Listed in Table 4.2 are the properties of the SWP employed in the calculation of the equivalent shell elements. Although the Poisson ratios for the OSB sheathing are actually 0.16 and 0.23 in the x and y directions, respectively (Thomas, 2004), the Poisson ratio value of 0.23 is here used in both directions because SAP2000 allows only one Poisson ratio value in each plane. The number of studs in each SWP, n_F, is presented in Table 4.3, together with the properties of the equivalent shell elements. The equivalent properties should be the same for all nine SWP. However, since the ratio of length-to-number of studs is not the same for all the SWP, the equivalent properties of the SWP are in fact different. The number of studs in the SWP is computed as the length of the SWP divided by the spacing of the studs, plus one to account for the end-stud.

Given in Table 4.4 are the x, y and z displacements of node 1 predicted by CFEA and SFEA; these results are also plotted in Figure 4.6. The maximum axial forces and

bending moment in the SWP studs, listed in Table 4.5 and shown in Figures 4.7 and 4.8, are determined from the most critical stud in each SWP, regardless the location of the studs; specifically, the maximum axial forces for the nine SWP analyzed were found at the bottom of the end-studs, while the maximum bending moments were found at the bottom of the middle studs.

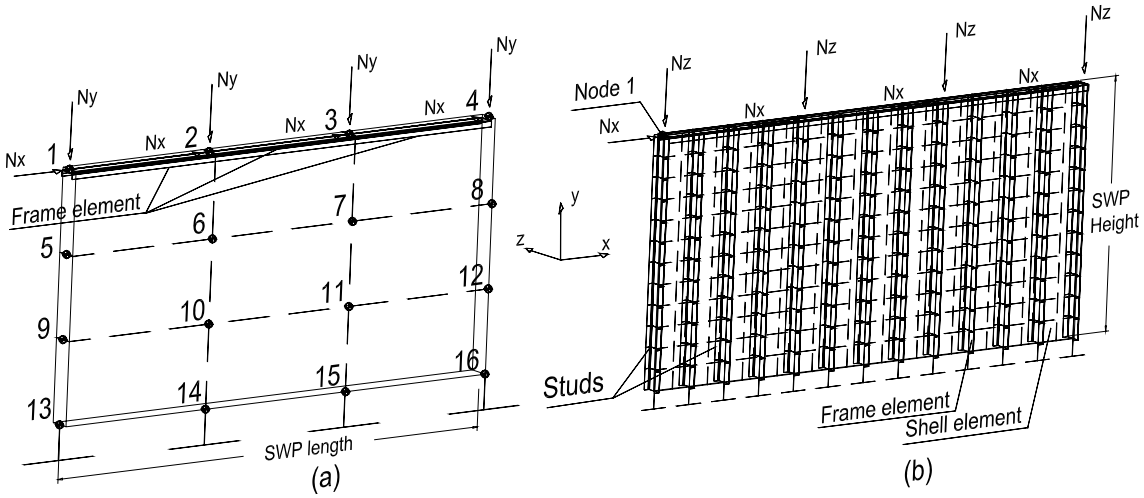

Figure 4.5. SWP model for (a) SFEA and (b) CFEA

Table 4.1 Number of shell and frame elements in the modeling of the SWP

SWP Aspect ratio	CFEA			SFEA		
mm	Shell	Frame	Total	Shell	Frame	Total
0.25	18	20	**38**	1	3	**4**
0.50	54	42	**96**	1	3	**4**
1.00	108	75	**183**	1	3	**4**
1.50	162	108	**270**	1	3	**4**
2.00	216	141	**357**	1	3	**4**
2.50	270	174	**444**	1	3	**4**
3.00	324	207	**531**	1	3	**4**
3.50	378	240	**618**	1	3	**4**
4.00	432	273	**705**	1	3	**4**

Table 4.2 Properties of the sheathing and framing studs employed for determining the properties of the equivalent shell elements

Sheathing						Stud				
Ma-	E_x	E_y	G	t	ν	E	G	t	A	I
terial	MPa	MPa	MPa	mm		MPa	MPa	mm	mm^2	mm^4
OSB	1983	9917	925	11.11	0.23	203000	77000	1.18	292.49	9.7×10^5

Table 4.3 Properties of the equivalent shell elements

SWP Aspect ratio	n_F	E_{xeq}	E_{yeq}	G_{eq}	t_{eq}
		MPa	MPa	MPa	mm
0.25	2	315.97	1676.74	58.44	175.85
0.50	4	315.97	1676.74	58.44	175.85
1.00	7	282.65	1489.10	56.31	182.51
1.50	10	271.71	1428.03	55.57	184.92
2.00	13	266.28	1397.78	55.20	186.17
2.50	16	263.03	1379.73	54.97	186.94
3.00	19	260.87	1367.73	54.82	187.45
3.50	22	259.33	1359.18	54.72	187.82
4.00	25	258.18	1352.78	54.63	188.10

Table 4.4 Displacements (mm) of node 1 for the SWP, predicted with SFEA and CFEA

SWP Aspect ratio	CFEA			SFEA		
mm	x	y	z	x	y	z
0.25	7.78	0.56	6.87	14.00	1.55	6.20
0.50	5.62	0.50	6.83	7.01	0.88	6.19
1.00	4.66	0.34	7.65	5.21	0.59	6.20
1.50	4.42	0.24	7.69	4.76	0.47	6.18
2.00	4.31	0.15	7.49	4.58	0.38	6.17
2.50	4.27	0.07	7.34	4.48	0.30	6.17
3.00	4.24	-0.02	7.29	4.43	0.24	6.18
3.50	4.24	-0.10	7.29	4.42	0.19	6.19
4.00	4.25	-0.18	7.30	4.34	0.15	6.08

Table 4.5 Maximum axial forces in the studs of the SWP from CFEA and SFEA

SWP Aspect ratio	CFEA			SFEA		
	Axial		Moment	Axial		Moment
mm	kN	kN	kN-mm	kN	kN	kN-mm
0.25	28.30	-37.18	903.62	32.51	-101.11	1716.81
0.50	27.57	-35.40	1001.38	34.52	-41.73	1151.63
1.00	22.56	-31.64	1092.84	23.39	-33.53	1160.44
1.50	20.02	-31.29	1151.67	21.38	-30.46	1157.63
2.00	17.95	-32.15	1197.59	18.09	-32.54	1155.16
2.50	16.01	-33.53	1221.19	15.40	-33.41	1152.76
3.00	14.15	-35.17	1230.24	14.59	-33.27	1151.05
3.50	12.36	-36.96	1229.16	13.48	-32.62	1149.51
4.00	10.64	-35.85	1224.37	17.64	-31.48	1255.51

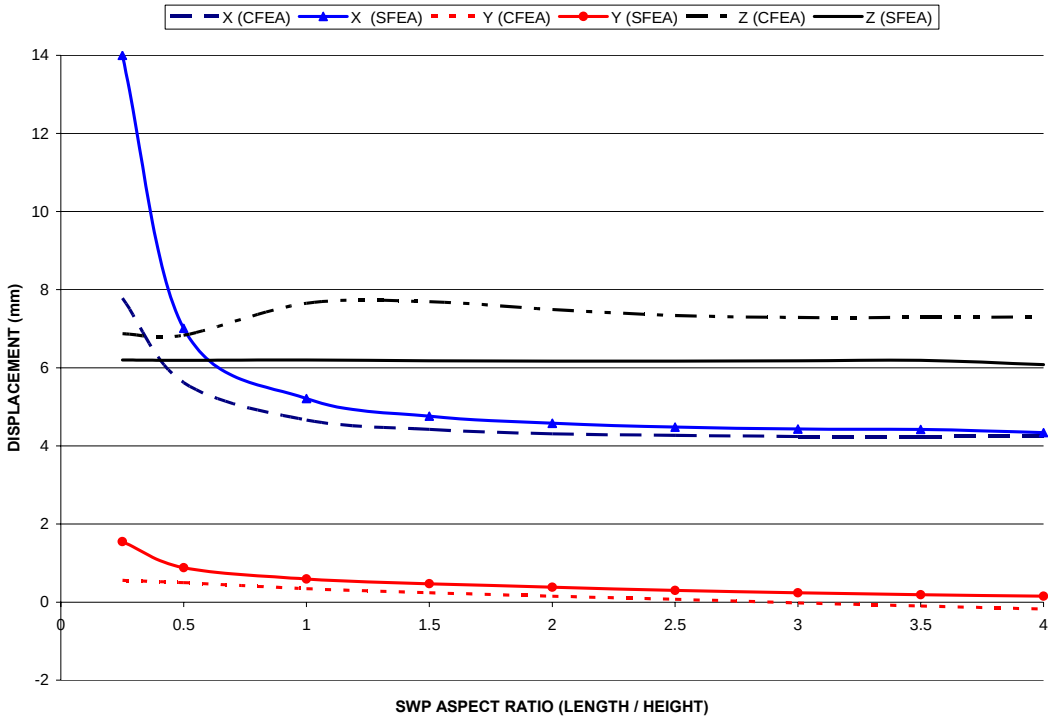

Figure 4.6. Displacement comparisons at node 1 with SFEA and CFEA

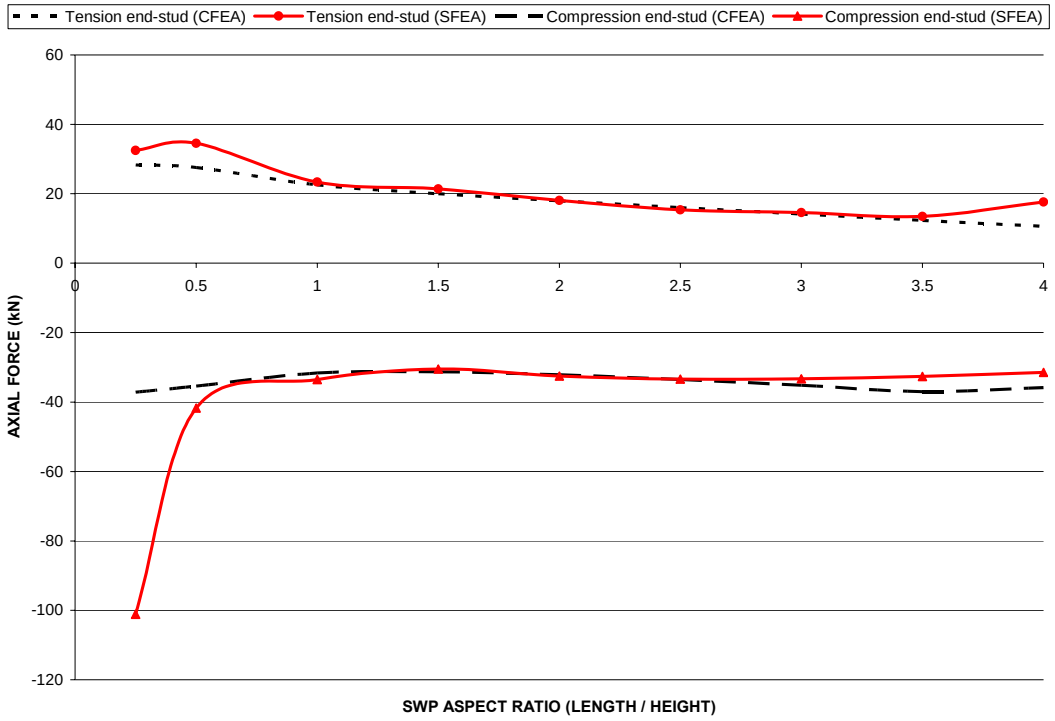

Figure 4.7. Maximum axial forces in the studs of the SWP

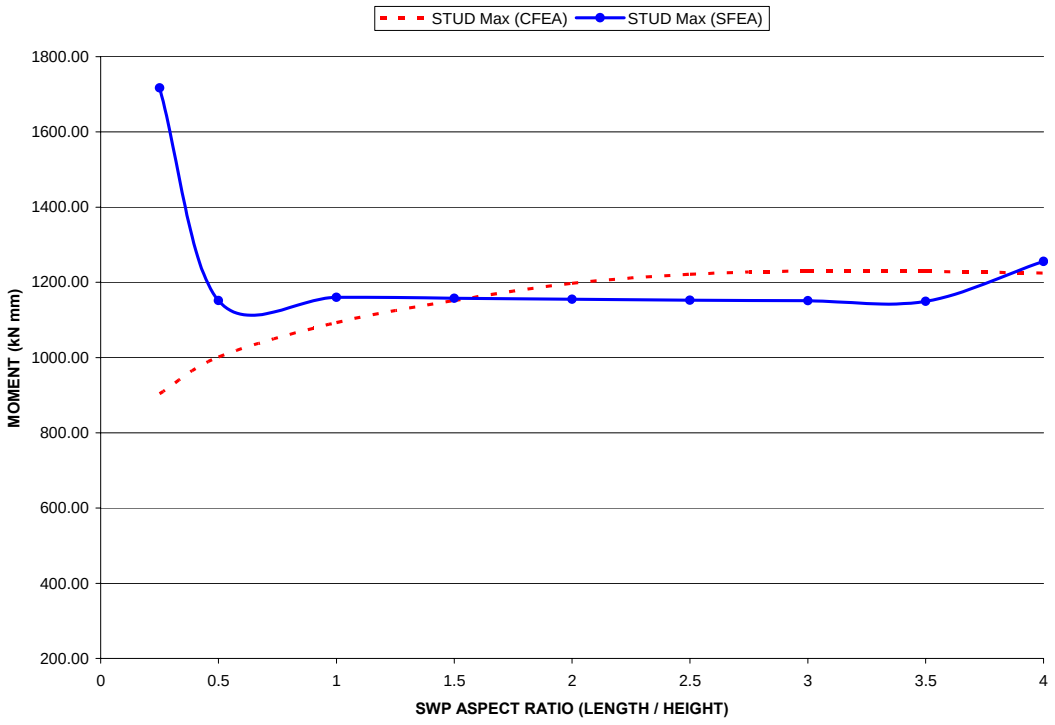

Figure 4.8. Maximum bending moment in studs of the SWP

Figure 4.6 indicates good agreement for the in-plane displacements of the SWP computed using SFEA and CFEA. However, the predicted out-of-plane displacements are different because, even though the sheathing is attached to the flange of the studs, SAP2000 (2006) models the shell and frame elements in the same plane, so that the offset of the sheathing from the centerline of the studs is not considered. Conversely, the equivalent shell elements consider the offset of the sheathing. In this case, however, the differences are not significant since the sheathing is relatively thin compared to the depth of the studs.

The predictions of the maximum axial force in the studs of the SWP are in good agreement, as shown in Figure 4.7, except for the studs of the SWP with an aspect ratio equal to 0.25. The predictions of the bending moments depicted in Figure 4.8 are acceptable, except for the two SWP with aspect ratio of 0.25 and 4.0, respectively; the error may be caused by the narrow shape of the shell elements in one direction, for which the cubic shape functions are not suitable. Therefore, based on the comparisons of the nine SWP, it is concluded that the SFEA model predicts reasonably accurate results when the aspect ratio for the equivalent shell elements is in the range of 0.5 to 3. For panels with aspect ratios outside of this range, it is recommended to use more than one equivalent shell element to model each panel.

In the analysis of the nine SWP, the loads were applied on the same four top nodes in both CFEA and SFEA models, leads to good agreement in the prediction of the axial forces. Typically, the CFEA model has a node on the top of each stud, whereas the SFEA model has only four nodes on the top of the SWP, regardless of the number of studs. To test how the accuracy of the analysis results is affected when uniformly distributed loads are applied on the top of the panel, the analysis of the nine SWP was carried out again. This time, the loads in the x and y directions are uniformly distributed on the top of the panel. Listed in Table 4.6 are the displacements and axial forces obtained from the CFEA. The displacements in the z direction and the maximum bending moments are not in Table 4.6 since they have the same magnitude as those presented in Table 4.4. The reason is that in both cases, the loads acting in the z direction are not applied on the nodes but on the face of each shell element.

Table 4.6 Displacements of node 1 and axial forces of the SWP, predicted with CFEA

SWP Aspect ratio	Displacements (mm)		Axial force (kN)	
mm	x	y	Tens	Com
0.25	7.78	0.59	28.28	-37.15
0.50	5.62	0.52	27.61	-35.32
1.00	4.66	0.41	23.17	-31.00
1.50	4.41	0.38	21.72	-29.55
2.00	4.30	0.37	21.08	-28.92
2.50	4.24	0.36	20.73	-28.58
3.00	4.20	0.36	20.52	-28.38
3.50	4.18	0.35	20.39	-28.25
4.00	4.16	0.35	20.29	-28.16

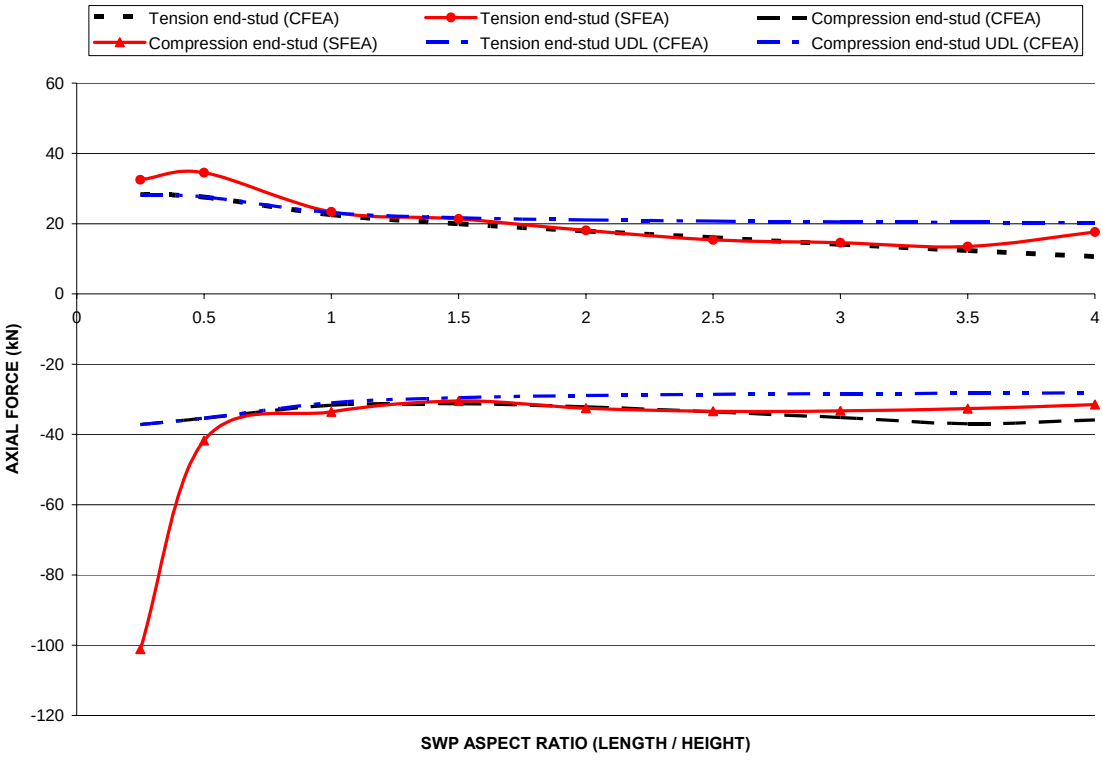

Figure 4.9. Maximum axial forces in the studs of the SWP

The displacements in the *x* and *y* direction in Tables 4.6 and 4.4 show a small difference that can be neglected. Shown in Figure 4.9 are the predicted axial forces in the studs listed in Table 4.6 and also the curves in Figure 4.7 in order to appreciate the difference in the predictions. Although the difference in the predicted axial forces for the SWP with concentrated loads and uniformly distributed load is not significant, the tendency is different. This means that in the modeling of a building, the aspect ratio of the shell elements may affect the prediction of the axial forces in the studs due to the different distribution of the loads in the equivalent shell elements.

4.6. Stiffness Degradation Model for SWP

Experimental investigations, such reported by COLA-UCI (2001), Fulop and Dubina (2004), NAHBRC (1997), and Branston et al. (2004, 2006), have shown that the load-displacement relationship for SWP is nonlinear. In addition, it is observed in the aforementioned experimental investigations that the loss of stiffness and the failure of SWP is primarily due to looseness of the sheathing-to-framing connections. Therefore, the nonlinear relationship between load and displacement of SWP needs to be accounted for in the finite element model of analysis.

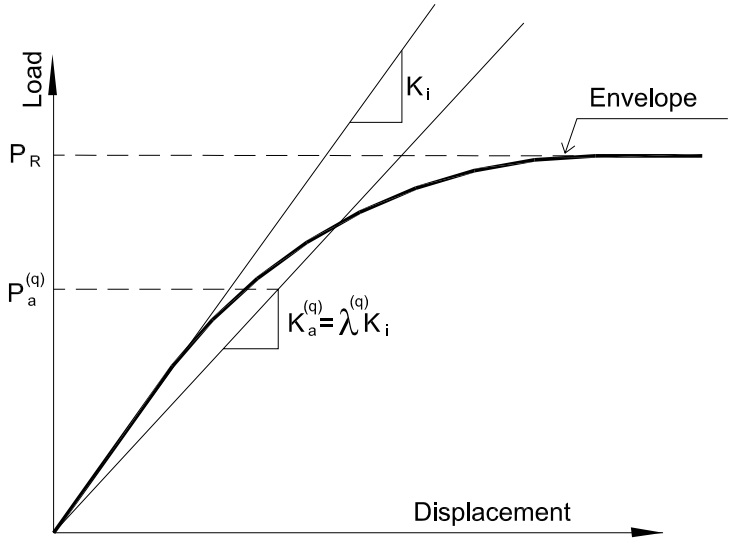

Figure 4.10. Characterization of the SWP loss in strength

Shown in Figure 4.10 is the proposed nonlinear model to characterize the stiffness degradation of SWP subjected to lateral forces: K_i is the initial stiffness of the SWP, tangent to $P_r = 0$, and is computed with SFEA using the equations in Section 4.2; $K_a^{(q)}$ is the secant stiffness corresponding to the load increment, q; P_R is the lateral strength of the SWP, computed using the method described in Chapter 3 (P_R can also be obtained from experimental investigations or design tables, such as AISI (2004)); P_a is the magnitude of the total lateral force applied on the top of the panel at load increment q; $\lambda^{(q)}$ is the stiffness degradation coefficient that characterizes the nonlinear behaviour of the SWP under the applied lateral forces until failure, and is defined by,

$$\lambda^{(q)} = 1 - \left(\frac{P_a^{(q)}}{P_R} \right)^{\beta} \qquad \textbf{(4. 52)}$$

where $\beta=(1.5\ in/s_C)$ is a stiffness degradation nonlinearity exponent, calibrated in accordance with experimental results from Branston et al. (2004) and COLA-UCI (2001). Described in the Appendix C is the calibration of β. It is observed from the results of the experimental investigations that the nonlinear load-displacement relationship for a SWP is primarily influenced by the sheathing material and edge screw spacing; for reasons of simplicity, in this study β was calibrated considering the screw spacing only.

When the stiffness degradation coefficient is computed, using Eq. (4.52), $\lambda^{(q)}$ is equal to unity at the initial load increment, which indicates that the SWP lateral stiffness has not yet been affected. When the applied load P_a is equal or greater than the maximum strength P_R, $\lambda^{(q)}$ becomes zero. This indicates that the SWP has completely lost its stiffness to resist lateral deformation induced by the applied lateral loads. However, the modulus of elasticity of the CFS studs remains unchanged in the y direction of the shell element, which means the equivalent shell may still have sufficient stiffness contributed by the studs to allow the SWP to continue to carry vertical loads.

Having the stiffness degradation coefficient $\lambda^{(q)}$ calculated at load increment q, the degraded stiffness of the SWP for the next load increment of the analysis is calculated by first multiplying the modulus of elasticity of the sheathing by $\lambda^{(q)}$. Then, the reduced

modulus of elasticity is used to calculate the modulus of elasticity of the equivalent shell element in accordance with the method described in Section 4.2. Afterwards, the constitutive matrix for the sixteen-node shell element is formed using Eq. (4.43).

4.7. Prediction of the Nonlinear Response of SWP Subjected to Lateral Loading.

Experimental results for single SWP, such as from Branston et al. (2004), NAHBRC (1997) and COLA-UCI (2001), are used to validate the accuracy of the proposed method for the analysis of SWP. The accuracy of the predicted response is generally correlated with the material properties and the geometric dimensions of the components. As not all properties are reported in the foregoing literature, the material properties adopted in the evaluation may not match with those of the tested materials. In this study, the geometric gross properties of the steel studs are computed for each case, and the material properties of the sheathing and steel being used in the calculations are defined in each case.

Branston et al. (2004) conducted a series of experimental investigations of SWP with different sheathing materials. Shown in Figures 4.11 to 4.16 are predicted and experimental force-displacement curves for the SWP tested by Branston et al. (2004). The predicted force-displacement curves were obtained using the SFEA and stiffness degradation models proposed by this study in the foregoing. The sheathing materials investigated were 11 mm (7/16 in) OSB, and 12.5 mm (1/2 in) DFP, fastened on one side of the panel with No. 8 screws (diameter = 4.06 mm) spaced every 305 mm (12 in) in the field. The screw spacing at the edge of the SWP is indicated at the foot of each figure. The same 92S41-1.12 mm (362S162-44 mils) C-shape CFS studs were used for all the SWP test specimens. The studs were spaced 610 mm (24 in) on centre, and double back-to-back C-shape studs were placed at the ends of the panel. Three edge screw spacings (s_C) of 76 mm (3 in), 102 mm (4 in) and 152 mm (6 in) were investigated. The tested SWP were 2438 mm (8 ft) in height and 1219 mm (4 ft) in length.

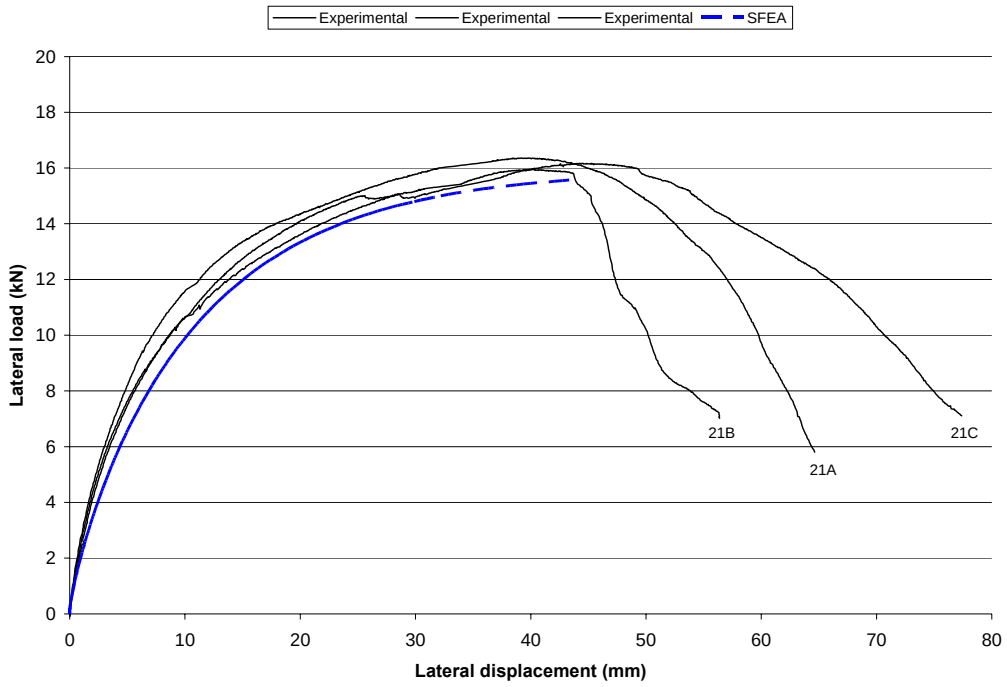

Figure 4.11. Predicted vs. experimental (Branston et al., 2004) curves of OSB SWP (s_C = 152mm)

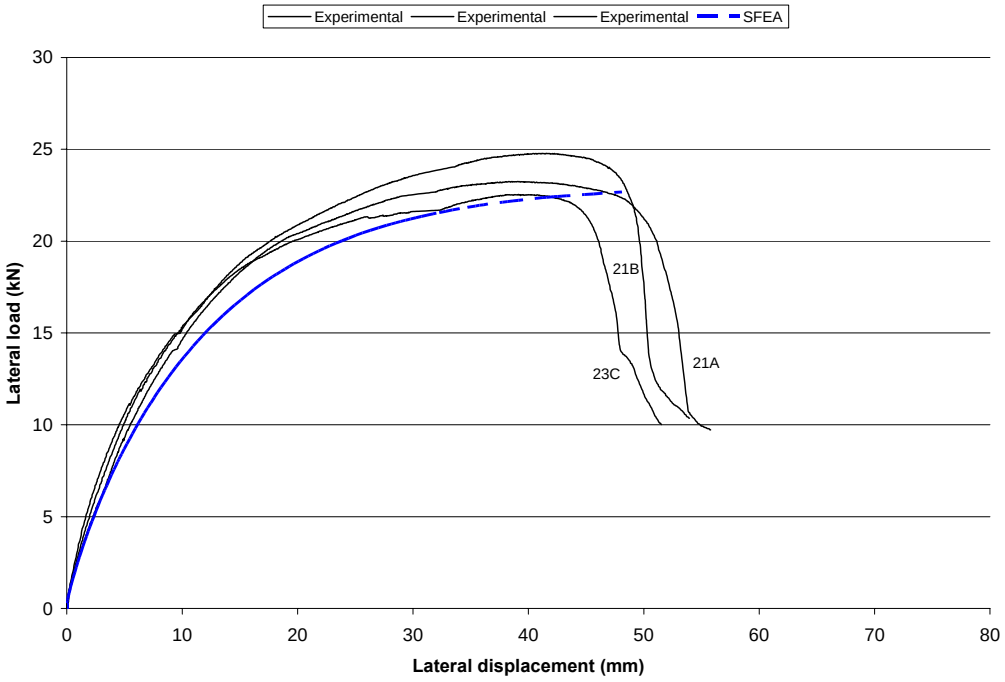

Figure 4.12. Predicted vs. experimental (Branston et al., 2004) curves of OSB SWP (s_C = 102mm)

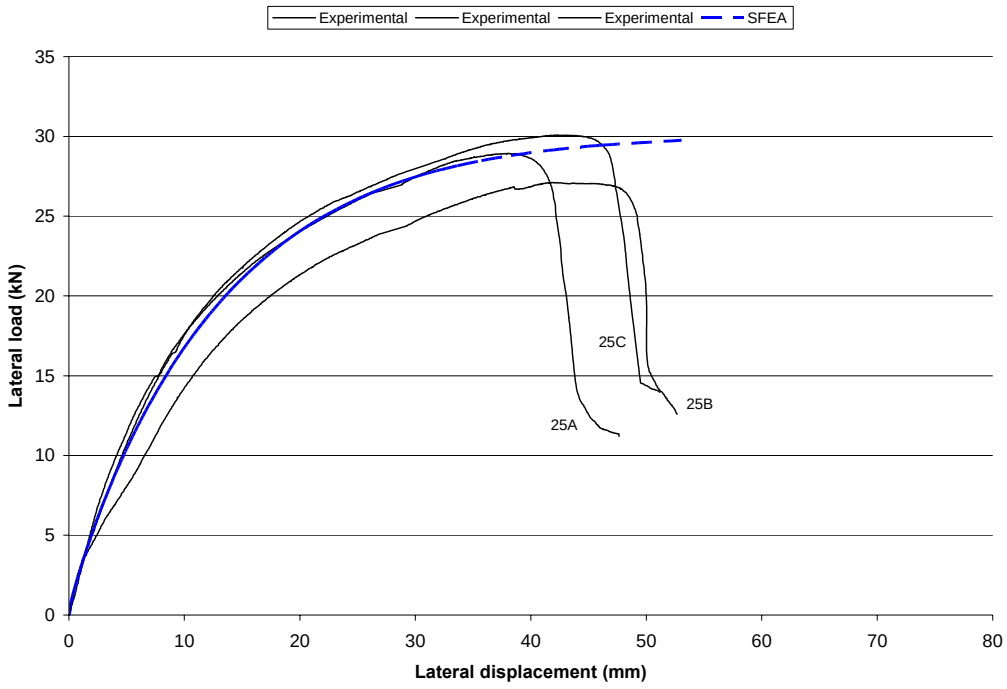

Figure 4.13. Predicted vs. experimental (Branston et al., 2004) curves of OSB SWP (s_C = 76 mm)

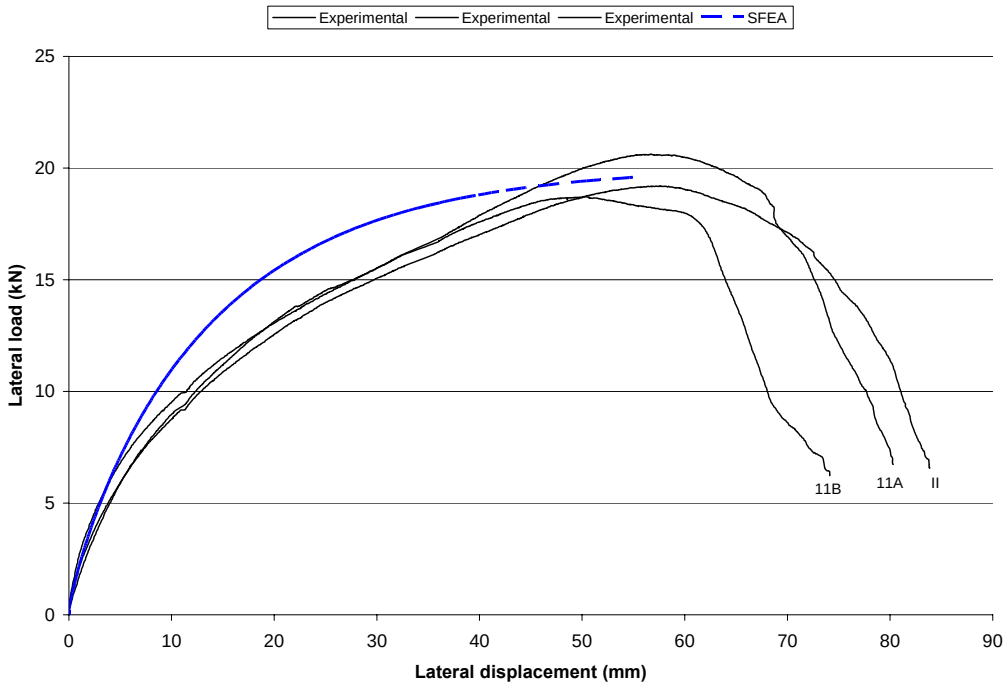

Figure 4.14. Predicted vs. experimental (Branston et al., 2004) curves of DFP SWP (s_C = 152mm)

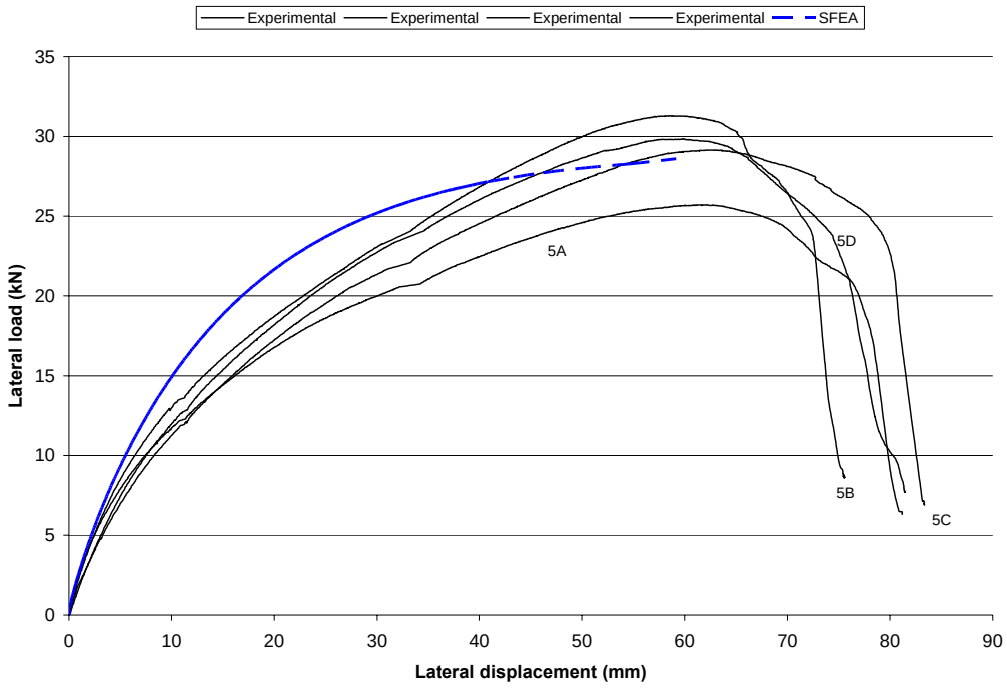

Figure 4.15. Predicted vs. experimental (Branston et al., 2004) curves of DFP SWP (s_C = 102mm)

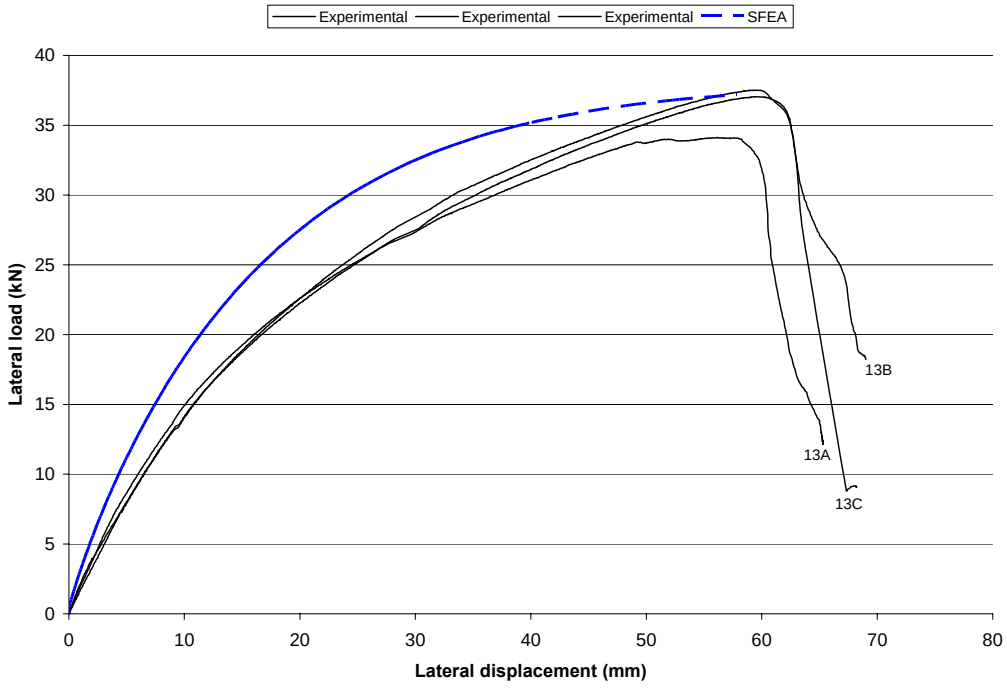

Figure 4.16. Predicted vs. experimental (Branston et al., 2004) curves of DFP SWP (s_C = 76 mm)

The National Association of Home Builders Research Center (NAHBRC, 1997) published a report that presents experimental results for long shear wall panels that are 12190mm (40 ft) in length and 2438mm (8ft) in height. Figure 4.17 presents a comparison of the experimental results with those predicted herein for the force-displacement curve of a long SWP without openings. NAHBRC (1997) does not specify the dimensions of the studs, but it states that "The wall framing is consistent with usual construction practices." Therefore, 92S41-1.12 mm (362S162-44mils) C-shape CFS studs were assumed in this comparison. OSB sheathing of 11.11 mm (7/16 in) thickness was fastened on one side of the SWP using No. 8 screws spaced at 305 mm (12in) in the field and at 152mm (6in) at the edge of the panel. GWB of 12.7 mm (1/2 in) thickness was fastened on the other side of the SWP using No. 6 screws spaced at 254 mm (10 in) in the field and at 178 mm (7 in) at the edge.

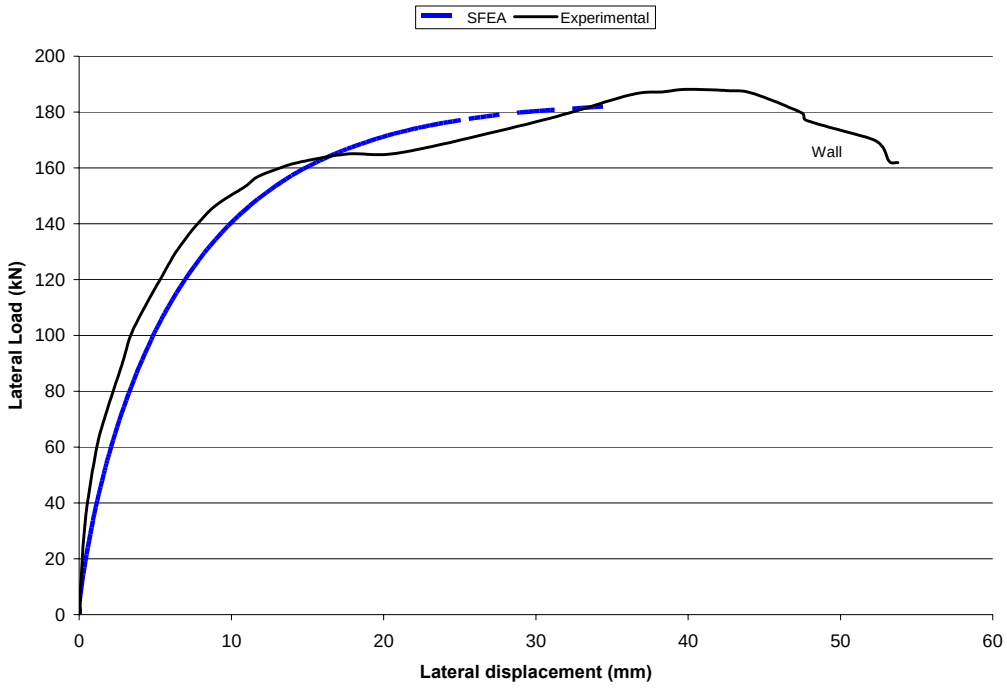

Figure 4.17. Predicted vs. experimental (NAHBRC, 1997) curves of a 40 ft OSB SWP (s_C = 152mm)

Plotted in Figures 4.18 to 4.20 are comparisons of experimental versus predicted force-displacement curves for SWP with different characteristics. The experimental curves were obtained from investigations carried out by COLA-UCI (2001). The three SWP that

are compared have the same dimensions: 2438 mm (8 ft) in length and 2438 mm (8 ft) in height. The studs used in the test were 89S41-0.86 mm (350S162-33mils) spaced 610 mm (24 in) on centre; double end-studs were used. The sheathing used in the comparisons, presented in Figures 4.10 and 4.19, was 4-ply Structural I Rated (STR) of 11.91mm (15/32 in) thickness. The sheathing was fastened to the framing on one side only with No. 8 screws spaced 305 mm (12 in) in the field and either 152 mm (6 in) or 51 mm (2 in) at the edge. The SWP, corresponding to Figure 4.20, had the same characteristics as the SWP corresponding to Figure 4.18, except that the sheathing material used for the test in Figure 4.20 was OSB of 11.11 mm (7/16 in) thickness.

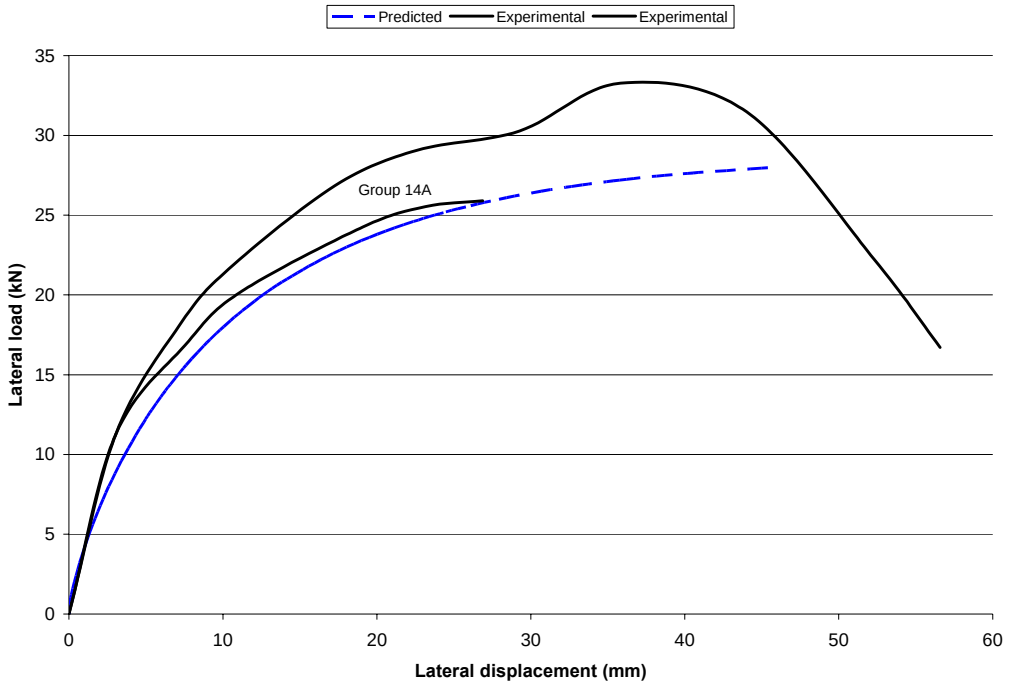

Figure 4.18. Prediction vs. experimental (COLA-UCI, 2001) curves of STR SWP (s_C = 152mm)

The following material properties were used for SFEA of the SWP. The shear modulus of elasticity for STR was 8490 MPA (COMPLY, 1999), whereas for OSB and DFP it was 925 MPa and 825 MPa (Okasha, 2004), respectively. The modulus of elasticity associated with STR, OSB, and DFP were 675 MPa (COMPLY, 1999), 9917MPa (OSB, 1995), and 10445 MPa (CANPLY, 2003), respectively. For GWB, the Young and shear modulus of

elasticity were 1290 MPa (GA-235, 2002) and 561 MPa, respectively. Furthermore, the yielding strength of the studs for all the calculations was 230 MPa.

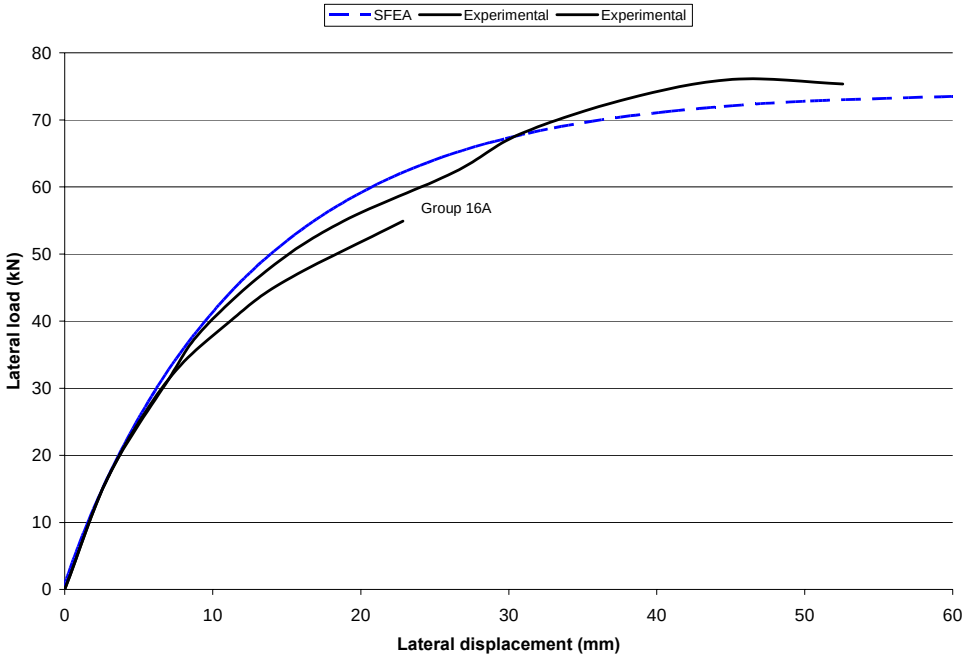

Figure 4.19. Predictied vs. experimental (COLA-UCI, 2001) curves of STR SWP (s_C = 51mm)

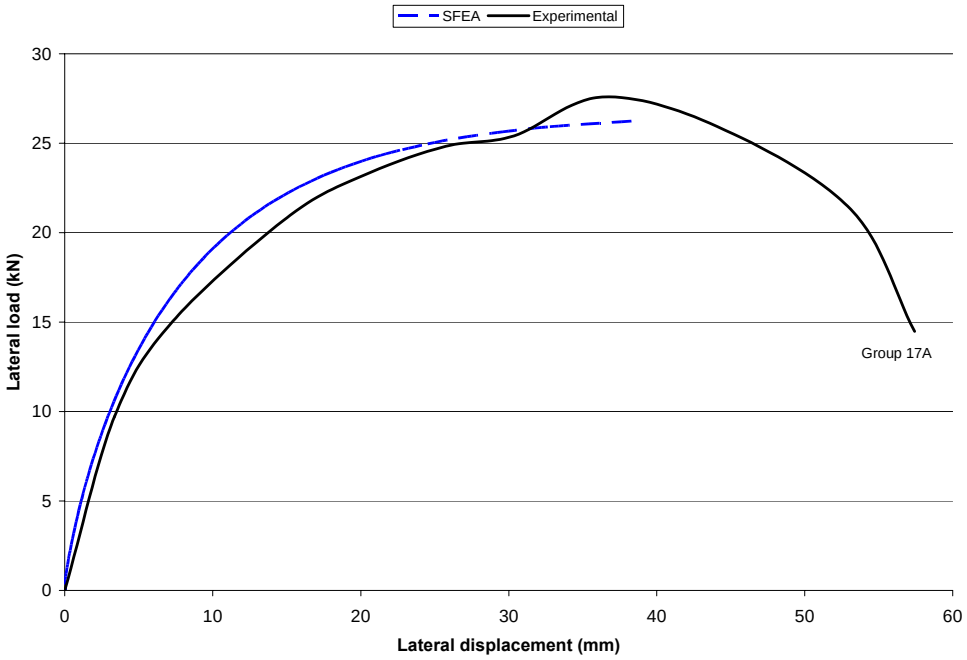

Figure 4.20. Prediction vs experimental (COLA-UCI, 2001) curves of OSB SWP (s_C = 152mm)

The comparisons in this section are for SWP having different characteristics and properties, such as different type of sheathing, length, screw spacing and so on. The force-displacement curves for the SWP were obtained experimentally from the different researchers mentioned. The predicted force-displacement curve was obtained using SFEA and the stiffness degradation model proposed in this chapter. In general, the predictions are in good agreement with the experimental results for all the SWP. However, the difference in the shapes of the predicted and experimental curves for DFP is evident. The shape of the curve is significantly affected by the factor β (nonlinearity exponent), included in the stiffness degradation model defined in Eq. (4.52). For simplicity, the stiffness degradation model was calibrated without accounting for the type of sheathing material, thus it may be more appropriate for some type of sheathing materials than for others. Another factor that significantly affects the prediction of the force-displacement curve is the lateral strength of the SWP that establishes the failure load, which is the highest point in the force-displacement response curve. Therefore, the accuracy in the lateral strength calculation also affects the prediction of the nonlinear behaviour of SWP.

Chapter 5

Pushover Analysis for Performance-Based Design Assessment of CFS Buildings

5.1. Introduction

The purpose of the Performance-Based Design (PBD) is to design buildings that satisfy the performance objectives specified by the designer and the governing code(s) of practice. The application of PBD assessment does not follow a fixed procedure, however, nor is it the same procedure for all structural systems, since it depends on the building characteristics and designer's preferences. For instance, several methods for carrying out the seismic assessment of buildings for PBD are available in the literature, such as those discussed in Section 2.2. The complexity of the application of each method is different and so are their capabilities; as a result, some of the methods might not be suitable for analyzing certain types of structures. The linear methods, particularly, have limited applications as they can produce incorrect results when used to analyze structures having a nonlinear response. From the methods discussed in Section 2.2, the nonlinear static procedure, better known as pushover analysis, is selected in this study for conducting the PBD assessment of CFS buildings. Pushover analysis is simpler than dynamic analysis; yet, accurate results can be obtained for structures with a predominant first mode of vibration (Krawinkler and Seneviratna, 1998). For the medium height and relatively high lateral stiffness of low and mid-rise CFS buildings, the framework structures are expected to have a predominant first mode of vibration. Therefore, reasonably correct results can be expected from pushover analysis of cold-formed steel (CFS) buildings.

A performance objective involves the combination of a seismic hazard and a performance level. The seismic hazards are represented by site spectra, which are determined from a geotechnical study of the site or from seismic maps, provided by FEMA 450 (2003) and USGS (2002). Typically, geotechnical studies are costly, and so, for conventional

structures, seismic maps are preferred. A performance level is a measure of the maximum damage that a building is allowed to undergo, where the level of damage is associated with the cost of the building.

PBD assessment involves transforming each selected performance objective, to be satisfied by the structure, into a tangible parameter that can be characterized in a seismic analysis. This study adopts a spectrum-based pushover analysis approach, also known as the force-based approach, in which the performance objectives are transformed into target base shears. From the maximum target base shear, the overall lateral load that the building is going to be subjected to can be determined. When the lateral loads applied on the building are equal to the target base shear for any one of the governing performance objectives, the shear wall panels (SWP) are checked to determine if they comply with the acceptance criteria corresponding to that performance level. In this chapter, the procedure for carrying out the PBD assessment of CFS buildings is described.

The equations to transform the performance objectives into spectral accelerations, and then into target base shears are described in Sections 5.2 and 5.3, respectively. In Section 5.4, the limit lateral drifts defining the acceptance criteria for the SWP are identified, and the limit drift ratios are obtained for each performance level. In Section 5.5 the procedure for carrying out the PBD assessment of CFS buildings is presented, and in Section 5.6 a computer program created for this study is described.

5.2. Spectrum-Based PBD Assessment of CFS Buildings

In this thesis, the spectrum-based approach is preferred over the displacement-based approach for the PBD assessment of CFS buildings. Typically, such design is carried out by using design spectra from seismic codes. The design spectra are used to compute the target base shears employed to calculate the pattern of lateral loads applied on the building. Conversely, if the displacement-based approach is chosen for carrying out the PBD assessment of a building, lateral displacement is used as a target parameter. In this approach, arbitrary lateral load increments or lateral displacements are applied on the

building, until the target displacement is reached or until the structure collapse occurs. Then, with the total load applied on the building during the analysis, the acceleration is computed and compared with the site design spectra to determine if the building satisfies the site requirements. In this approach, the designer does not know whether the building satisfies the site requirements until the analysis is complete. This can lead to unnecessary load or displacement increments. On the other hand, the spectrum-based approach is directly consistent with the seismic codes. A discussion on the advantages and disadvantages of both approaches is available in the literature (Grierson et al., 2006). Although Grierson et al. (2006) focus their discussion on steel frameworks, the principles of PBD assessment also apply to CFS buildings.

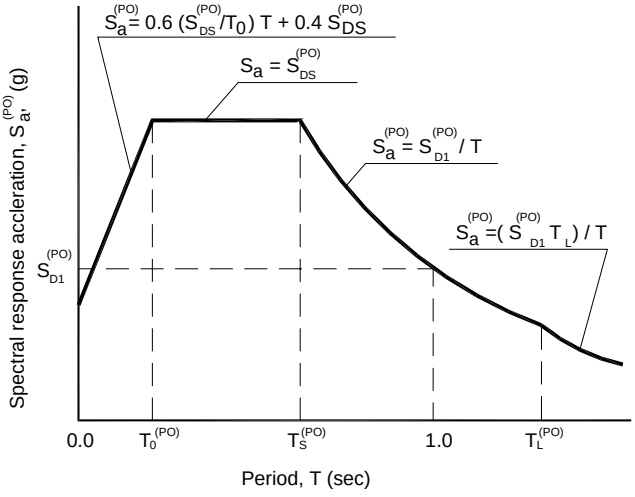

Figure 5.1. General response spectrum (FEMA 450, 2003)

For spectrum-based PBD assessment, each performance objective is associated with a particular design earthquake. The corresponding base shear is adopted as the damage target parameter, which represents the maximum base shear that a building can undergo during that earthquake. The target base shear for a building is computed as a function of the spectral acceleration (S_a), structural seismic weight (W), and gravity acceleration constant (g) for each selected performance objective as follows: For each of multiple performance objectives possible for a building (see Table 2.1), the base shear is computed by the following expression:

$$V_b^{PO} = S_a^{PO} \frac{W}{g} \qquad \textbf{(5.1)}$$

Figure 5.1 signifies a general response spectrum provided by FEMA 450 (2003), in which the spectral acceleration is given as a function of the earthquake hazard associated with the performance objective under consideration, and is defined by the following equations:

$$S_a^{PO} = 0.60\frac{S_{DS}^{PO}}{T_0^{PO}}T + 0.4S_{DS}^{PO} \quad \text{for} \quad T \le T_0^{PO} \qquad \textbf{(5.2 a)}$$

$$S_a^{PO} = S_{DS}^{PO} \quad \text{for} \quad T_0^{PO} \le T \le T_S^{PO} \qquad \textbf{(5. 2 b)}$$

$$S_a^{PO} = \frac{S_{D1}^{PO}}{T} \quad \text{for} \quad T_S^{PO} \le T \le T_L \qquad \textbf{(5. 2 c)}$$

$$S_a^{PO} = \frac{S_{D1}^{PO}T_L}{T^2} \quad \text{for} \quad T > T_L \qquad \textbf{(5. 2 d)}$$

where T is the fundamental period of the structure, which can be found by computing the eigenvalues of the building or by using the simplified method described in Appendix A. The parameter T_L is the ground long-period transition period, provided in regional hazard seismic maps by FEMA 450 (2003). Finally, the parameters T_S^{PO} and T_0^{PO} are the ground characteristic period and a fraction of the ground characteristic period, respectively; both are shown in Figure 5.1, and computed using the following expressions:

$$T_S^{PO} = \frac{S_{D1}^{PO}}{S_{DS}^{PO}} \qquad \textbf{(5. 3)}$$

$$T_0^{PO} = 0.2T_S^{PO} \qquad \textbf{(5.4)}$$

where S_{DS}^{PO} and S_{D1}^{PO} are the design acceleration parameters, expressed as,

$$S_{DS}^{PO} = \frac{2}{3}S_{MS}^{PO} \qquad \textbf{(5.5)}$$

$$S_{D1}^{PO} = \frac{2}{3}S_{M1}^{PO} \qquad \textbf{(5. 6)}$$

in which S_{MS}^{PO} and S_{M1}^{PO} are the spectral response accelerations parameters for a short period (0.2 second) and one second period, respectively, given by,

$$S_{MS}^{PO} = F_a^{PO}S_S^{PO} \qquad \textbf{(5. 7)}$$

$$S_{M1}^{PO} = F_v^{PO} S_1^{PO} \quad \textbf{(5. 8)}$$

where F_a and F_v are factors to adjust the spectral acceleration in the short-period range and one- second period range, respectively, for the site class, and are found from Tables 5.2 and 5.3 (FEMA 450, 1997). The site class is defined as A, B, C, D, E, and F for hard rock, rock, very dense soil and soft rock, stiff soil, soft soil, and soils requiring site-specific evaluations, respectively. S_S^{PO} and S_1^{PO} are the site response acceleration parameters corresponding to a short period and a one-second period, respectively, for a structure with 5% damping. These parameters are obtained from regional seismic hazard maps such as FEMA 450 (2003) and USGS (2002). However, these documents provide response acceleration parameters for earthquakes having only 2% and 10% probability of exceedance in a fifty-year period. The response acceleration parameters for earthquakes with 20% and 50% probability of exceedance in a fifty-year period are computed by using equations provided by FEMA 273 (1997). Table 5.1 provides sample values of S_S and S_1 for two locations in California and Nevada, USA (Gong, 2003).

Once the target base shears for a building are computed, based on the selected performance objectives, the distribution of the lateral loads applied on the building are computed by the equations described in the next section.

Table 5.1. Performance objective site parameters, Gong (2003)

Site Location	Performance Level	Earthquake Level[a]	S_s (g)	S_1 (g)
Latitude 36.9°N, Longitud 120°W	OP	50% / 50	0.126	0.061
	IO	20% / 50	0.209	0.100
	LS	10% / 50	0.290	0.140
	CP	2% / 50	0.500	0.230
Latitude 41°N, Longitud 115.2°W	OP	50% / 50	0.109	0.035
	IO	20% / 50	0.180	0.058
	LS	10% / 50	0.250	0.080
	CP	2% / 50	1.100	0.410

[a] Eccedance probability / years

Table 5.2. Values of F_a as a function of the Site Class and Mapped Short-Period Maximum considered earthquake spectral acceleration, *FEMA 450 (2003)*

Site Class	Mapped Maximum Considered Earthquake Spectral Response Acceleration at Short Periods				
	$S_s \leq 0.25$	$S_s = 0.50$	$S_s = 0.75$	$S_s = 1.00$	$S_s \geq 1.25$
A	0.8	0.8	0.8	0.8	0.8
B	1.0	1.0	1.0	1.0	1.0
C	1.2	1.2	1.1	1.0	1.0
D	1.6	1.4	1.2	1.1	1.0
E	2.5	1.7	1.2	0.9	0.9
F	a	a	a	a	a

NOTE: Use linear interpolation for intermediate values of S_s.

[a] Site-specific geotechnical investigation and dynamic site response analyses shall be performed.

Table 5.3. Values of F_v as a Function of the Site Class and Mapped 1 Second Period Maximum considered earthquake spectral acceleration, *FEMA 450 (2003)*

Site Class	Mapped Maximum Considered Earthquake Spectral Response Acceleration at Short Periods				
	$S_s \leq 0.10$	$S_s = 0.20$	$S_s = 0.30$	$S_s = 0.40$	$S_s \geq 0.50$
A	0.8	0.8	0.8	0.8	0.8
B	1.0	1.0	1.0	1.0	1.0
C	1.7	1.6	1.5	1.4	1.3
D	2.4	2.0	1.8	1.6	1.5
E	3.5	3.2	2.8	2.4	2.4
F	a	a	a	a	A

NOTE: Use linear interpolation for the intermediate values of S_1.

[a] Site-specific geotechnical investigation and dynamic site response analyses shall be performed.

5.3. Spectrum-Based Pushover Analysis for CFS Buildings.

For the PBD assessment of CFS buildings, a pushover analysis is employed to carry out the seismic analysis for reasons of practicality. In the spectrum-based pushover analysis, adopted in this study, the building is subjected to incrementally applied lateral loads, until the target base shear is reached or the structure collapses. Throughout this analysis

process, the gravity loads are maintained constant on the building. Upon applying a lateral load increment on the structure, the structural analysis is carried out by using a suitable method for the type of structure under consideration. In this study, the structural analysis is performed by using the finite element method, presented in Chapter 4, with account for both geometric and material nonlinearities of the elements. From the structural analysis results, the incremental nodal displacements are obtained, and then the accumulated total displacements up to the current stage of the loading process are found.

The maximum base shear computed for the selected performance objective by Eq. (5.1) is expressed as,

$$V_{b\max} = \max\left[V_b^{PO}\right] \tag{5. 9}$$

The lateral load increments are applied on the building until V_{bmax} is reached or the structure collapses. Each load increment is a small portion of V_{bmax}, and selecting the appropriate size for the lateral load increment is important to obtain the correct analysis results. If the size of the selected load increment is excessively small, the program used in the calculations might not be able to handle the required precision, causing incorrect results. On the contrary, if the size of the load increment is excessively large, the response curve from the analysis can be in significant error relative to the correct curve. In order to achieve correct results, the size of the load increment is varied depending on the type of structure. For example, Grierson et al. (2005) have applied a 5% increment of the total lateral loads for analysis of steel frameworks. To determine the appropriate size of the load increment for CFS buildings, the OSB shear wall panel analyzed in Section 4.7, and presented in Figure 4.10, is analyzed by varying the size of the load increment to be, 10%, 3.5%, 2%, 1% and 0.5% of the total seismic load. Figure 5.2 exhibits the response curves for the different sizes of the load increments. It is noted that the difference in the response for the load increments ranging from of 0.5% to 3.5% is not significant. Moreover, the curves for the load increments of 1% and 0.5% are almost the same. Therefore, in this thesis a 1% load increments are used for the pushover analysis.

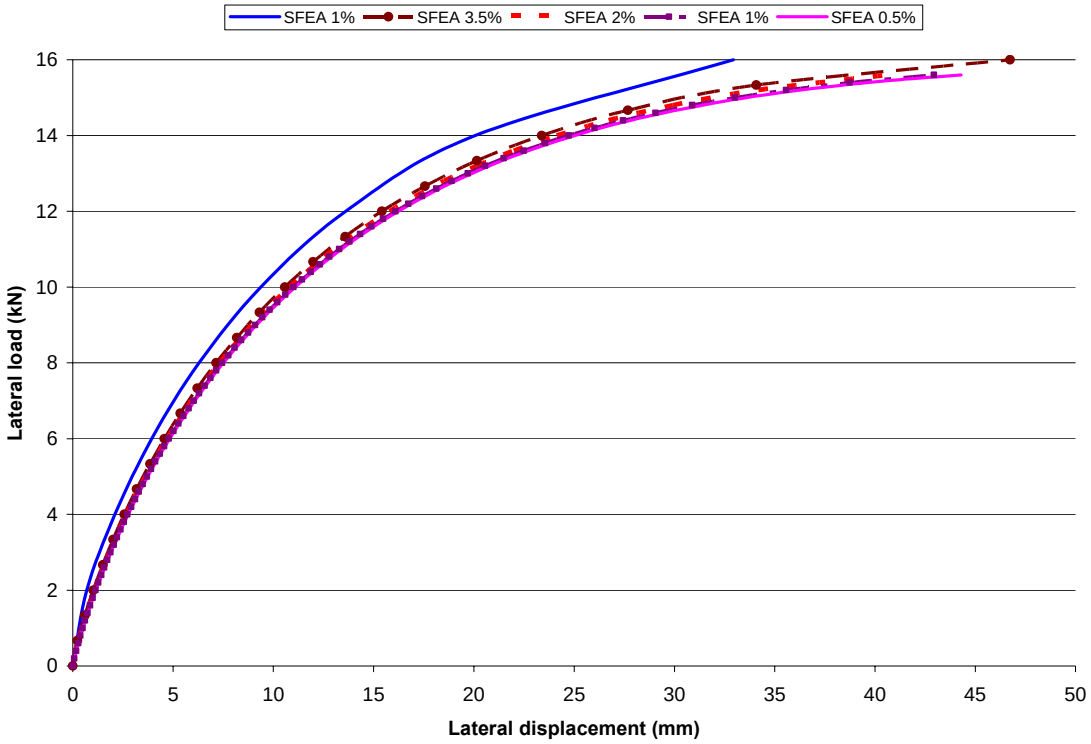

Figure 5.2. Sensitivity tests of the response curve for different sizes of lateral load increments.

The seismic loads are distributed over a building's height with a pre-defined profile, determined as,

$$F_x = C_{vx} V_{b\ \max} \qquad \textbf{(5. 10)}$$

where F_x is the lateral seismic load to be applied on the building, at height x from the building base. C_{vx} is the lateral load distribution coefficient which represents the lateral load pattern (FEMA 273, 1997) such that,

$$C_{vx} = \frac{w_x h_x^{\kappa}}{\sum_{z=1}^{n_t} w_z h_z^{\kappa}} \qquad \textbf{(5. 11)}$$

where w_z and w_x are portions of the total seismic weight of the structure, corresponding to storey levels z and x, respectively; h_z and h_x are the height from the building base to storey levels z and x, respectively; and n_t is the number of storeys in the building. The exponent κ is a function of the structure fundamental period T; for structures with T≤

0.5sec κ=1, and for structures with T≥ 2.5sec κ=2. For the intermediate values of T, a linear interpolation is used to find κ. Note that the coefficients C_{vx} found from Eq. (5.11) over all n_t storeys satisfy the condition,

$$\sum_{z=1}^{n_t} C_{vx,z} = 1 \qquad \textbf{(5. 12)}$$

In the PBD assessment of a CFS building, the acceptance criteria of the shear wall panels (SWP) are checked when the base shear of the building is equal to the target base shear for any selected performance objective, V_b^{PO}. Thus, if the structural elements satisfy the deformation and strength requirements, the acceptance criteria for the specified performance objective are satisfied.

5.4. Performance Acceptance Criteria for CFS Buildings

The acceptance criteria determine if a building is properly designed to satisfy the demands imposed by the seismic hazards. The acceptance criteria limit the damage that the elements in a building are allowed to undergo, and are expressed in terms of strength, displacement, deformations, stresses, and so on. In PBD assessment, the acceptance criteria are given as a function of the performance levels. If FEMA criteria (FEMA 273, 1997) are adopted, as herein, the damage in the building goes from low to high for the OP, IO, LS and CP performance levels, respectively.

In CFS buildings, the SWP's are the primary structural elements in resisting the lateral loads. Consequently, acceptance criteria based on SWP lateral drift is established. However, the strength of each SWP also needs to be checked to prevent premature failure prior to reaching the limit drift. In some cases, the lateral drift of a SWP might be less than the limit value but the applied lateral loads exceed the SWP strength, or vice versa. Therefore, both the lateral drift and strength of the SWP need to be checked to determine if the panel has been designed appropriately.

FEMA 273 (1997) provides acceptance criteria defined by "limit" drift ratios for different types of lateral-load resisting structural systems such as steel frameworks, concrete walls, masonry walls, and wooden stud walls. In Chapter 8 of FEMA 273 (1997), the magnitudes of the limit drift ratios are associated with three performance levels for several types of SWP. For instance, the limit drift ratios for SWP with plywood sheathing and wood framing are 1.4%, 2.6%, and 3.0% for the IO, LS, and CP performance levels, respectively.

Chapter 2 of FEMA 273 (1997) includes descriptions of the expected damages and corresponding limit drift ratios for different structural systems corresponding to the OP, IO, LS and CP performance levels. Typically, these limit drift ratios are adopted to establish the target displacements, which are likely to be experienced by a structure in a seismic event. These ratios have been used in different studies (Hassan et al., 2002; and Filiatrault and Folz, 2002) to calculate the target displacements for displacement-based pushover analysis. For SWP with wood framing, the limit drift ratios are 3%, 2% and 1% for the CP, LS and IO performance levels, respectively (FEMA 273, 1997). However, no such limit drift ratios, neither as acceptance criteria nor for estimating target displacements, are provided for CFS SWP.

Although wood and CFS shear wall panels are built in a similar fashion, their force-displacement curves are not similar, and so the limit drift ratios for wood-framed SWP cannot be used for CFS-framed SWP. Although there is no evidence of studies in the literature where the behaviour of SWP with wood and steel framing is compared. SEAOC and COLA-UCI (2001) have carried out extensive testing of SWP with wood and steel framing under the same testing conditions. Shown in Figure 5.3 is the superposition of the cycling test curves of SWP with wood and steel framing with structural sheathing (STR 1) and two different edge screw spacings. The curves show that the wood-framed SWP has greater ductility and smaller strength, and therefore, that limit drift values for wood SWP are not suitable for modelling CFS SWP. Instead, in this thesis, the limit drift ratios for CFS shear walls are estimated from experimental data (Branston et al., 2006).

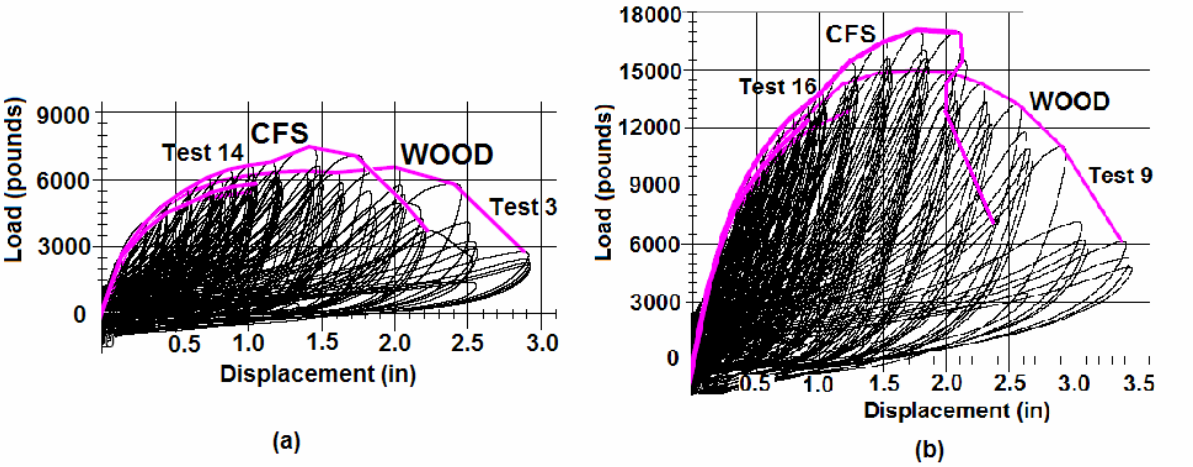

Figure 5.3. Comparison of the behaviour of SWP with wood and CFS framing for different edge screw spacing: (a) 152mm and (b) 51mm (SEAOC and COLA-UCI, 2001)

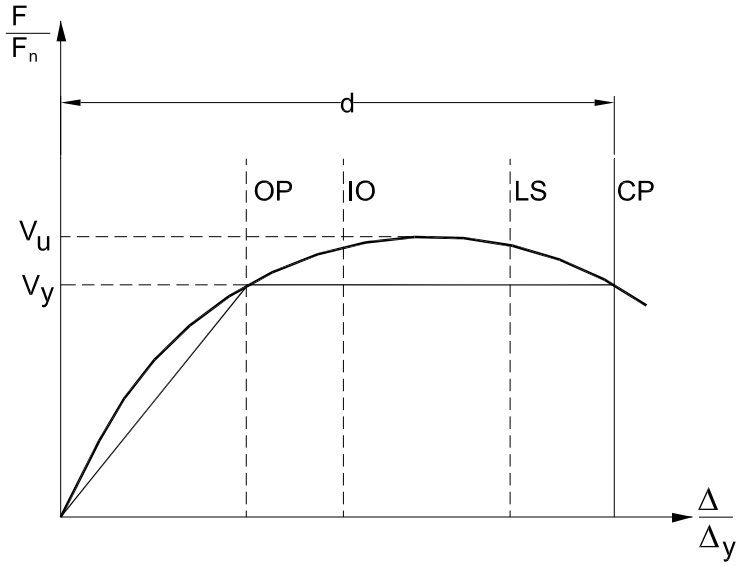

Figure 5.4. Normalized force versus deformation ratio for wood elements (Fig. 8-1, FEMA 273, 1997)

FEMA 273 (1997) establishes the relationship between performance levels using the normalized bilinear force-deformation curve for SWP depicted in Figure 5.4. In addition, FEMA 273 (1997) provides the equations for determining the normalized deformation associated with the three performance levels CP, LS and IO. The equations are expressed as a function of the ductility *d* of the SWP, which is the normalized lateral deformation of the SWP at the CP performance level:

$$\Delta_{CP}/\Delta_y = d \quad \textbf{(5. 13)}$$

$$\Delta_{LS}/\Delta_y = 1.0 + 0.8(d-1) \quad \textbf{(5. 14)}$$

$$\Delta_{IO}/\Delta_y = 1.0 + 0.2(d-1) \quad \textbf{(5. 15)}$$

where Δ_{PL} is the deformation of the SWP at the selected performance level CP, LS or IO, and Δ_y is the deformation at yielding of the SWP. The equation for the normalized deformation corresponding to the OP performance level is not provided by FEMA 273 (1997). For steel frameworks this deformation is generally computed at the onset of yielding in the elements (Hasan et al., 2002). For SWP it has been reported that forty percent of the yield displacement ($0.40\Delta_y$) represents the service load level (Chen et al., 2006). Accordingly, this study adopts forty percent of the yielding deformation as being representative of the OP performance level for CFS SWP. The limit drift ratios for SWP are given by the following equation:

$$LDR(\%) = \left(\Delta_{PL}/\Delta_y\right)\frac{\Delta_y}{h} \times 100 \quad \textbf{(5. 16)}$$

where *LDR* is the limit drift ratio for the selected performance level, given as a percentage; h is the height of the SWP; and $\left(\Delta_{PL}/\Delta_y\right)$ is the normalized deformation evaluated using Eqs. (5.13) to (5.15). Table 5.4 presents the yielding deformation and normalized deformation at the failure of the SWP, found from the experimental testing conducted by Branston et al. (2006). With this information, the limit drift ratios are evaluated for the four performance levels and presented in the last row of Table 5.4.

The limit drifts for the performance objectives need to be computed before the pushover analysis of a CFS building is initiated. The limit drifts for a SWP are evaluated by multiplying the SWP height by the corresponding performance level *LDR* (i.e., 2.5%, 2.1%, 1.0% and 0.20% for the CP, LS, IO and OP performance levels, respectively). If the SWP lateral drifts computed by the pushover analysis are smaller than the corresponding limit drifts, the performance criteria are satisfied.

Table 5.4. Determination of the limit drift ratios for CFS shear wall panels

Branston et al (2006)										
	Specimen	Disp. at yielding (Δ_y) mm	d ($\Delta_{failure}/\Delta_y$)	Normalized displacement (5.13) CP	(5.14) LS	(5.15) IO	Drift ratio CP	LS	IO	OP
Average negative values	4 – A,B,C	-16.2	3.8	3.83	3.26	1.57	2.54%	2.17%	1.04%	0.27%
	6 – A,B,C	-15.5	4.1	4.08	3.46	1.62	2.59%	2.20%	1.03%	0.25%
	8 – A,B,C	-12.3	4.7	4.72	3.98	1.74	2.38%	2.01%	0.88%	0.20%
	10 – A,B,C	-18.5	3.1	3.07	2.66	1.41	2.33%	2.02%	1.07%	0.30%
	12 – A,B,C	-11.2	5.1	5.13	4.30	1.83	2.36%	1.98%	0.84%	0.18%
	14 – A,B,C,D	-15.5	4.1	4.05	3.44	1.61	2.57%	2.19%	1.02%	0.25%
	16 – A,B,C	-15.8	4.4	4.44	3.75	1.69	2.88%	2.43%	1.09%	0.26%
	18 – A,B,C	-18.4	3.3	3.34	2.87	1.47	2.52%	2.17%	1.11%	0.30%
	20 – A,B,C	-12.8	6.3	6.33	5.26	2.07	3.32%	2.76%	1.08%	0.21%
	22 – A,B,C	-8.2	5.9	5.86	4.89	1.97	1.97%	1.64%	0.66%	0.13%
	24 – A,B,C	-8.8	4.6	4.62	3.90	1.72	1.67%	1.41%	0.62%	0.14%
	26 – A,B,C	-8.9	4.4	4.39	3.71	1.68	1.60%	1.36%	0.61%	0.15%
	28 – A,B,C	-15.9	4.7	4.68	3.94	1.74	3.05%	2.57%	1.13%	0.26%
	30 – A,B,C	-15.6	3.8	3.78	3.22	1.56	2.42%	2.06%	1.00%	0.26%
	32 – A,B,C	-16.9	4.0	4.00	3.40	1.60	2.77%	2.36%	1.11%	0.28%
	34 – A,B,C,D	-16.5	3.8	3.77	3.22	1.55	2.55%	2.18%	1.05%	0.27%
Average positive values	4 – A,B,C	14.9	4.9	4.85	4.08	1.77	2.96%	2.49%	1.08%	0.24%
	6 – A,B,C	16.2	4.2	4.21	3.57	1.64	2.80%	2.37%	1.09%	0.27%
	8 – A,B,C	10.1	6.4	6.41	5.33	2.08	2.66%	2.21%	0.86%	0.17%
	10 – A,B,C	17.3	3.8	3.79	3.23	1.56	2.69%	2.29%	1.11%	0.28%
	12 – A,B,C	13.1	5.0	5.02	4.22	1.80	2.70%	2.27%	0.97%	0.21%
	14 – A,B,C,D	19.3	3.5	3.51	3.01	1.50	2.78%	2.38%	1.19%	0.32%
	16 – A,B,C	22.6	2.8	2.79	2.43	1.36	2.59%	2.25%	1.26%	0.37%
	18 – A,B,C	27.0	2.3	2.27	2.02	1.25	2.51%	2.23%	1.39%	0.44%
	20 – A,B,C	16.1	4.5	4.54	3.83	1.71	3.00%	2.53%	1.13%	0.26%
	22 – A,B,C	7.5	7.4	7.38	6.10	2.28	2.27%	1.88%	0.70%	0.12%
	24 – A,B,C	8.1	5.4	5.38	4.50	1.88	1.79%	1.50%	0.62%	0.13%
	26 – A,B,C	10.6	4.6	4.55	3.84	1.71	1.98%	1.67%	0.74%	0.17%
	28 – A,B,C	15.7	3.9	3.90	3.32	1.58	2.51%	2.14%	1.02%	0.26%
	30 – A,B,C	10.7	6.0	6.01	5.01	2.00	2.64%	2.20%	0.88%	0.18%
	32 – A,B,C	15.7	4.3	4.34	3.67	1.67	2.79%	2.36%	1.07%	0.26%
	34 – A,B,C,D	17.3	4.0	4.01	3.41	1.60	2.85%	2.42%	1.14%	0.28%
				Average rounded to two decimals			2.53%	2.15%	0.99%	0.24%
				Average rounded to one decimal			**2.5%**	**2.1%**	**1.0%**	**0.2%**
				Standard deviation			**0.004**	**0.003**	**0.002**	**0.001**
				Coefficient of variation			**0.156**	**0.156**	**0.196**	**0.297**

In addition to checking the limit drifts of the SWP, it is necessary to check their lateral strength. To determine if the lateral strength of the SWP P_R is adequate, the lateral strength of the SWP is computed in accordance with Eq. (3.1) and compared to the lateral forces P_a found from the analysis. Thus, P_a must be smaller than P_R; otherwise, the design is not adequate and the SWP needs to be redesigned to satisfy the strength

requirements. To design or redesign a SWP, the factors that most affect their lateral strength must be considered so that the strength can be effectively increased. The following are typical modifications that have a major impact on the lateral strength of SWP: increasing the sheathing thickness, attaching sheathing on the two sides of the SWP (if it is being used only on one side), reducing the spacing of the screws for the sheathing-to-framing connections at the edge of the SWP, and increasing the diameter of the screws. The modifications that are considered to have a minor impact on the lateral strength of a SWP include: increasing the thickness and depth of the CFS studs, reducing the spacing between studs, and reducing the spacing of the screws for the sheathing-to-framing connections in the field of the SWP. The influence of these factors on the lateral strength of a SWP have been determined from experimental tests (Branston et al., 2006; Serrette, 2002), and confirmed by the method described in Chapter 3.

The vertical strength of the SWP is evaluated and compared with the vertical forces that result from the gravity and lateral loads applied on the structure. Although the sheathing can contribute to the vertical strength of the SWP, it is assumed that only the studs resist the vertical forces. This assumption is widely adopted in current practice and design standards (AISI, 2004). The studs' axial strength is computed according to the standard for design of CFS structural members (S136-01, 2002). The effective length coefficients described in Section 3.4 that consider the lateral support of the sheathing are considered.

5.5. Procedure of PBD Assessment for CFS buildings

In this section, a step-by-step description of the procedure for carrying out the PBD assessment of CFS buildings is provided to summarize the proposed methodology. Also presented in Figure 5.5 is a flowchart illustrating the described procedure for conducting pushover analysis for the PBD assessment of CFS buildings. The step numbers annotated in the flowchart match the step numbers of the PBD assessment procedure described in the following.

1. Establish the CFS building information. Specifically, create the preliminary design of the building, which may be obtained from a design derived for gravitational loads only. Determine the cross-sectional properties of the steel studs and material properties of the structural sheathing. Also, establish the following seismic design information:
    a. Select the performance objectives to be satisfied by the building from Table 2.1. Custom performance objectives can be formed by combining the expected performance level for a building with seismic hazards.
    b. Establish the seismic parameters of the site, such as response acceleration parameters S_s and S_1, site coefficients F_a and F_v, and long-period transition period T_L. These values are available in Tables 5.1, 5.2 and 5.3 (FEMA 450, 2003; USGS, 2002).

2. Determine the applicable gravity loads, W_g, as the summed magnitude of the dead and live loads: the dead loads are computed from the self-weight of the elements and components in the building; the live loads are computed from the applicable code, such as the National Building Code of Canada (NBCC, 2005), or the ASCE/SEI 7 (2005).

3. Evaluate the lateral strength of all the SWP for the building, P_R, in accordance with the analytical method presented in Chapter 3, using the properties of the SWP established in Step 1.

4. Compute the fundamental period of the structure, T, by employing the procedure described in Appendix A. Alternatively, the period can be computed by applicable eigenvalue analysis.

5. Compute the target base shear, V_b^{PO}, for each performance objective: based on the seismic parameters in Step 1, first calculate the seismic spectral acceleration using Eq. (5.2) for each performance objective; then compute the target base shear for each performance objective using Eq. (5.1).

6. Evaluate the maximum target base shear, $V_{b\max}$, using Eq. (5.7).

7. Determine the lateral-load distribution coefficients, C_{vx}, using Eq. (5.9); then, compute the lateral force, F_x, in each storey using Eq. (5.10).

8. Determine the limit drift of each SWP for each performance objective, $Drift^{PO}$, by multiplying the height of each SWP by the drift ratio of the performance level under consideration (i.e., by 2.5%, 2.1%, 1.0% and 0.6% for the CP, LS, IO and OP performance levels, respectively).

9. Initially set the lateral strength reduction coefficient $\lambda = 1$, and the load increment index $q = 1$.

10. Determine the constitutive properties, E_{xeq}, $E_{yeq,}$ and G_{xyeq}, of the equivalent shell elements in accordance with Eqs. (4.10), (4.14), and (4.18), respectively.

11. Form the linear and nonlinear stiffness matrices for all elements, by using Eqs. (4.41) and (4.42), respectively. Then, form the linear and nonlinear structural stiffness matrices by using Eqs. (4.44) and (4.45), respectively.

12. If q=1, apply the totality of the gravity loads on the building. Otherwise, go to step 13

13. Apply a lateral load increment on each floor, ΔF_{xi}, which is taken by this study to be 1% (i.e., Δ=0.01) of the lateral load found from Step 7 (the magnitude of the load increment remains constant throughout the pushover analysis).

14. Determine the nodal displacements and reactions of the building by solving Eq. (4.46) or Eq. (4.48).

15. Calculate the building base shear at load increment q, $V_a^{(q)}$

    The base shear is computed by summing the lateral load increments applied on the building.

16. If the accumulated base shear is equal to the target base shear of any performance objective, or greater (i.e., $V_a^{(q)} - V_b^{PO} < \Delta F_{xi}$), go to step 17. Otherwise, go to step 20.

17. Determine the SWP lateral-drift, using the nodal displacements from step 14. Verify if the SWP satisfy the acceptance criteria, by comparing the lateral drift of the SWP (i.e., inter-storey drift) to the limit drift for the performance objective being verified.

18. Determine the SWP lateral force, using the nodal displacements and element stiffness matrices. Verify if the SWP lateral strength satisfy the acceptance criteria, check if the lateral forces in the SWP have not exceeded their lateral strength.

19. If the building base shear is equal or greater than the maximum base shear, the analysis is complete. Otherwise, go to step 20.

20. Update the stiffness degradation coefficient λ, using Eq. (4.52) to reflect the SWP loss of stiffness due to the lateral forces on the CFS building. Update the equivalent shell elements constitutive matrix C, using Eq. (4.43). Increase the load increment index q. Proceed to Step 11.

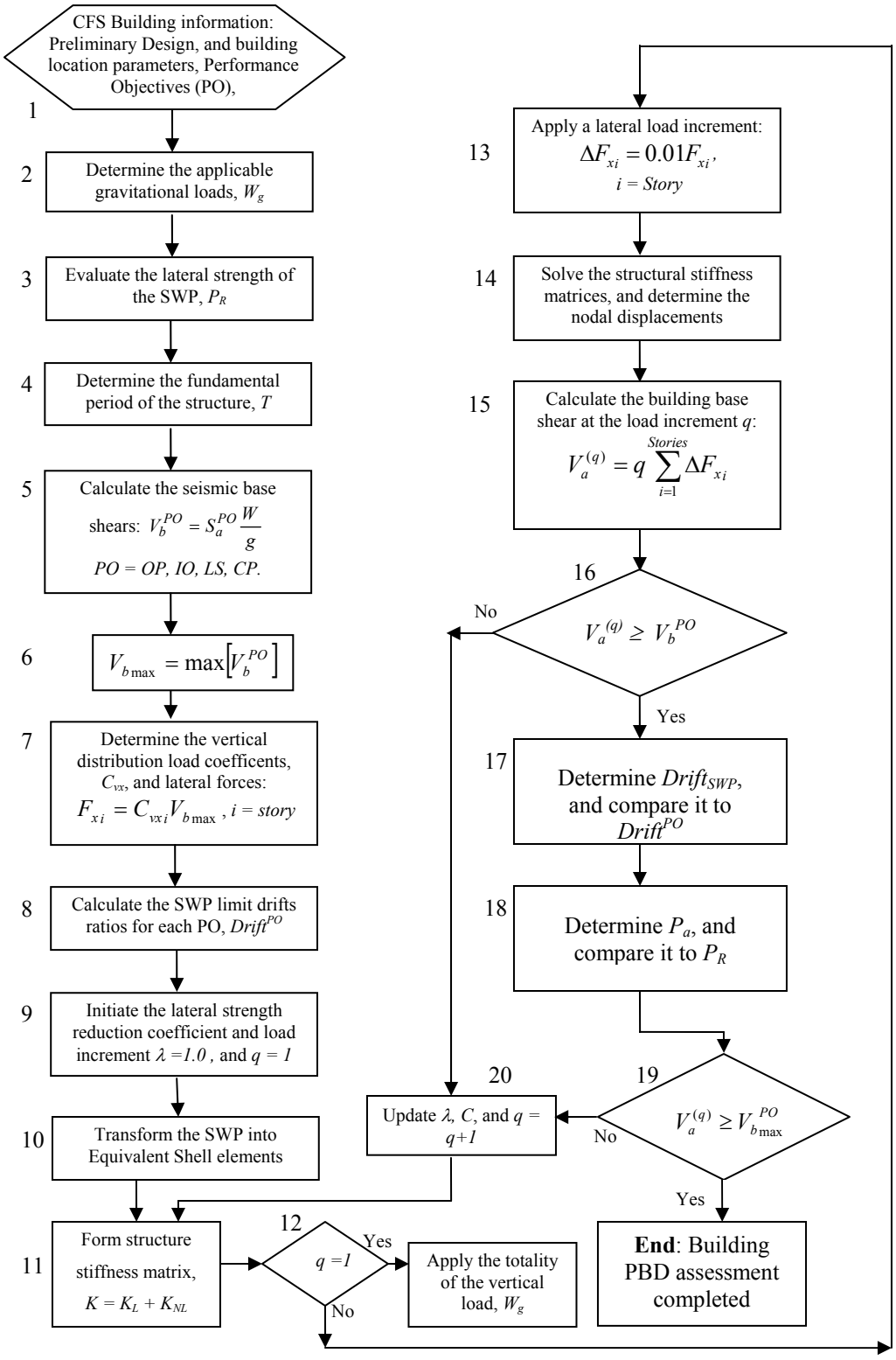

Figure 5.5. Flowchart for the PBD assessment of CFS buildings

5.6. Computer Program for the PBD assessment of CFS Buildings

As part of this study, a computer program has been developed to conduct the PBD assessment of three-dimensional CFS buildings. The program is developed on the basis the Structural Optimization and Design Analysis software (SODA, 1999), originally developed at the University of Waterloo. The software, SODA, has the capability to conduct the structural analysis and design for three-dimensional structural steel frameworks. In this study, new modules to carry out the PBD assessment of CFS buildings have been implemented. Thus, the resulting program is capable of conducting pushover analysis and the PBD assessment for CFS buildings that can be modeled using shell and frame elements as that demonstrated in Chapter 6.

To conduct the PBD assessment of CFS buildings using the computer program, the input file must contain the geometry information of the building such as nodal coordinates, member connectivity, boundary conditions, and material and cross-sectional properties of structural frame elements and panels. In addition, response acceleration parameters of the site and applicable loads are required. Based on the foregoing input information, the computer program calculates the lateral strength of the SWP, the fundamental period of vibration of the building, limit lateral drifts for the SWP, and the target base shears for the performance objectives. The program also determines the constitutive properties of the equivalent shell elements used to model the SWP. The program conducts the pushover analysis of the building. The SWP inter-storey drifts and lateral forces are computed at each performance objective, and compared to the limit inter-storey drifts and SWP strength, to determine if the SWP satisfy the acceptance criteria.

The output files generated by the computer program contain the following information:

- Weight and the fundamental period of the building
- Target base shear for each performance objective
- Frame-element end forces
- Nodal displacements
- Support reactions
- SWP lateral strength

- SWP lateral force for each performance objective
- Studs axial strength
- Studs axial force for each performance objective
- Limit inter-storey drift for each performance objective
- SWP inter-storey drift for each performance objective
- Stiffness degradation factor for each performance objective

Chapter 6

Examples

6.1. Introduction

The principal objective of this chapter is to present examples for the PBD assessment of CFS buildings using the spectrum-based pushover analysis procedure described in Section 5.5. Two different building models are created, and linear and pushover analyses are carried out for each model by using simplified finite element analysis (SFEA). The results from the linear and the pushover analyses are compared to determine the differences. Moreover, the results from the linear analyses are compared to the results from conventional finite element analysis (CFEA). The CFEA of the CFS buildings are conducted by using SAP2000 (2006). The purpose of the comparison between linear SFEA and linear CFEA is to determine the extent of the simplifications in SFEA that affect the accuracy of the results. The results from the pushover analyses are not compared, because to the author's knowledge there is no commercial software which is capable of carrying out the PBD assessment of CFS buildings.

In addition to presenting the practical application of the methodology developed in this study for the PBD assessment of CFS buildings, the examples serve to illustrate the nonlinear response of CFS buildings (as predicted by SFEA). Consequently, problems that may arise when designing a CFS building are identified, and recommendations can be made to avoid or reduce such problems.

6.2. Comparison of Linear SFEA and CFEA

The computer program developed in this study for carrying out the SFEA of CFS buildings employs the equivalent shell element formulation, described in Chapter 4. The modeling of CFS buildings using SFEA involves transforming all the panels in the

building, including those for walls, floors and roof, into equivalent shell elements. Each equivalent shell element is modeled with a sixteen-node shell element. Based on the comparison of the results from SFEA and CFEA presented in Section 4.4, it is recommended to use shell elements with a length-to-height ratio between 0.5 and 3.0. Otherwise, more than one shell element should be used to model the panels.

To transform the panels into flat shell elements of equivalent properties, the sheathing and studs are accounted for in the calculations, but not the top and bottom tracks. The reason for this is that the tracks do not provide lateral strength to the SWP, their primary function being to distribute the loads on the studs and maintain the integrity of the panels. However, if the tracks need to be included in the building model, they should be added as frame elements. As described in Section 5.6, the computer program created for this study has the capability to analyze frame elements in combination with shell elements. However, the material nonlinear behaviour of frame elements is not accounted for. For gravity wall panels, only the properties of the studs are accounted for when determining the equivalent properties of the shell elements. The floor and roof panels are transformed into equivalent shell elements using the same equations as that for SWP, which are presented in Section 4.2. If a floor or roof is built as a flat slab without joists, the constitutive properties of the slab and equivalent shell element are equal.
For the linear CFEA of CFS buildings, the studs, tracks and joists are modeled with frame elements, while the sheathing is modeled with meshes of shell elements.

6.2.1. Example 1: Analysis of an Isolated SWP Using SFEA and CFEA

The objective of analyzing the isolated SWP in Figure 6.1 is to determine how the two proposed simplifications of the SFEA affect the accuracy of the results. The two simplifications involve 1) the transformation of the SWP into an equivalent shell element, and 2) the modeling of the panel using one sixteen-node shell element.

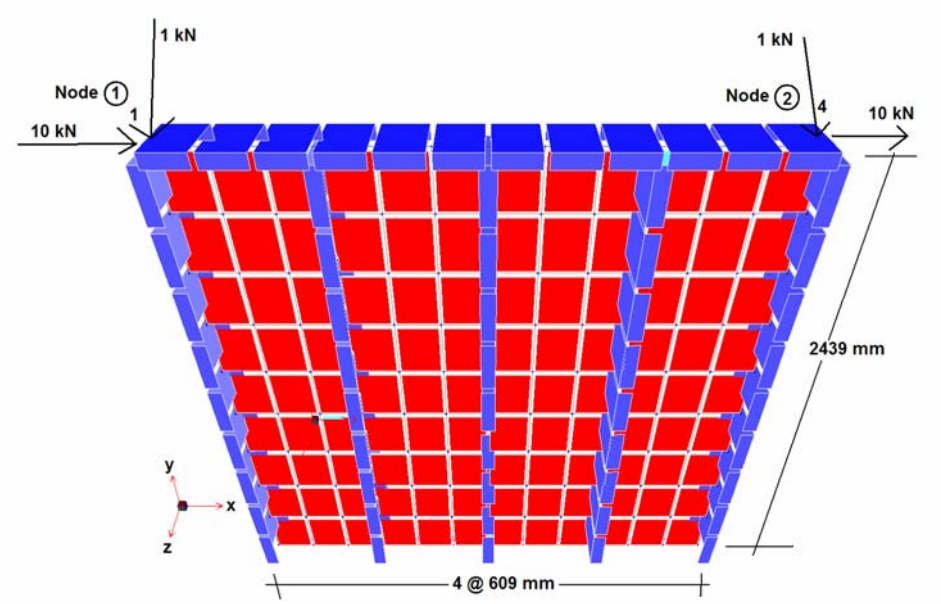

Figure 6.1. SWP model for CFEA

The SWP is built with 152 mm (6 in) depth studs (i.e., 152S51-1.37mm), and 11.11 mm (7/16in) OSB sheathing. The SWP, in Figure 6.1, has fixed support. CFEA is carried out using both SAP2000 (2006) and the computer program mentioned in Section 5.6; the two analyses are called CFEA and CFEA1, respectively. A total of 57 frame elements are included in each model to represent the studs and top track. In the CFEA model a total of 108 four-node shell elements are employed to model the sheathing, whereas in the CFEA1 model only 12 sixteen-node shell elements are employed to model the sheathing. A larger number of four-node shell elements is employed in the model because, usually, the sixteen-node shell elements offer more accuracy due their higher order shape functions. In fact, both models have the same number of nodes so that similar results can be achieved with both models.

The SFEA analyses are carried out in two different ways: for the SFEA1 analysis the SWP is transformed into equivalent shell elements modeled with 12 sixteen-node shell elements and the top track is modeled with 12 frame elements; for the SFEA2 analysis the SWP is modeled with one sixteen-node element, and three frame elements. The numbers of elements for each model, as well as their size, are presented in Table 6.1. For all cases, a 1.0 kN/m^2 out-of-plane load is applied on the surface of the panels. In-plane

nodal forces of magnitude of 1 kN and 0.1 kN in the *x* and *y* direction, respectively, are applied on nodes 1 and 2. Although in reality it is very unlikely to have a situation in which a structure is subjected to combined wind and earthquake loads, in this example both lateral and out-plane loads are applied on the SWP to compare the results obtained from different types of analysis.

Table 6.1. Quantity of elements

Analysis Model	Quantity of elements			Dimension (mm)			
	Shell	Frame		Shell		Frame	
		Track	Stud	width	height	Track	Stud
CFEA	108	12	45	203	271	203	271
CFEA1	12	12	45	609	813	203	271
SFEA1	12	12	0	609	813	203	0
SFEA2	1	3	0	2436	2439	609	0

Presented in Table 6.2 are the results obtained from the four SWP analyses for the displacements at node 1, the end-stud axial forces and the maximum bending moment in the centre stud. The CFEA results are taken as the benchmark to compare the other three analyses results. Since CFEA1 is carried out in the same fashion as CFEA, the results are similar. The displacements in the *x* and *y* directions from SFEA1 are larger than those from CFEA, but the axial forces are similar. Also, the displacements and axial forces from SFEA2 are larger than those from CFEA. The difference in the displacements from SFEA1 and SFEA2 is small, but the difference for the stud axial forces is relatively large.

Table 6.2. Comparison of results for Example 1

Analysis Model	Displacements (Node 1), mm			Forces in end-stud		
	x	y	z	Comp, kN	Tension, kN	Moment, kN-mm
CFEA	2.24	0.21	8.90	13.50	12.51	1526.43
CFEA1	2.28	0.22	8.95	13.72	12.71	1530.01

SFEA1	2.47	0.27	5.89	14.41	14.20	1859.28
SFEA2	2.58	0.39	6.12	18.81	17.59	1741.04

According to the results in Table 6.2**,** the use of equivalent shell element(s) decreases the accuracy of the *x* and *y* displacements and the bending moments, and also the accuracy of the axial forces in a minor way. On the contrary, the displacements are less sensitive to the number of equivalent shell elements in the model, while the axial forces are more sensitive to the number of elements. As mentioned in Section 4.6, the difference in the displacements in the *z* direction is caused by the SAP2000 model, which models the sheathing at the mid-plane of the studs.

6.2.2. Example 2: Three-storey Building

Shown in Figure 6.2 is a three-storey CFS building. The typical floor plan of the building is shown in Figure 6.3. All the SWP in the building are built with cold-formed studs 152S51–1.73 mm (600S200-68 mils), sheathed on both sides with 12.5 mm (1/2 in) DFP. The studs in SWP 2 are spaced 650 mm on centre, while the studs in the rest of the panels are spaced 600 mm on centre. Although, the stud spacing selected for this example is not common in practice, is selected for reasons of practicality. In all the SWP a single end-stud is used. No. 8 screws are used to attach the sheathing to the framing at 102 mm and 305 mm spacing on the edge and in the field of the SWP, respectively. The size and spacing of the screws are included to evaluate the lateral strength of the SWP in accordance with the procedure described in Chapter 3. All the SWP on the first storey have pin supports. The floor panels consist of a concrete slab of 127 mm thickness, supported by 254 mm (10 in) deep CFS joist, designated 254S64-1.37 mm (1000S250-54 mils). The height for all the storeys is 2850 mm, and the pitched roof has 17% slope. For this example, the structural details of the roof panels are identical to the details of the floor panels. Listed in Table 6.3 are the properties of the sheathing, studs, and floor and roof joists used in the building. In addition, the axial strength of the studs is presented in the table, which is computed in accordance with S136-02 (2002).

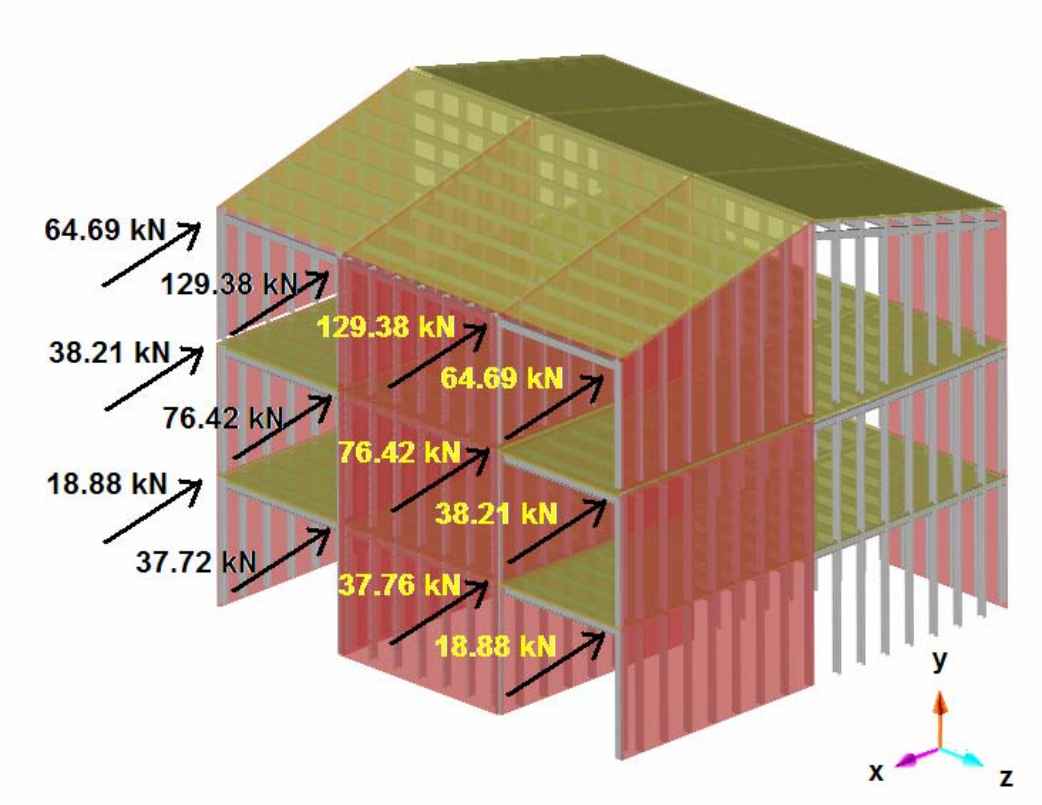

Figure 6.2. Three-storey CFS building

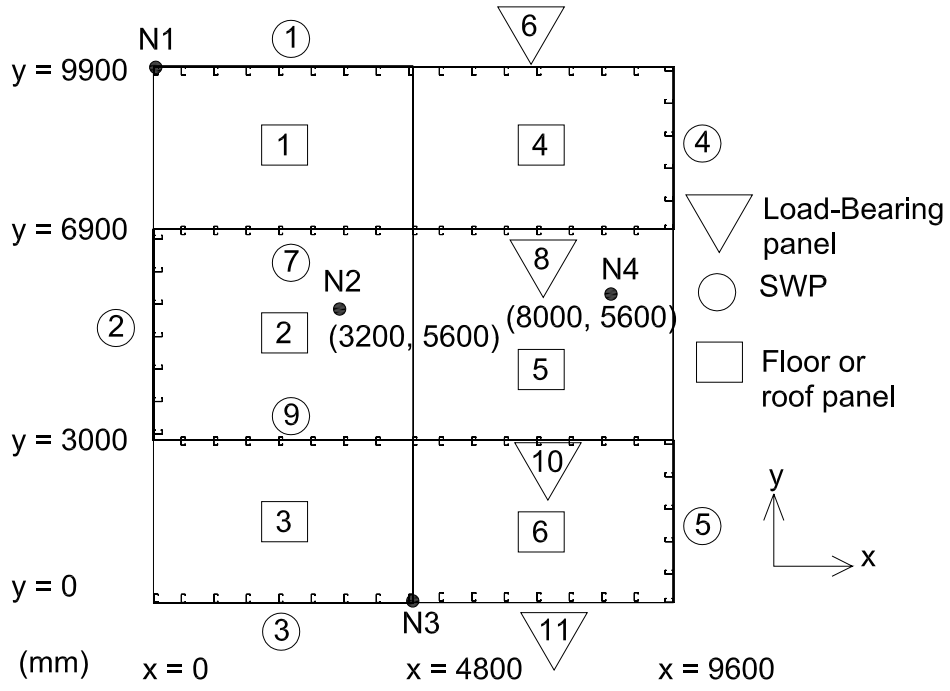

Figure 6.3. Typical plan and element identification of the three-storey CFS building

A CFEA of the CFS building is conducted using SAP2000 (2006), where the sheathing is modeled using shell elements that are 600 or 650 mm in length by 950 mm in height, and the studs are modeled with C-section frame elements that are 950 mm in length. Thus, a total of 1232 four-node shell elements and 1647 frame elements are used to model the three-storey CFS building. The sheathing and framing elements are joined at their mid-plane so that the offset between the shell elements and studs' flange is neglected. In the SFEA model of the CFS building, each SWP is modeled by an equivalent shell element, while each floor and roof panel is modeled with six equivalent shell elements. The floor and roof transversal joists in Figure 6.2 are modeled with three frame elements each. Therefore, a total of 51 sixteen-node shell elements and 72 frame elements are used to model the building. Table 6.4 records the properties for the equivalent shell elements for the floor and roof panels in the SFEA model, evaluated in accordance with Section 4.2.

Table 6.3. Properties of the sheathing and CFS framing material

Properties	Sheathing DFP		Properties		Stud	Joist
E_x	(MPa)	1167	E	(MPa)	203000	
E_y		10445	G		77000	
G		825	Fy		345	
t	(mm)	12.7	t	(mm)	1.73	1.37
ν_x		0.23	A	(mm^2)	472	515
ν_y		0.23	I	(mm^4)	$1.63x10^6$	$4.5x10^6$
Screw	(mm)	4.06	P_n	(kN)	60.03	Not applicable
			T_n		97.38	

The CFS building is subjected to both gravitational and lateral loads. The magnitudes of the factored gravity loads (Dead + Live load) are 3.24 kN/m^2 and 1.32 kN/m^2 for the floors and roof, respectively. The factored gravity loads are uniformly applied on the floor and roof elements, whereas the lateral seismic loads are applied on the top of the SWP along the *x* direction, as shown in Figure 6.2. The lateral seismic loads are computed by assuming that the building is located in California at latitude 41.0° N and longitude 115.2°W; the detailed calculations of the seismic loads are shown in Example 4

(in Section 6.3.1). The live loads and the factored load combinations are taken from ASCE/SEI 7 (2005) for a housing building.

Shown in Table 6.5 are the displacements obtained from SFEA and CFEA for linear analysis. For comparison, only the displacements of four joints (N1 to N4) are presented. Figure 6.3 illustrates the locations of the selected joints N1 to N4. The displacement of each joint is given in the *x*, *y* and *z* directions. The lateral inter-storey drift computed at joints N1 to N4 is also indicated in Table 6.5.

Table 6.4. Constitutive properties of the equivalent shell elements

Panel	SWP				Floor			
	E_{xeq}	E_{yeq}	G_{eq}	t_{eq}	E_{xeq}	E_{yeq}	G_{eq}	t_{eq}
	MPa	MPa	MPa	mm	MPa	MPa	MPa	mm
	Storeys 1 and 2							
1, 3	159.03	1482.85	52.69	195.72	5054.47	5057.21	1986.36	652.66
2	153.85	1432.09	52.11	197.89				
7, 9	159.03	1482.85	52.69	195.72				
5, 6	167.19	1563.08	53.58	192.48				
	Storey 3							
1, 3	155.41	1447.33	52.29	197.22	5041.63	5044.27	1984.67	653.21
2, 4, 5, 6	Same as for storeys 1 and 2							

The displacements in the *x* direction predicted from SFEA and CFEA are in good agreement. The displacements along the *y* direction are small, since no loads are applied in this direction. Conversely, the difference in the displacements of the floor panels in the *z* direction at joints N2 and N4 is large. The reason is that in the modeling with CFEA, the studs and joists are modeled at the mid-plane of the shell elements. This yields a smaller value of the moment of inertia of the combined cross-section, and consequently, the resulting deflections are larger. The SFEA accounts for the offset of the sheathing from the centroid of the studs.

The lateral strengths P_R of the SWP in Table 6.6 are evaluated with the procedure described in Chapter 3. The table also lists the lateral force P_a in each SWP that is obtained from SFEA and CFEA. In SFEA, the lateral forces in the SWP are predicted by adding up the lateral forces at the nodes of the SWP, which are computed by multiplying the stiffness matrices of the shell elements by the nodal displacements of the building. In SAP2000, it is not possible to obtain the forces in the nodes; instead the lateral forces are computed using the average shear force in the shell elements obtained from the CFEA. The average shear force is multiplied by the length of the SWP to determine the lateral force in the SWP.

Table 6.5. Displacement and lateral drift at selected joints, mm

Joint	SFEA				CFEA			
	X	Y	Z	Drift	X	Y	Z	Drift
	Storey 1							
N1	5.94	-0.04	1.25	5.94	6.01	0.00	1.59	6.01
N2	5.96	-0.02	-0.45	5.96	5.99	0.00	-0.90	5.99
N3	6.01	0.00	-0.79	6.01	5.99	0.00	-1.33	5.99
N4	5.96	0.03	-0.69	5.96	6.00	0.00	-0.94	6.00
	Storey 2							
N1	11.78	-0.05	1.67	5.84	12.08	0.01	2.08	6.07
N2	11.80	-0.02	-0.63	5.84	12.04	0.00	-1.22	6.05
N3	11.87	0.00	-1.12	5.86	12.02	0.00	-1.85	6.03
N4	11.80	0.05	-1.07	5.84	12.03	0.00	-1.28	6.03
	Storey 3							
N1	16.60	-0.09	1.66	4.82	17.18	0.03	2.08	5.10
N2	17.13	-0.07	-0.59	5.33	17.88	0.00	-1.03	5.84
N3	17.34	-0.05	-1.15	5.47	18.09	0.00	-1.92	6.07
N4	17.24	0.01	-1.18	5.44	18.29	0.00	-1.15	6.26

The lateral forces listed on Table 6.6 are obtained from the SFEA and CFEA, and are computed by multiplying the average lateral force on the SWP by its length. Although this approach is not exact it provides acceptable results, and integration of forces over the SWP area is not required. The results in Table 6.6 indicate that the force in each SWP is

less than the SWP strength; That is, the seismic design of the SWP is appropriate for resisting the lateral loads since none of the SWP fail. The lateral forces in SWP 1 and 3 are larger on the first storey than on the top storey, because the forces are transmitted from top to bottom. On the contrary, SWP 4 and 5 on the third storey have the largest force while the SWP on the first storey have the smallest force. Although no lateral forces are applied on SWP 4 and 5, lateral deformation is induced in the SWP by the flexural deformation of roof and floor panels under the gravity loads, as shown in Figure 6.4. As a result, small lateral forces are found in SWP 4 and 5. No shear deformation is produced in SWP 2 since it is located in the center bay of the building. Therefore, the lateral force in SWP 2 is zero. In general, all the predictions of the lateral forces in the SWP are in good agreement with the results obtained from CFEA. The lateral strength for SWP 1, 3, 7 and 9 is larger for the SWP in the third storey than for the SWP in the first and second storeys because the average height of the SWP in the third storey is larger.

Table 6.6. SWP lateral strength P_R and lateral force P_a, kN

SWP	Storey 1			Storey 2			Storey 3		
	$\mathbf{P_R}$	P_a		$\mathbf{P_R}$	P_a		$\mathbf{P_R}$	P_a	
		SFEA	CFEA		SFEA	CFEA		SFEA	CFEA
1, 3	**212.80**	177.44	160.80	**212.80**	146.59	122.40	**226.75**	88.79	84.12
7, 9	**212.80**	177.60	163.20	**212.80**	149.66	120.00	**226.75**	94.50	87.12
4,5	**128.21**	1.99	0.48	**128.21**	3.72	1.92	**128.21**	4.72	3.36

Presented in Table 6.7 is the maximum compression force in the most critical stud of each SWP. For all the SWP the most critical stud is an end stud: for SWP 1, 3, 7, 9, 4 and 5 the end-stud located towards the centre of the building is critical; for SWP 2 both end-studs have the same maximum compression force. The axial forces in the studs are estimated using Eq. (4.50) after the analysis of the building is carried out.

The compression forces predicted from SFEA and CFEA are presented in Table 6.7, and demonstrate a large difference for SWP 1 and 3 in the third storey for the example building. The size of the shell elements also affect the accuracy, as described in Example 1. Since only one shell element is used to model each SWP, the SWP 1, 3 and 9 are each

4800 mm in length and 2850 mm in height; (i.e., a length-to-height ratio = 1.68). Moreover, the predicted compression forces in the end-studs for SWP 1, 3, 7 and 9 are larger than the studs' strength, so those studs need to be reinforced by using double end-studs.

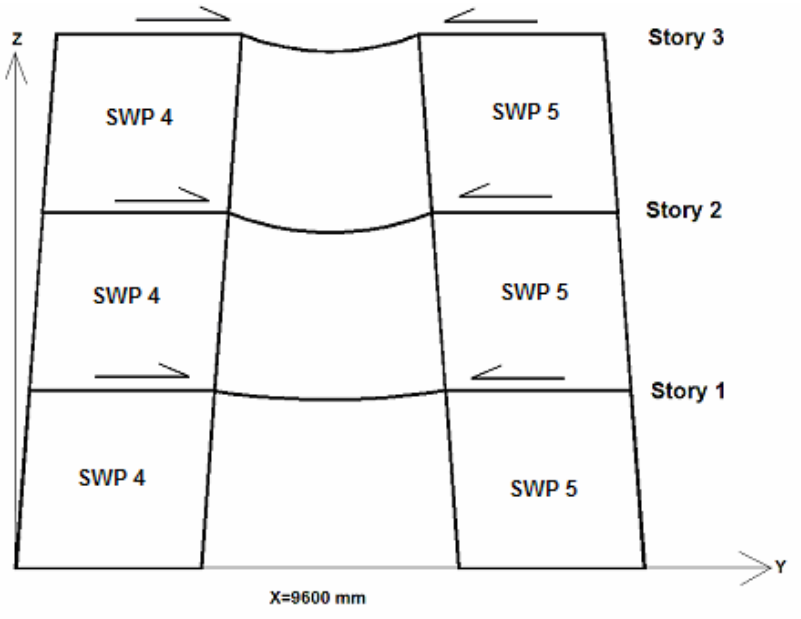

Figure 6.4 Building deformation due to gravity loads

Table 6.7. Compression force in the most critical stud of each SWP, kN

SWP	SFEA			CFEA		
	Storey 1	Storey 2	Storey 3	Storey 1	Storey 2	Storey 3
1, 3	64.27	41.16	19.36	61.13	30.67	12.99
2	0.00	0.00	3.09	0.00	0.00	8.28
4, 5	3.65	2.71	1.55	5.33	3.62	1.50
7, 9	65.94	43.53	13.82	63.64	34.69	14.96
Load-Bearing Wall						
8, 10	28.94	18.31	10.88	39.31	18.91	2.79
6, 11	27.31	17.40	13.82	31.01	16.09	4.33

Table 6.8 presents the maximum tension force in the most critical stud of each SWP. The difference is small in the predicted forces in storeys 1 and 2 for SWP 1 and 3 from both

analysis approaches. However, the difference is large for the SWP in storey 3. The studs in SWP 4, 5, 6, 8, 10 and 11 do not have a tension force.

Table 6.8. Tension force in the most critical stud of each SWP, kN

SWP	SFEA			CFEA		
	Storey 1	Storey 2	Storey 3	Storey 1	Storey 2	Storey 3
1, 3	89.14	46.12	28.14	65.61	26.36	5.43
2	8.45	4.92	1.13	15.87	9.28	2.31
7, 9	72.96	41.37	12.89	37.61	13.79	1.87

When the SFEA and CFEA results are compared, the differences in the displacements in the *z* direction and the axial forces in the studs are large. However, the purpose of the SFEA is to facilitate the PBD assessment of CFS buildings. In this context, the SWP lateral displacements and lateral forces are employed as acceptance criteria. Since these quantities are in good agreement with both approaches, the SFEA can be employed with confidence for carrying out the preliminary performance-based design of this CFS building.

6.2.3. Example 3: Five-Storey Building

The building in Figure 6.5 is analyzed using SFEA and CFEA for the loading indicated in the *x* direction, and the results from both methods are compared. The dimensions of the building typical plan and the identification of the panels are illustrated in Figure 6.6. The storey height is 2850 mm for each of the five storeys. The primary load-carrying elements in the building are the load-bearing panels and SWP, built with studs 152S41–1.73 mm (600S162-68 mils) spaced at 609 mm on centre. The SWP 1, 5, 13, and 17 are covered with 11.11 mm OSB sheathing on the two sides, and SWP 3, 6, 12, 15, 19, and 20 are covered with the same type of sheathing on one side. The sheathing is attached with No. 8 screws at 152 mm and 305 mm spacing on the edge and in the field of the SWP, respectively. The rest of the panels are load-bearing panels, with no sheathing. All the SWP on the first floor are pin-connected to the foundation. In addition, the panels that

intersect at a ninety-degree angle (e.g., panels 3 and 27 in Figure 6.6) are joined at the top and bottom nodes, but not at intermediate nodes. Therefore, the vertical and lateral forces that those panels receive come from the floor. The floor consists of a 127-mm thick concrete slab, supported by the load-bearing panels and SWP. This example CFS building has several differences compared to the building in Example 2: different geometry and size, different material properties, SWP with sheathing on the two sides of the framing, and gravity wall panels are used. Listed in Table 6.9 are the properties of the sheathing, studs and joist for the analysis. The compression and tension strengths of the studs, P_n and T_n, respectively, are computed based on S136-02 (2002), and presented in the last two rows of the table.

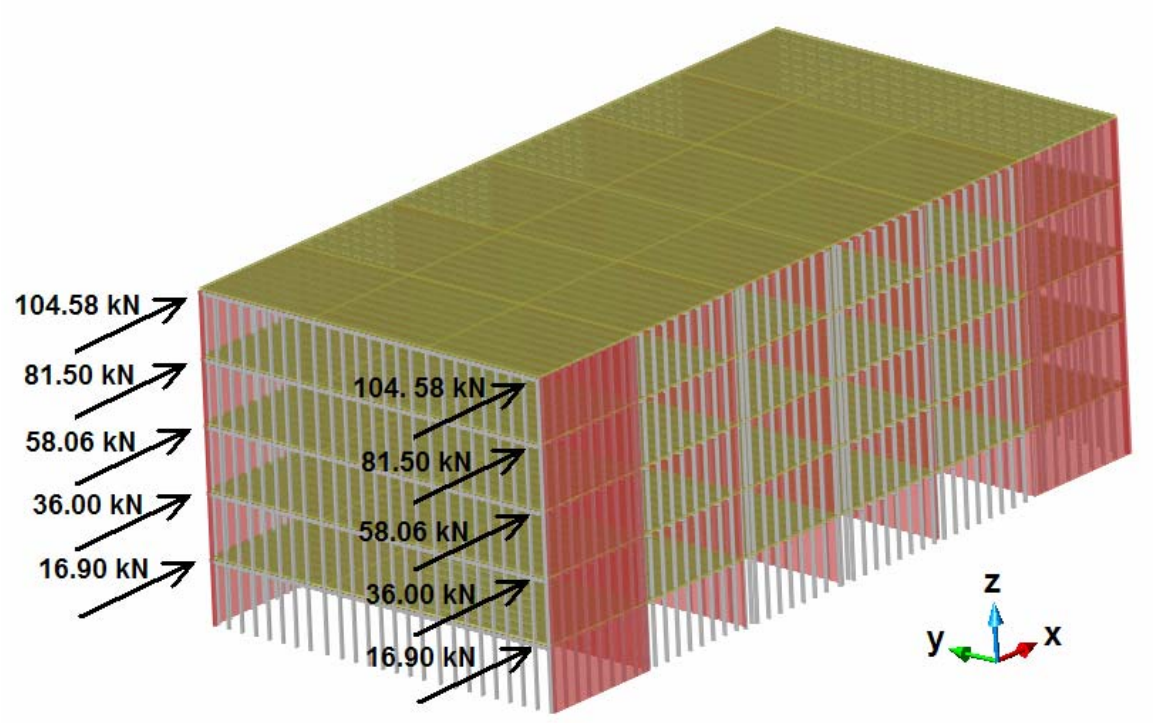

Figure 6.5. Five-storey CFS building

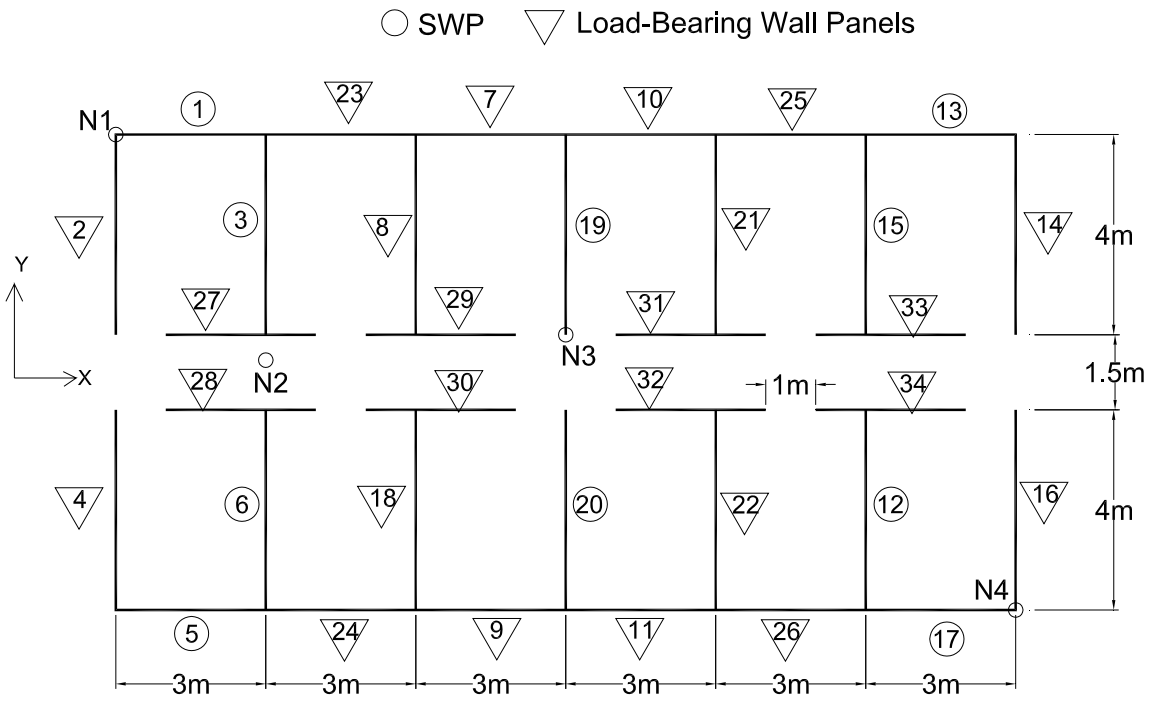

Figure 6.6. Typical plan and element identification of the five-storey CFS building

The CFEA of the CFS building is carried out using SAP2000 (2006); the sheathing is modeled using 600 mm × 950 mm shell elements, and the studs are modeled with 640-mm long C-section frame elements. A total of 3480 four-node shell elements and 2580 frame elements are employed to model the CFS building. For the SFEA of the building, each one of the 34 wall panels and SWP are transformed into a single shell element, and the floors and roof are divided into 18 shell elements: 12 of 3000 mm × 4000 mm side length, and 6 of 3000 mm × 1500 mm side length. Thus, the CFS building is modeled with a total of 260 equivalent shell elements. Listed in Table 6.10 are the constitutive properties of the equivalent shell elements in the SFEA, evaluated from the formulation in Section 4.2. The parameters E_{xeq} and G_{xyeq} for the wall panels are equal to zero since these panels have no sheathing.

Table 6.9. Sheathing and CFS framing material properties

Properties	OSB Sheathing		Properties		Studs	Joists
E_x	(MPa)	1983	E	(MPa)	203000	
E_y		9917	G		77000	

G		925	Fy		345	
t	(mm)	11.11	t	(mm)	1.73	1.37
ν_x		0.23	A	(mm^2)	425	479
ν_y		0.23	I	(mm^4)	$1.39x10^6$	$3.91x10^6$
Screw (∅)	(mm)	4.06	P_n	(kN)	63.77	Not applicable
			T_n		87.73	

Table 6.10 Constitutive properties of the equivalent shell elements

Panels	E_{xeq}	E_{yeq}	G_{xyeq}	t_{eq}
	MPa	MPa	MPa	mm
Shear wall 1, 5, 13, 17	407.65	2095.43	99.92	205.70
Shear wall 3, 6, 12, 15, 19, 20	312.00	1623.21	57.58	178.49
Load-Bearing 2, 4, 8, 14, 16 18, 21, 22, 23	0.00	4421.06	0.00	41.13
Load-Bearing 7, 9, 10, 11, 23, 24, 25, 26	0.00	4584.81	0.00	41.13
Floors and Roof	24500	24500	10500	127.00

The CFS building is subjected to both gravitational and lateral loads: the magnitudes of the factored gravity loads (Dead + Live loads) are 4.00 kN/m^2 and 1.60 kN/m^2 for the intermediate floors and the roof, respectively. The factored gravity loads are uniformly applied on the floor and roof elements, whereas the lateral seismic loads are applied as point loads on the top of the SWP, as depicted in Figure 6.5. The seismic load applied on each frame is distributed among the SWP (e.g., the load of 104.58 kN applied on the fifth storey is equally distributed to SWP 1 and 13). The lateral seismic loads are computed by assuming that the building is located in California at latitude 36.9°N and longitude 120°W (the detailed calculations of the seismic loads are shown in Example 5 in Section 6.3.2). The live loads and load combinations are determined from ASCE/SEI 7 (2005) for an office building.

Table 6.11 presents the displacements found from the SFEA and CFEA linear analyses of the CFS building. For comparison, only the x, y and z displacements of the four joints N1 to N4 shown in Figure 6.6 are listed. Also given in Table 6.11 are the inter-storey drifts at joints N1 to N4.

It is noted in Table 6.11 that the displacements in the *x* and z directions are slightly larger by SFEA, and the displacements in the *y* direction tend to zero since no forces are applied in that direction. The *y* displacements at joints N1 and N4 are positive because of the deformation pattern of the building. Shown in (b)
Figure 6.7(a) is the building deformation in the fifth storey caused by the lateral loads, the storeys below follow the same deformation pattern except the first storey which has no lateral deformation. The difference in the deformation in the *z* direction is caused by the small number of shell elements employed to model the floor.

Table 6.11. Displacement and lateral drift at selected joints (mm)

Joint	SFEA				CFEA			
	X	Y	Z	Drift	X	Y	Z	Drift
	Storey 1							
N1	9.76	0.00	3.54	9.76	9.35	0.00	3.14	9.35
N2	9.76	0.00	-0.80	9.76	9.34	0.00	-0.79	9.34
N3	9.76	0.00	-1.05	9.76	9.34	0.00	-0.62	9.34
N4	9.77	0.00	-4.14	9.77	9.35	0.00	-3.44	9.35
	Storey 2							
N1	23.08	0.01	5.47	13.32	21.87	0.01	4.87	12.52
N2	23.05	0.00	-1.53	13.29	21.84	0.00	-1.37	12.50
N3	23.05	0.00	-1.83	13.29	21.84	0.00	-1.13	12.50
N4	23.08	0.01	-6.52	13.31	21.87	0.01	-5.44	12.52
	Storey 3							
N1	37.71	0.01	6.40	14.63	35.44	0.01	5.69	13.57
N2	37.69	0.00	-2.09	14.64	35.41	0.00	-1.95	13.57
N3	37.69	0.00	-2.34	14.64	35.41	0.00	-1.50	13.57
N4	37.72	0.01	-7.78	14.64	35.45	0.02	-6.47	13.58
Joint	Storey 4							

N1	52.18	0.02	6.64	14.47	48.67	0.02	5.88	13.23
N2	52.13	0.00	-2.45	14.44	48.62	0.00	-2.28	13.21
N3	52.13	0.00	-2.62	14.44	48.62	0.00	-1.76	13.21
N4	52.18	0.02	-8.21	14.46	48.67	0.02	-6.79	13.22
	Storey 5							
N1	64.86	0.04	6.57	12.68	60.04	0.04	5.79	11.37
N2	64.78	0.00	-2.64	12.65	59.96	0.00	-2.44	11.34
N3	64.78	0.00	-2.67	12.65	59.95	0.00	-1.89	11.33
N4	64.86	0.04	-8.21	12.68	60.03	0.04	-6.74	11.36

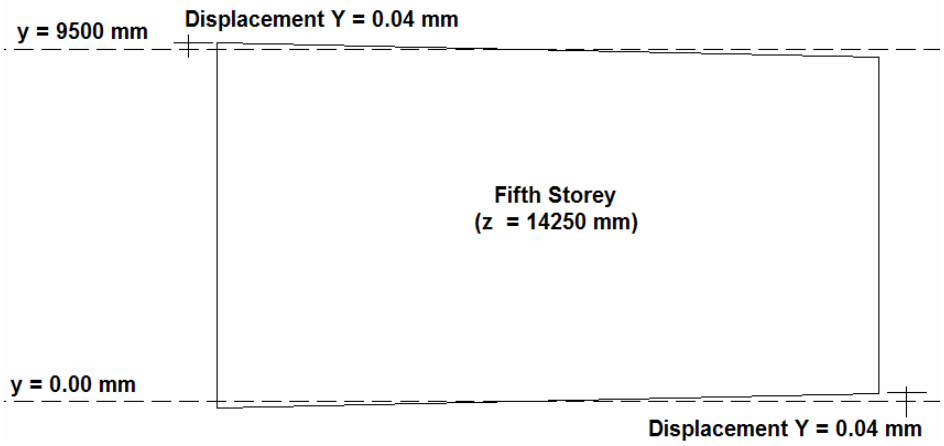

(a)

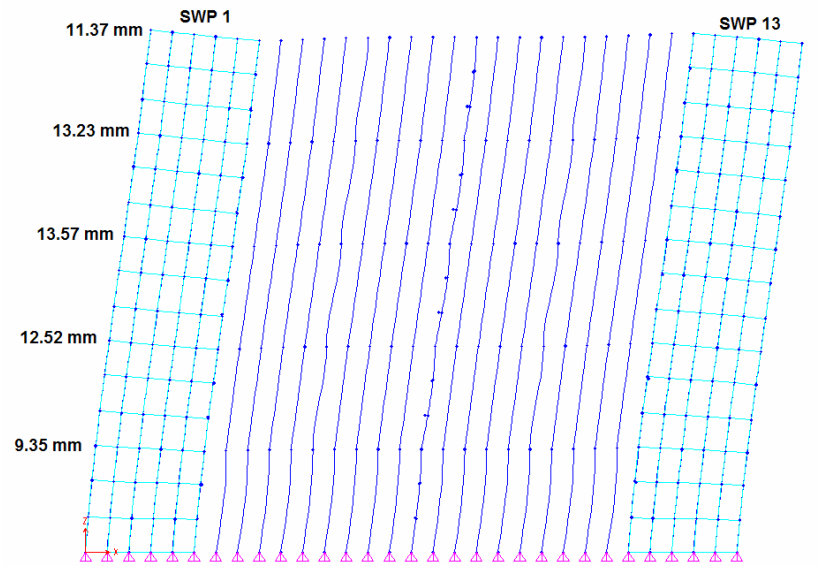

(b)

Figure 6.7 a) Fifth storey displacement in the *y* direction, b) Building inter-storey drift

The lateral loads accumulate from top to bottom. Thus the lateral load in the first storey is larger than in the storeys above, the lateral load in the second storey is larger than in the storeys above, and so on. However, the inter-storey drifts listed in Table 6.11 do not follow the same tendency, since the largest inter-storey drift is obtained for the third storey. The reason is that SWP undergo shear and bending deformation, and for this building the bending deformation is significant. Shown in Figure 6.1(b)
Figure 6.7 is the deformed shape of the building, and the inter-storey drift for SWP 1.

Table 6.12 presents the lateral strengths of the SWP, and their lateral forces predicted from SFEA and CFEA. Upon comparing the lateral strengths and forces, it is observed that the SWP in storeys 1 and 2 are not properly designed to resist the seismic forces since the lateral forces in the SWP are larger than their strengths.

From Table 6.12 it is noted that SWP 1, 5, 13 and 17 have the largest lateral forces, with the largest being on the SWP in the first storey. The small lateral forces in SWP 3, 6, 12, 15, 19, and 20 are caused by the deformation of the building, as illustrated in Figure 6.4 for Example 2. The lateral forces in the SWP predicted by SFEA and CFEA, and described in Table 6.12, are in good agreement.

Table 6.12. SWP lateral strength P_R and lateral force P_a on the, kN

SWP	P_R	P_a									
		SFEA					CFEA				
		Storey					Storey				
		1	2	3	4	5	1	2	3	4	5
1, 5	101.13	140.41	126.87	101.13	82.69	43.03	133.71	112.74	93.59	69.01	40.62
13, 17	101.13	140.54	127.74	108.65	85.31	46.00	136.38	115.70	99.08	71.73	44.34
3, 6	48.85	4.31	10.54	12.96	13.06	12.01	2.46	7.32	9.98	10.53	10.29
12, 15	48.85	6.39	16.60	22.45	25.00	25.42	4.74	14.55	21.15	24.72	26.64
19, 20	48.85	1.87	4.98	7.00	8.11	8.52	0.61	2.49	3.96	5.04	5.58

Table 6.13 exhibits a notable difference in the compression force in the most critical stud of each panel predicted by SFEA and CFEA. According to the results of Example 1, and

as explained in Section 4.4, the number of equivalent shell elements affects the accuracy in the prediction of the axial forces. Since SFEA provides an approximation of the maximum axial forces in the studs, these values are not intended for design purposes. The reason is that in some cases, the error in the prediction is large (e.g., twice as large). Moreover, according with the results, the end studs in SWP 1, 5, 13 and 17 have failed as a consequence of the lateral loading, so those studs need to be reinforced.

Table 6.13. Compression force in the most critical stud of each SWP, kN

SWP	SFEA					CFEA				
	Storey					Storey				
	1	2	3	4	5	1	2	3	4	5
1, 5	137.89	106.95	77.31	50.85	25.32	92.10	63.03	42.98	26.31	12.25
13, 17	225.24	140.00	85.41	49.27	35.74	128.44	78.55	45.94	21.39	4.04
3, 6,	17.58	12.08	7.87	5.62	3.79	44.29	34.02	21.99	11.94	4.75
12, 15	5.15	0.00	0.00	7.38	12.85	11.44	8.46	5.55	3.14	1.25
19, 20	15.06	11.49	8.83	6.21	5.23	18.79	14.92	11.12	7.33	3.58
	Load-Bearing Wall									
2, 4	0.00	0.00	0.00	0.00	0.00	0.00	0.00	0.00	0.00	0.00
14, 16	26.60	14.10	8.62	4.33	0.00	61.41	44.88	28.29	14.54	5.09
23, 24	70.86	54.95	37.89	22.27	9.13	50.32	35.28	21.08	9.70	1.99
25, 26	7.25	4.07	1.58	0.00	14.94	7.32	6.14	4.49	2.82	1.19
7, 9	19.25	15.03	10.93	6.88	3.35	12.52	11.12	8.94	6.23	3.05
10, 11	16.95	16.95	12.49	8.14	3.65	10.84	9.25	7.14	4.70	2.07
8, 18	12.91	8.85	7.97	6.84	1.73	44.26	34.00	21.79	11.91	4.75
21, 22	10.13	5.25	4.28	3.49	0.00	21.83	17.73	13.18	8.64	4.18
27, 28	39.09	34.08	25.26	15.65	7.08	26.41	20.93	15.85	10.55	5.06
33, 34	40.98	28.71	18.98	11.35	5.45	16.53	11.34	7.80	4.82	1.95
29, 30	40.14	32.29	23.49	14.34	5.29	25.64	20.14	15.21	10.29	5.31
31, 32	36.22	28.81	20.37	11.90	3.99	22.84	17.11	12.37	8.03	3.88

Presented in Table 6.14 is the maximum tension force in the most critical stud of each panel. The SWP that do not have tension force are not listed in the table. The prediction of the tension forces from SFEA and CFEA differ.

Table 6.14. Tension force in the most critical stud of each SWP, kN

SWP	SFEA					CFEA				
	Storey					Storey				
	1	2	3	4	5	1	2	3	4	5
1, 5	198.66	120.55	71.94	35.88	28.75	119.06	69.32	38.31	15.89	1.13
13, 17	110.02	85.66	63.29	44.13	0.00	78.45	52.04	35.65	22.85	12.85
3, 6,	N/A	N/A	N/A	N/A	1.07	N/A	N/A	N/A	N/A	3.24
12, 15	11.66	14.14	13.93	12.92	6.92	22.76	17.47	9.96	4.27	1.53
19, 20	N/A	N/A	N/A	N/A	3.79	N/A	N/A	N/A	N/A	N/A
	Load-Bearing Wall									
2, 4	13.96	13.12	11.45	10.66	5.32	46.41	32.96	19.40	8.71	2.33
25, 26	47.22	35.55	26.34	18.22	7.08	34.06	21.62	10.59	4.38	1.60

Similar to Example 2, the analysis results from SFEA and CFEA display differences, where the largest differences are found for the axial forces in the studs. Also, it is determined that analysis by SAP2000 does contribute to the differences in the results, since SAP2000 does not account for the offset of the sheathing and studs. Despite the differences in the stud axial forces, the lateral displacements and lateral forces in the SWP are consistently found by both approaches. Therefore, conducting the pushover analysis by SFEA can provide appropriate results for carrying out the PBD assessment of CFS buildings, i.e., as lateral displacements and forces are the two key parameters in that regard.

6.3. Performance-Based Design Assessment of CFS Buildings

In this section, the PBD assessment of the CFS buildings analyzed in Examples 2 and 3 is carried out in accordance with the methodology described in Chapter 5, where a single-mode spectrum-based pushover analysis is employed. After the lateral loads in the building corresponding to the specified performance objectives are computed, the pushover analysis is conducted. For the pushover analysis, the totality of the gravity loads are applied on the building, and a lateral load increment of 1% of the maximum target base shear is also applied. Then, the structural analysis is carried out. Before applying the next lateral load increment, the lateral stiffness of the SWP is updated by multiplying the

constitutive properties of the SWP by the lateral strength reduction factor, as explained in Section 4.6. When the lateral load applied on the building is equal to the target base shear corresponding to any of the specified performance objectives, the analysis is "paused" to check the acceptance criteria of the SWP. If all the specified performance objectives are satisfied, the PBD assessment of the building is completed.

The lateral stiffness of the sheathing on the SWP is updated as the lateral loads on the building increase. When the lateral stiffness of a SWP is zero, it is considered that the sheathing fails. In this case, the SWP is treated as a wall panel with no lateral stiffness, and only the vertical stiffness of the studs is considered for subsequent load increments. However, if one or several SWP fail, the performance objective in consideration is not satisfied, and the lateral design of the building needs to be improved accordingly.

The results from the pushover analyses applied to assess the PBD of the example CFS buildings are not validated, since no commercial software capable of performing this task is available to allow for a comparison of results. However, the SWP inter-storey drifts, lateral forces and stud forces found from both the linear analysis and the pushover analysis, are compared to determine the difference in the results from both approaches.

6.3.1. Example 4: Three storey building

The PBD assessment of the building shown in Figure 6.2 is carried out. The material properties and geometry of the building described in Example 2 are adopted as the preliminary design for this example. According to the analysis results of Example 2, the SWP lateral strength is greater than required and, so, the SWP can be redesigned to reduce the lateral strength and gain a more economical design. In addition, a double end-stud is required in several SWP. However, the design is not modified, so that the results from the pushover analysis in this example can be compared later to the results from the linear elastic analysis. In addition, the building is subjected to the same set of seismic loads as shown in Figure 6.2, applied in load increments of 1%. The gravity loads are maintained constant on the building throughout the analysis. Also, the stiffness

degradation model (Section 4.6) is used to reduce the lateral stiffness of the SWP after each load increment.

The three-storey building is considered to be ordinary according to the categories established by SEAOC (1995), so that the building must satisfy the four performance objectives described in Table 2.1. The building is assumed to be located in California at latitude 41.0° N and longitude 115.2°W on a site class B. The corresponding seismic parameters needed to calculate the spectral acceleration for the four performance objectives are obtained from Table 5.1. The four performance objectives are the following: OP for a 50%/50 year earthquake, IO for a 25%/50 year earthquake, LS for a 10%/50 year earthquake, and CP for a 2%/50 year earthquake.

The gravity dead loads are computed from the building's self-weight, and the gravity live loads are obtained from ASCE/SEI 7 (2005) for residential buildings: Dead load (D) = 1.1 kN/m^2 ; Live load floor (L) = 1.92 kN/m^2 ; Live load roof (L_r) = 0.96 kN/m^2

The ASCE/SEI 7 (2005) describes two load combinations that include earthquake loads (E):

$$1.2(D)+1.0(E)+L+0.2S \quad \textbf{(6. 1)}$$

$$0.9(D)+1.0(E)+1.6H \quad \textbf{(6. 2)}$$

where H is the load due to earth pressure, ground pressure, or bulk material pressure, and S is the load due to snow. Bulk material pressure and snow load are not applicable for this example because the building is not going to be built underground or in a city with risk of snow. The most critical load combination is chosen to determine the factored loads to be applied on the building As such, the factored gravity load applied on the floors of the building is computed using Eq. (6.1), such that,

$$1.2(1.1)+1.92=3.24kN/m^2$$

Also from Eq. (6.1), the factored gravity load applied on the roof of the building is computed by,

$$1.2(1.1) = 1.32 kN/m^2$$

The seismic weight of the building is W=405 kN. The natural period of the building is T=0.324 second in the x direction, which is computed according to the procedure described in Appendix A.

Table 6.15 gives the target base shears corresponding to the specified four performance objectives, which are computed as functions of the zone seismic parameters and natural period of the building. The variables from the second to the ninth column are defined in Section 5.2. After the base shears are computed, the lateral load for the pushover analysis is defined by the maximum target base shear $V_{b\ max}$=730.70 kN. The lateral loads are applied on the building in 1% increments of 7.307 kN, until the maximum target base shear is reached or the structure collapse occurs. The factors to adjust the spectral acceleration in the short period and one second period range, F_a and F_v, are provided by Tables 5.2 and 5.3, respectively. Listed in Table 6.16 are the lateral loads for each storey, $F_{a,}$ computed by multiplying the maximum target base shear by the lateral load distribution coefficient C_{vx} for each storey, which is computed using Eq. (5.63), for κ = 1.0 since the building's period is smaller than 0.5 second. The variables h, w, and C_{vx} in Table 6.16 are the inter-storey height, storey weight, and lateral load distribution coefficient, respectively.

Table 6.15. Target base shears, kN

PO	S_S	S_1	S_{MS}	S_{M1}	S_{DS}	S_{D1}	T_o	T_s	S_a	V_b
	(g)						(sec)		(g)	(kN)
OP	0.109	0.035	0.109	0.035	0.073	0.023	0.064	0.321	0.073	**71.75**
IO	0.180	0.058	0.180	0.058	0.120	0.039	0.064	0.322	0.120	**118.91**
LS	0.250	0.080	0.250	0.080	0.167	0.053	0.064	0.320	0.167	**164.01**
CP	1.100	0.410	1.100	0.410	0.733	0.273	0.075	0.373	0.733	**730.70**

Table 6.16. Lateral loads in the building

Storey, x	*h* (m)	*w* (kN)	C_{vx}	F_x (kN)
1	2.85	309.23	0.16	**113.29**
2	5.70	312.91	0.31	**229.27**
3	8.55	309.69	0.53	**388.14**
	Σ	**931.83**	**1.00**	**730.70**

Table 6.17 presents the inter-storey drifts and limit drifts for the SWP related to each performance objective, which are computed by the limit drift ratios developed in Section 5.4 (i.e., 0.2%, 1.0%, 2.1% and 2.5% for the OP, IO, LS and CP performance levels). The limit inter-storey drifts are obtained by multiplying the lateral drift ratios by the height of the SWP. SWP 1 and 3 exhibit the largest lateral drifts, because the seismic loads are applied on these panels. Yet, the limit drifts are not exceeded, so that the SWP are well designed to resist the seismic loads.

Table 6.17. SWP inter-storey drift, mm

SWP	Performance objective											
	OP (limit=4.8)			IO (limit=24.0)			LS (limit=50.4)			CP (limit=60.0)		
	Storey			Storey			Storey			Storey		
	1	2	3	1	2	3	1	2	3	1	2	3
1	0.34	0.39	0.43	0.76	0.77	0.76	1.22	1.19	1.10	21.40	14.84	9.44
3	0.36	0.40	0.43	0.78	0.78	0.76	1.25	1.20	1.11	21.50	14.89	9.46
6	0.34	0.39	0.43	0.75	0.76	0.76	1.22	1.18	1.11	21.38	14.81	9.48
7	0.35	0.39	0.43	0.76	0.77	0.75	1.23	1.19	1.10	21.43	14.85	9.41
9	0.35	0.39	0.43	0.77	0.77	0.75	1.24	1.19	1.10	21.47	14.87	9.41

The results from the pushover analysis at the CP performance level are compared to the results from the linear analysis to determine the influence of each type of analysis. At the CP performance level, the building is subjected to the same loading condition as that for the linear analysis. The difference in the displacements predicted from linear and pushover analysis is significantly large. The inter-storey drift for the pushover analysis is more than triple that for the linear analysis. The reason is that the pushover analysis

accounts for the geometric nonlinearities and the stiffness degradation of the SWP. Figure 6.8 is a comparison of the inter-storey drifts and lateral displacements for SWP 1, obtained from linear and pushover analysis.

Table 6.18 indicates the lateral strengths P_R and lateral forces P_a for the SWP. The lateral strengths are computed in accordance with Section 3.3 of Chapter 3, and the lateral forces are obtained from the SFEA (in Section 4.3). Since the lateral forces in the SWP are smaller than their strengths, the performance objectives are deemed to be satisfied. The largest forces are obtained for the CP performance objective, since it is associated with the maximum target base shear. The forces from linear analysis are slightly larger than the forces from pushover analysis. Yet, the difference is small, indicating that the prediction of the lateral forces acting on the SWP is not affected by the method of analysis (i.e., linear or pushover analysis).

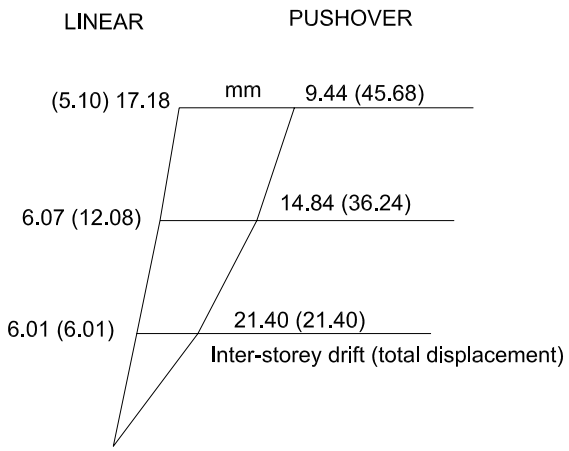

Figure 6.8. Inter-storey drifts and displacements of the SWP 1: Linear and pushover analysis

In Table 6.18, the summation of lateral forces in the SWP is different to the lateral loads applied on the building, i.e., for the CP performance objective the summation of forces is 677 kN while the lateral force applied on the building is 730 kN. The reason for the difference is that the panels in the *y* direction (i.e., perpendicular to the SWP 1, 3, 7 and

9) are taking a proportion of the lateral loads: i.e., SWP 2 is taking 23.79 kN, SWP 4 is taking 14.85 kN, and SWP 5 is taking 14.77 kN.

Table 6.18. SWP lateral strength P_R and lateral force P_a, kN

SWP	P_R	Lateral force, P_a											
		OP			IO			LS			CP		
		Storey			Storey			Storey			Storey		
		1	2	3	1	2	3	1	2	3	1	2	3
1	212.80	9.14	7.66	4.31	17.89	14.77	8.60	26.66	21.91	12.89	171.46	140.23	85.71
3	212.80	9.29	7.77	4.18	18.13	14.92	8.47	26.97	22.08	12.76	171.71	140.41	85.66
7	212.80	8.14	6.62	4.47	16.93	14.02	9.10	25.64	21.34	13.67	166.81	138.51	87.89
9	212.80	8.43	6.75	4.43	17.23	14.16	9.06	25.95	21.49	13.64	167.02	138.67	87.86

Listed in Table 6.19 is the stiffness degradation coefficient, represented by λ, for each SWP, which is computed using Eq. (4.52). When λ is equal to zero the SWP has failed; for this example none of the SWP failed.

Table 6.19. SWP stiffness degradation coefficient λ

SWP	OP			IO			LS			CP		
	Storey			Storey			Storey			Storey		
	1	2	3	1	2	3	1	2	3	1	2	3
1	0.69	0.71	0.77	0.60	0.63	0.71	0.54	0.57	0.66	0.08	0.14	0.30
2	0.93	0.95	0.93	0.92	0.95	0.91	0.91	0.94	0.90	0.85	0.90	0.80
3	0.69	0.71	0.78	0.60	0.63	0.71	0.54	0.57	0.66	0.08	0.14	0.30
4	0.82	0.76	0.75	0.82	0.76	0.75	0.82	0.76	0.75	0.79	0.74	0.75
5	0.84	0.77	0.75	0.84	0.77	0.74	0.84	0.77	0.74	0.85	0.75	0.71
7	0.70	0.73	0.77	0.61	0.64	0.70	0.55	0.58	0.65	0.09	0.15	0.30
9	0.70	0.72	0.77	0.61	0.64	0.70	0.54	0.58	0.65	0.09	0.15	0.30

The maximum compression force in the most critical stud of each SWP, resulting from the gravity and seismic loads applied on the building, are provided in Table 6.20. The studs in the building have not exceeded their axial compression strength for the LS and

CP performance objectives, which is 60.03 kN as shown in Table 6.3. The compression forces predicted by pushover analysis are smaller than the forces predicted by linear analysis, especially for SWP 2, 4, 5 and 6.

Table 6.20. Compression force in most critical stud of each SWP, kN

SWP	Performance objective											
	OP			IO			LS			CP		
	Storey			Storey			Storey			Storey		
	1	2	3	1	2	3	1	2	3	1	2	3
1	12.96	8.08	7.21	14.71	9.12	6.42	26.81	16.84	11.90	40.62	28.65	10.44
2	1.23	0.91	0.53	0.96	0.91	0.67	1.90	1.82	1.32	0.00	0.00	4.24
3	12.73	8.00	7.07	14.57	9.06	6.26	26.69	16.75	11.64	40.40	28.56	10.08
4	3.16	1.91	0.81	3.21	1.98	0.87	6.41	3.95	1.74	6.58	4.80	2.79
5	3.17	1.91	0.81	3.22	1.97	0.87	6.44	3.93	1.74	6.59	4.69	2.79
6	8.32	6.07	4.49	8.91	6.40	5.18	17.88	12.81	10.37	53.73	31.73	23.77
7	22.93	12.46	4.73	24.14	13.29	4.70	44.16	24.56	8.74	48.88	30.89	16.08
8	13.48	7.85	2.95	14.15	8.02	3.31	28.32	16.06	6.64	59.53	32.74	18.93
9	23.12	12.51	4.67	24.25	13.31	4.63	44.26	24.59	8.62	48.49	30.82	15.32
10	13.49	7.82	2.96	14.16	8.01	3.30	28.33	16.03	6.60	59.60	32.74	18.83
11	8.24	6.07	4.48	8.93	6.40	5.18	17.91	12.81	10.37	53.58	31.65	23.83

Table 6.21 indicates the maximum tension force in the most critical stud of each SWP, as a result of the gravity and seismic loads applied on the building. SWP 1, 3, 7 and 9 exhibit one end-stud in compression and the other in tension. Also, SWP 2 has studs in tension for the CP performance objective. None of the studs in the SWP exceeds the axial tension strength, which is 97.38 kN. The stud forces predicted by linear analysis are slightly larger than the forces predicted by pushover analysis.

Table 6.21. Tension force in most critical stud of each SWP, kN

SWP	Performance objective											
	OP			IO			LS			CP		
	Storey			Storey			Storey			Storey		
	1	2	3	1	2	3	1	2	3	1	2	3
1	2.36	0.00	0.00	6.70	3.59	0.95	12.79	6.91	1.86	70.05	38.80	19.42
2	2.45	0.00	0.00	6.85	3.61	0.91	13.08	6.95	1.79	70.81	38.88	19.43
3	0.00	0.00	0.00	0.00	0.00	0.00	0.00	0.00	0.00	49.26	29.44	22.47
7	0.00	0.00	0.00	0.00	0.00	0.00	0.00	0.00	0.00	49.29	28.93	22.43
9	2.36	0.00	0.00	6.70	3.59	0.95	12.79	6.91	1.86	70.05	38.80	19.42

From the results of the spectrum-based pushover analysis, it is observed that the building satisfies all seismic requirements. The four performance objectives are deemed to be satisfied since the inter-storey drifts and lateral strengths for the SWP are smaller than the limit values. Therefore, the PBD assessment for seismic forces is completed, and the lateral design of the building does not require modification.

According to the pushover and linear analyses results, the prediction of the lateral forces in the SWP, and forces in the studs are not significantly affected by the type of analysis used. Conversely, the difference in the prediction of the lateral displacements by both approaches is significantly large. Therefore, CFS buildings can be designed for the strength limit state, according to seismic codes, with sufficient accuracy by linear analysis. However, the PBD assessment of a CFS building must not be carried out by linear analysis since the acceptance criteria are established as functions of the displacements. In summary, then, if linear analysis is employed to assess the seismic behaviour of a CFS building, the results can lead to inappropriate seismic designs.

6.3.2. Example 5. Five-Storey Building

The PBD assessment of the building in Example 3 is conducted with the seismic loads applied in the x and y directions (see Figure 6.5). Since the building is for offices, the performance objectives for ordinary structures described in Table 2.1 can be used, but a

higher level of performance is desirable. Consequently, it is designed to satisfy the performance objectives for hazardous facilities (SEAOC, 1995): OP for a 10%/50 year earthquake and IO for a 2%/50 year earthquake. These performance objectives provide the CFS building with higher performance since the considered earthquakes are the largest possible, according to code requirements. Thus, by satisfying the OP and IO performance levels it is "assured" that the building is not going to collapse, since these levels result in less damage than that of the CP performance level. The building will be built in California on a site class B, and the site coordinates are latitude 36.9°N and longitude 120°W. The seismic weight (W) of the building is 1238.24 kN, and its natural period (T) is 2.05 seconds, as computed by the procedure described in Appendix A.

The maximum target base shear ($V_{b\,\max}$) is listed in Table 6.22 as 251.78 kN, representing the maximum lateral loads applied on the building for the pushover analysis. In Table 6.23, the seismic loads for each storey are defined by the lateral load distribution coefficients C_{vx} (Eq. 5.11), for exponent κ =1.75 since the building's natural period is larger than 0.5 seconds and smaller than 2.5 seconds.

Table 6.22. Target base shears in the *x* direction

PO	S_S	S_1	S_{MS}	S_{M1}	S_{DS}	S_{D1}	T_o	T_s	S_a	V_b
	(g)						(sec)		(g)	(kN)
OP	0.290	0.140	0.290	0.140	0.193	0.093	0.097	0.483	0.102	**339.19**
IO	0.500	0.230	0.500	0.230	0.333	0.153	0.092	0.460	0.179	**592.07**

Table 6.23. Lateral loads in the building in the *x* direction

Storey, x	h (m)	w (kN)	C_{vx}	F_x (kN)
1	2.85	642.03	0.054	**31.80**
2	5.70	642.03	0.122	**72.00**
3	8.55	642.03	0.196	**116.12**
4	11.40	642.03	0.275	**163.00**
5	14.25	633.23	0.353	**209.15**
	Σ	**2090.06**	**1.0**	**592.07**

The dead gravity loads are calculated from the self-weight of the building, and the live gravity loads are specified by ASCE/SEI 7 (2005) for office buildings: Dead load (D) = 1.3 kN/m^2 ; Live load (L) = 2.40 kN/m^2 ; Live load roof (Lr) = 0.96 kN/m^2 .

The factored gravity loads applied on the first two storeys of the building are computed by Eq. (6.1) as $1.2(1.1)+2.4=3.72kN/m^2$. Also from Eq. (6.1), the factored gravity load applied on the roof of the building is computed as $1.2(1.1)=1.32kN/m^2$.

Table 6.24 presents the inter-storey drifts of the SWP, which are computed in the local *x* direction of the SWP (see Figure 4.2). In the first row of the table are the limit drifts associated with the OP and IO performance levels, computed by multiplying the height of the panels by the limit drift ratios in Section 6.4. According to Table 6.24, both performance objectives are not satisfied, since the SWP inter-storey drifts are much larger than the limit drifts. Comparing the lateral drifts predicted by the pushover analysis and those predicted by the linear analysis, it can be noted that the lateral drifts obtained with pushover analysis are much larger. The inter-storey drifts and lateral displacements for SWP 1 predicted by both approaches are depicted in Figure 6.9.

Table 6.24. SWP inter-storey drift in the *x* direction, mm

SWP	OP (Limit: 5.70 mm)					IO (Limit: 28.5 mm)				
	Storey					Storey				
	1	2	3	4	5	1	2	3	4	5
1	11.25	11.97	11.80	10.29	8.11	41.11	53.60	38.29	25.71	17.27
5	11.25	11.97	11.79	10.29	8.11	41.07	53.55	38.26	25.71	17.28
13	11.25	11.96	11.78	10.29	8.09	41.10	53.56	38.27	25.71	17.24
17	11.25	11.95	11.79	10.28	8.09	41.06	53.51	38.25	25.70	17.24

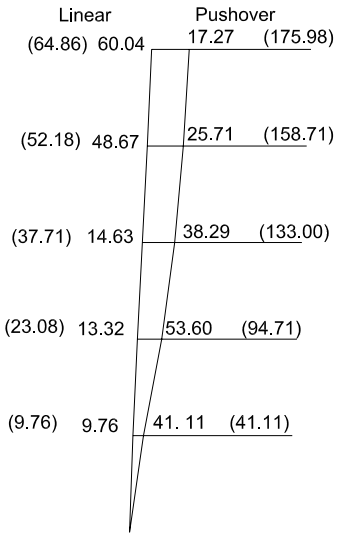

Figure 6.9. Inter-storey drifts and displacements of the SWP 1: Linear and pushover analysis

Listed in Table 6.25 is the stiffness degradation coefficient λ for each SWP, which is computed using Eq. (4.52). For this example, the SWP in the first and second storeys have failed for the IO performance objective since their λ value is equal to zero, and the SWP on the third storey are at a point of imminent failure.

Table 6.25. SWP stiffness degradation coefficient λ

SWP	OP					IO				
	Storey					Storey				
	1	2	3	4	5	1	2	3	4	5
1	0.13	0.17	0.22	0.30	0.45	0.00	0.00	0.02	0.10	0.28
5	0.13	0.17	0.22	0.30	0.45	0.00	0.00	0.02	0.10	0.28
13	0.13	0.17	0.21	0.29	0.43	0.00	0.00	0.02	0.10	0.28
17	0.13	0.17	0.21	0.29	0.43	0.00	0.00	0.02	0.10	0.28

The lateral strengths and lateral forces for the SWP are listed in Table 6.26. Comparing the SWP strengths and lateral forces, it is observed that lateral force acting on the SWP in the first story is larger than the SWP strength. Therefore, those SWP have failed; it is for this reason that the lateral displacements are so large. Also, it can be noted in Table 6.26 that the lateral forces predicted by the linear analysis are slightly larger than the forces predicted by the pushover analysis.

Table 6.26. SWP lateral strength P_R and lateral force P_a, kN

SWP	P_R	Lateral force, P_a									
		OP					IO				
		Storey					Storey				
		1	2	3	4	5	1	2	3	4	5
1	101.13	69.63	60.97	52.57	39.31	20.18	132.34	101.89	96.69	76.59	41.38
5	101.13	69.60	60.95	52.55	39.30	20.17	132.15	101.90	96.67	76.54	41.30
13	101.13	69.31	60.98	53.16	40.60	22.27	130.61	101.42	96.12	76.41	41.85
17	101.13	69.29	60.97	53.15	40.59	22.27	130.48	101.42	96.10	76.39	41.86

Table 6.27 indicates the maximum compression force in the most critical studs of each panel, caused by the gravity and seismic loads. In several cases, the force in the studs is greater that their strength. For all the SWP, as was found in Example 3, the largest compression force is registered at the end studs. The compression forces in the studs from the pushover analysis are larger than the compression forces from linear analysis; especially for the end-studs in the SWP that have failed, SWP 1, 5, 13 and 17, because these studs are subjected to larger forces due to the over-turning of the building.

Table 6.27. Compression force in the most critical stud of each SWP, kN

Panel	OP					IO				
	Storey					Storey				
	1	2	3	4	5	1	2	3	4	5
1	65.53	52.61	39.46	26.12	13.51	200.47	47.74	46.59	38.86	16.93
2	0.21	0.10	0.08	0.00	0.00	0.00	0.00	0.00	0.00	0.00
3	23.00	16.65	13.03	8.16	2.64	24.23	17.14	9.44	5.95	3.52
4	0.22	0.10	0.08	0.06	0.00	0.12	0.00	0.00	0.00	0.00
5	65.54	52.63	39.48	26.14	13.51	201.00	47.94	46.72	38.92	16.90
6	23.04	16.68	13.00	8.15	2.64	24.05	17.22	9.53	5.82	3.53
7	36.79	32.04	24.11	14.94	5.90	38.53	32.25	25.92	16.75	7.29
8	24.42	15.25	13.27	11.58	2.76	23.65	13.88	13.20	12.01	0.00
9	36.80	31.99	24.06	14.89	5.87	38.62	32.21	25.81	16.62	7.20
10	40.94	34.10	24.80	14.85	5.29	47.79	38.52	26.53	15.33	6.24
11	40.90	34.05	24.75	14.80	5.32	47.68	38.15	26.26	15.20	6.29
12	15.15	11.27	9.71	9.31	8.80	8.19	6.66	4.02	2.86	10.86

13	119.52	87.24	53.25	33.56	22.71	397.18	90.17	64.08	41.66	35.89
14	38.05	18.57	12.11	7.33	0.00	49.43	25.98	15.44	7.02	0.00
15	15.12	11.24	9.67	9.25	8.75	8.02	6.54	3.91	2.72	10.67
16	38.05	18.57	12.11	7.33	0.00	49.43	25.98	15.44	7.02	0.00
17	119.50	87.20	53.21	33.56	22.71	397.20	90.26	64.08	41.66	35.93
18	24.42	15.25	13.27	11.58	2.76	23.65	13.88	13.20	12.01	0.00
19	25.08	17.85	13.29	9.63	7.81	21.68	15.13	10.82	9.20	0.37
20	25.09	17.86	13.31	9.65	7.83	21.66	15.12	10.83	9.25	0.37
21	2.20	1.34	1.15	0.93	0.00	0.19	0.08	0.08	0.07	0.00
22	2.20	1.34	1.15	0.93	0.00	0.19	0.08	0.08	0.07	0.00
23	67.97	50.86	35.24	20.34	8.08	116.86	85.17	60.01	35.58	15.80
24	67.95	50.92	35.32	20.42	8.03	116.91	85.60	60.37	35.86	15.64
25	32.27	22.73	15.47	14.89	11.61	34.52	22.41	15.67	1.59	21.69
26	32.26	22.71	15.45	14.89	11.61	34.23	22.23	15.63	1.58	21.72
27	75.71	57.30	39.78	24.56	11.64	83.62	66.81	46.26	27.10	12.48
28	75.71	57.30	39.79	24.57	11.65	83.64	66.76	46.25	27.12	12.49
29	78.95	62.01	44.47	26.58	9.48	87.32	67.47	47.20	28.59	10.80
30	78.96	62.06	44.53	26.65	9.52	87.37	67.74	47.40	28.74	10.93
31	79.91	62.85	44.33	25.99	8.65	84.83	66.41	45.23	25.74	8.45
32	79.95	62.93	44.40	26.05	8.68	84.89	66.71	45.46	25.89	8.52
33	98.44	74.80	50.82	28.22	11.49	117.77	88.64	58.67	32.15	11.65
34	98.45	74.81	50.83	28.22	11.48	117.72	88.82	58.75	32.15	11.60

Table 6.28 provides the maximum tension forces in the most critical stud of each panel. According to the results obtained, the tension forces in several studs are much larger than their axial strength, especially for the studs in the SWP that have failed.

Table 6.28 Tension force in the most critical stud of each SWP, kN

Panel	OP					IO				
	Storey					Storey				
	1	2	3	4	5	1	2	3	4	5
1	81.99	49.62	29.61	3.03	N/A	335.93	82.51	60.85	32.38	26.00
2	11.40	14.12	13.34	N/A	N/A	28.76	30.66	21.43	17.98	13.23
3	N/A	N/A	N/A	N/A	4.26	N/A	N/A	N/A	N/A	3.01

4	11.40	14.12	13.34	N/A	N/A	28.76	30.66	21.43	17.98	13.23
5	81.90	49.61	29.60	3.00	N/A	335.10	82.08	60.67	32.33	26.05
6	N/A	N/A	N/A	N/A	4.26	N/A	N/A	N/A	N/A	3.09
12	5.12	7.83	N/A	N/A	5.85	12.68	15.13	13.28	11.41	7.19
13	34.07	27.08	N/A	N/A	N/A	149.35	42.63	39.71	33.44	13.21
15	5.17	7.89	N/A	N/A	5.89	12.93	15.37	13.56	11.66	7.35
17	34.05	27.03	N/A	N/A	N/A	148.70	42.42	39.68	33.44	13.23
25	26.66	19.49	3.26	N/A	4.90	67.50	48.53	38.66	27.00	11.66
26	26.63	19.47	3.27	N/A	4.86	67.70	48.37	38.59	26.98	11.61

The pushover analysis in the *y* direction is conducted in the same fashion as the analysis in the *x* direction. However, since the period of the building in the *y* direction differs from the period in the *x* direction, the *y*-direction target base shears and lateral loads are different. The fundamental period of the CFS building in the *y* direction is 1.11 seconds. Tabulated in Table 6.29 are the target base shears for the specified two performance levels. Table 6.30 tabulates the lateral loads applied on each storey of the building. The pushover analysis is carried out by the same procedure as that for the previous examples.

Table 6.29. Target base shears for analysis in the *y* direction

PL	S_S	S_1	S_{MS}	S_{M1}	S_{DS}	S_{D1}	T_o	T_s	S_a	V_b
	(g)						(sec)		(g)	(kN)
OP	0.290	0.140	0.290	0.140	0.193	0.093	0.097	0.483	0.102	**339.19**
IO	0.500	0.230	0.500	0.230	0.333	0.153	0.092	0.460	0.179	**592.07**

Table 6.30. Lateral loads in the building for analysis in the *y* direction

Storey, x	*h* (m)	*w* (kN)	C_{vx}	F_x (kN)
1	2.85	642.03	0.054	**31.80**
2	5.70	642.03	0.122	**72.00**
3	8.55	642.03	0.196	**116.12**
4	11.40	642.03	0.275	**163.00**
5	14.25	633.23	0.353	**209.15**
	Σ	**2090.06**	**1.0**	**592.07**

Table 6.31 lists the lateral drifts for the SWP for the OP performance level. The lateral drifts for the IO performance level are not presented because the building has collapsed before reaching the associated lateral load level. Since the building inter-storey drifts are larger than the limit drift for the OP performance level and the building failed before reaching the IO lateral load level, the OP and IO performance objectives have not been satisfied. Therefore, the design of the building must be improved to resist the seismic forces in the *y* direction (i.e., additional reinforcement of the SWP is required).

Table 6.31. SWP inter-storey drift, mm

SWP	OP (Limit: 5.7 mm)				
	Storey				
	1	2	3	4	5
3	18.36	13.19	11.10	7.94	4.43
6	18.36	13.19	11.10	7.94	4.43
12	18.36	13.19	11.10	7.94	4.43
15	18.36	13.19	11.10	7.94	4.43
19	18.35	13.20	11.10	7.94	4.42
20	18.35	13.20	11.10	7.94	4.43

Table 6.32 gives the SWP lateral strengths P_R, lateral forces P_a, and the stiffness degradation coefficient λ found from the pushover analysis for the OP performance level. It can be observed in the table that λ is close to zero for the SWP in the first and second storeys.

Table 6.32. SWP lateral strength P_R, lateral force P_a, kN, and stiffness degradation coefficient, λ

SWP	P_R	Lateral force, P_a					λ				
		OP					OP				
		Storey					Storey				
		1	2	3	4	5	1	2	3	4	5
3	48.84	40.61	34.75	31.81	26.59	18.97	0.05	0.08	0.10	0.14	0.21
6	48.84	40.27	33.40	29.32	22.22	11.09	0.05	0.09	0.12	0.18	0.31
12	48.84	40.26	33.40	29.32	22.23	11.10	0.05	0.09	0.12	0.18	0.31

15	48.84	40.60	34.74	31.81	26.59	18.97	0.05	0.08	0.10	0.14	0.21
19	48.84	40.52	34.88	32.27	27.43	20.22	0.05	0.08	0.10	0.13	0.20
20	48.84	40.05	32.77	28.16	20.27	9.21	0.05	0.10	0.13	0.20	0.34

Listed in Table 6.33 are the maximum compression and tension forces in the most critical stud of each panel for the OP performance objective. The studs in several SWP have failed.

Table 6.33. Compression force in most critical stud of each SWP, kN

Panel	OP, Compression					OP, Tension				
	Storey					Storey				
	1	2	3	4	5	1	2	3	4	5
1	77.12	54.28	34.62	20.57	8.05	N/A	N/A	N/A	N/A	N/A
2	4.16	3.23	2.79	2.07	1.16	N/A	N/A	N/A	N/A	0.15
3	13.75	13.10	12.42	11.00	8.25	N/A	N/A	N/A	N/A	N/A
4	5.43	3.07	2.26	1.38	0.00	N/A	N/A	N/A	N/A	0.16
5	28.50	23.64	20.13	16.50	9.26	N/A	N/A	N/A	N/A	N/A
6	20.19	16.82	15.44	12.85	8.89	N/A	N/A	N/A	N/A	8.94
7	53.86	42.18	28.90	16.10	5.56	N/A	N/A	N/A	N/A	N/A
8	3.52	2.98	2.68	2.17	0.60	N/A	N/A	N/A	N/A	0.14
9	32.41	24.43	16.71	11.71	5.10	N/A	N/A	N/A	N/A	N/A
10	53.89	42.24	28.93	16.11	5.55	N/A	N/A	N/A	N/A	N/A
11	32.43	24.37	16.65	11.66	5.02	N/A	N/A	N/A	N/A	N/A
12	20.19	16.82	15.44	12.85	8.89	N/A	N/A	N/A	N/A	8.94
13	77.20	54.22	34.56	20.53	8.03	N/A	N/A	N/A	N/A	N/A
14	4.16	3.24	2.79	2.08	1.16	N/A	N/A	N/A	N/A	0.15
15	13.75	13.10	12.42	11.00	8.25	N/A	N/A	N/A	N/A	N/A
16	5.42	3.08	2.27	1.39	0.00	N/A	N/A	N/A	N/A	0.16
17	29.16	22.87	19.76	16.14	8.99	N/A	N/A	N/A	N/A	N/A
18	3.57	2.88	2.46	1.84	1.00	N/A	N/A	N/A	N/A	0.13
19	18.61	16.81	15.78	13.77	10.25	N/A	N/A	N/A	N/A	6.16
20	21.32	17.32	15.05	11.65	3.63	N/A	N/A	N/A	N/A	7.73
21	3.52	2.98	2.68	2.17	0.60	N/A	N/A	N/A	N/A	0.14
22	3.57	2.88	2.46	1.84	1.00	N/A	N/A	N/A	N/A	0.13

23	34.90	25.74	17.90	10.63	3.17	N/A	N/A	N/A	N/A	N/A
24	28.26	20.96	14.29	7.95	3.36	N/A	N/A	N/A	N/A	N/A
25	34.86	25.84	18.07	10.79	3.30	N/A	N/A	N/A	N/A	N/A
26	28.21	21.00	14.30	7.96	3.42	N/A	N/A	N/A	N/A	N/A
27	73.62	59.16	43.59	26.51	12.89	N/A	N/A	N/A	N/A	0.18
28	104.08	75.47	48.45	24.97	10.50	N/A	N/A	N/A	N/A	2.43
29	74.41	60.78	44.37	27.03	9.67	N/A	N/A	N/A	N/A	N/A
30	87.67	67.17	46.40	26.69	9.47	N/A	N/A	N/A	N/A	N/A
31	74.40	60.80	44.38	27.03	9.68	N/A	N/A	N/A	N/A	N/A
32	87.66	67.15	46.38	26.67	9.44	N/A	N/A	N/A	N/A	N/A
33	73.62	59.17	43.58	26.50	12.88	N/A	N/A	N/A	N/A	0.18
34	104.14	75.51	48.42	24.95	10.49	N/A	N/A	N/A	N/A	2.44

According to the PBD assessment of the building, conducted in the *x* and *y* directions, the building has not satisfied the OP and IO performance objectives. Therefore, the SWP in the building must be reinforced to increase both the building lateral and vertical strength capacities. To increase the building lateral strength, the screw spacing can be reduced, but if this is not sufficient then the number of SWP must be increased. To increase the vertical strength of the SWP, thicker studs can be used.

Although CFS buildings may be lighter than buildings built with other materials, such as steel, concrete and masonry, the live loads that are imposed on them are the same. As such, the lower weight of CFS buildings results in smaller seismic loads. However, an adequate number of SWP must be used in the building to resist the lateral loads.

Since CFS members are thin-walled, their axial strength is very limited. This may cause problems during the PBD of CFS buildings. In particular, it is important to pay strict attention to the design of studs for mid-rise CFS buildings.

Chapter 7

Conclusions and Recommendations

7.1. Conclusions

The principal contribution of this study is the development of a methodology for carrying out the Performance-Based Design (PBD) assessment of low and mid-rise buildings built with Cold-Formed Steel (CFS) shear wall systems. The proposed methodology includes the establishment of the acceptance criteria for Shear Wall Panels (SWP), a simplified nonlinear finite element technique for spectrum-based pushover analysis, and a stiffness degradation model for the SWP.

A primary difficulty to conduct the PBD assessment of a structural system is establishing the acceptance criteria associated with the performance levels of the structural elements. Since SWP are the primary lateral load-resistant elements in CFS buildings, the acceptance criteria are established according to the lateral drift and lateral strength of the SWP. For CFS SWP, the lateral drift ratios are 2.5%, 2.1%, 1.0% and 0.2% for the CP, LS, IO and OP performance levels, respectively. The limit drift ratios for CFS SWP are determined from experimental data, obtained by Branston et al. (2006).

A method for computing the lateral strength of the SWP is devised. The proposed method is used to evaluate the lateral strength of SWP with different sheathing and framing materials, panel dimensions, and construction details such as fastener spacing. The comparisons of the results from the proposed method and extensive experimental tests carried out by different researchers, are in good agreement. The method includes the formulation for estimating the lateral drift of SWP at the ultimate load level. According to comparisons made with experimental results, the proposed method yields better accuracy for lateral strength than for lateral displacements. Of the iterative and simplified procedures proposed for evaluating the lateral strength of SWP, the simplified procedure requires significantly less computational effort than the iterative one. As such, the

simplified procedure for evaluating the ultimate strength coefficient is an excellent alternative to design tables, such as AISI (2004). The comparison of experimental tests and predicted lateral strengths and displacements were in good agreement; the average of the ratios of experimental-to-predicted lateral strengths is 1.05 with a standard deviation of 0.11, while for lateral displacements the ratio average is 1.13 and the standard deviation is 0.19.

The predicted linear analysis results from Simplified Finite Element Analysis (SFEA) and Conventional Finite Element Analysis (CFEA) for isolated SWP of various lengths are in good agreement, except that the out-of-plane displacements are different because the CFEA models the sheathing in a way that does not fully represent the real conditions of the SWP. Whereas, the shell element properties employed for SFEA are equivalent to the SWP properties. It was found that the ratio length-to-height of the (sixteen-node) shell elements for modeling SWP should be in the range of 0.5 and 3.0. Comparisons of SWP force-displacement curves from experimental investigations and from SFEA using the proposed stiffness degradation model are in good agreement, except some difference exists in the shape of the response curve for SWP with Douglas Fir Plywood (DFP) sheathing material. This difference is caused primarily by the nonlinearity exponent in the stiffness degradation model, calibrated using different types of wood sheathing materials.

It is determined that the prediction of the displacements is affected more by the equivalent shell concept than by the number of elements in the model. However, the opposite exists for the prediction of the studs' axial forces. The comparison of the results of linear SFEA and CFEA for example three-storey buildings are in good agreement for both the lateral displacements and lateral forces in the SWP. However, some differences exist for the axial forces in the studs and displacements in the *z* direction: for SWP in the direction of analysis, the difference between the predicted stud axial forces is large, while the difference for the displacements in the *z* direction is large. It is not recommended to use the predicted stud forces for final design. Nevertheless, these differences do not otherwise affect the PBD assessment, since the SWP acceptance criteria are evaluated solely as functions of inter-storey drifts and lateral forces.

For linear analysis of an example five-storey building, the results from SFEA and CFEA show similar tendencies in the predicted displacements and SWP lateral forces. However, there are large differences in the predicted forces in the studs due to the limitations of the model proposed in Section 4.4. Another reason of the difference in the predictions is that since the models created in SAP2000 cannot match the conditions as accurately as the SFEA models, they are not reliable to validate the results of SFEA. Therefore, specialized software for finite element analysis should be employed to validate the results of SFEA in future studies.

For the example three-storey building considered, the lateral and axial strengths of SWP are sufficient to resist the applied loads. For the five-storey building, the SWP and studs in the first and second storey failed since those elements did not have the sufficient strength to resist the loads applied on the building. Although only two different building models were analyzed by this study, it is quite likely that similar behaviour may occur for other CFS buildings. An appropriate design should include a large enough number of SWP and load-bearing wall panels that result in a suitable distribution of the gravity loads in the building, and sufficient lateral strength.

Linear analysis can be consistently employed for carrying out the lateral seismic strength design of SWP since there is no significant difference in their lateral forces predicted by linear and pushover analysis. This suggests that linear analysis may be effectively used for preliminary sizing of CFS buildings. However, the results of this study suggest that linear analysis greatly underestimates the lateral drifts and the stud axial forces for SWP and, therefore, that pushover analysis is required to carry out the PBD assessment of CFS buildings.

The main feature of SFEA is the limited number of elements it requires to model a CFS building (e.g., for the example five-storey building, CFEA required 3480 four-node shell elements and 2580 frame elements, whereas SFEA required only 260 sixteen-node shell elements). The reduction in pushover analysis computing time using SFEA is very

significant. It can be concluded that the proposed methodology provides an efficient and practical technique for the PBD assessment of CFS buildings.

7.2. Recommendation for Future Work

The use of pushover analysis to assess the seismic behaviour and performance-based design of CFS buildings has notable advantages over prescriptive design based on seismic codes. The proposed methodology for carrying out the PBD assessment of CFS buildings can be extended to include account for other types of materials and elements, such steel columns and girders. Combining different types of structural elements may provide other advantages, such as the capability for designing high-rise composite hot-rolled and cold-formed steel buildings. In addition, though not explicitly dealt with herein, the PBD process itself can be optimized to find more economical and safer designs. Mentioned in the following are aspects of this work that extend or increase the robustness of the proposed methodology developed by this study.

- Develop optimization criteria to implement the performance-based design process for CFS buildings.

  An optimization algorithm can improve the methodology for the PBD of CFS buildings, producing more efficient designs. Different approaches are found in the literature for carrying out the PBD optimization of structural systems, such as those published by Gong (2003) and Grierson et al. (2006) for hot-rolled steel buildings, which may form a basis for PBD optimization of CFS buildings.

- Investigate the interaction of cold-formed steel shear wall panels with other structural elements, such as steel columns and beams.

  In construction practice, it is common to combine CFS SWP with structural steel elements. The interaction of these two material types in an integrated structural design context presents an interesting challenge. For example, the aforementioned method for carrying out the PBD of hot-rolled steel buildings can be combined

with the CFS methodology presented in this study to provide for the PBD of composite hot-rolled and cold-formed steel high-rise buildings.

- Extend the single-mode pushover analysis employed by this study to multi-mode or modal pushover analysis.

  The single-mode pushover analysis is appropriate for buildings with a predominant fundamental period of vibration, such that the building response is not affected by the participation of higher-frequency vibration modes. If higher modes do affect the response of a building, however, then modal pushover analysis should be used to assess seismic behaviour. FEMA 450 (2003) has established the basis for modal pushover analysis, which has been successfully implemented in other studies for a variety of structural systems, such as by Gong (2003) for multi-storey steel frames.

- Account for new generation PBD principles to establish performance objectives based on risk due to earthquake-induced losses.

  New generation PBD (ATC, 2005) provides for the establishment of performance objectives in terms of losses, which are directly associated with cost.

- Account for the shear buckling mode of failure in cold-formed steel shear wall panels.

  Since some construction materials used as sheathing for CFS SWP are prone to shear buckling, this mode of failure should be accounted for when determining the lateral strength of CFS SWP.

References

AISI. (2004). Standard for Cold-Formed Steel Framing-Lateral Design. *American Iron and Steel Institute*, Washington, DC.

AISI. (1998). Shear Wall Design Guide. *American Iron and Steel Institute*, Technical Data RG-9804, Washington, DC.

Argyris, J. H. (1982). An Excursion Into Large Rotations. *Computer Methods In Applied Mechanics and Engineering*, Vol. 32(85-155).

ATC. (2005). Guidelines for Seismic Performance Assessment of Buildings, 25% Complete Draft. *Applied Technology Council*; Redwood City, California.

ATC 58-2. (2003). Preliminary Evaluation of Methods for Defining Performance.

Bathe, K. J. (1996). Finite Element Procedures. *Prentice Hall*.

Bathe, K. J., and Bolourchi, S. (1982). A Geometric and Material Nonlinear Plate and Shell Analysis. *Computers and Structures*; Vol. 11, pp. 23-48.

Bertero, R. D., and Bertero, V. V. (2002). Performance-based seismic engineering: the need for a reliable conceptual comprehensive approach. *Earthquake Engineering and Structural Dynamics;* Vol. 31, pp. 627–652.

Brandt, G. D. (1982). Rapid Determination of Ultimate Strength of Eccentrically Loaded Bolt Groups. *Engineering Journal*, AISC.

Branston, A. E., Boudreault, F. A., Chen, C. Y. and Rogers, C. A. (2004). Light Gauge Steel Frame / Wood Panel Shear Wall Test Data: Summer 2003. *Research*

Report, Department of Civil & Applied Mechanics, McGill University, Montreal, Canada.

Branston, A.E., Chen, C.Y., Boudreault, F.A., and Rogers, C.A., (2006). Testing of Light-Gauge Steel Frame - Wood Structural Panel Shear Walls. *Canadian Journal of Civil Engineering,* Vol. 33 No. 5, 573-587.

CANPLY. (2003). Plywood Design Fundamentals. *Canadian Plywood Association*; Vancouver, BC.

Chopra, A. K., and Goel, R. K. (2002). A modal pushover analysis procedure for estimating seismic demands for buildings. *Earthquake Engineering and Structural Dynamics;* Vol. 31, pp. 561–582.

COLA-UCI. (2001). Report of a testing program of wall-framed walls with wood-sheathed shear panels. *Structural Engineers Association of Southern California*, *COLA-UCI Light Frame Committee.*

COMPLAY. (1999). Design Capacities of APA Performance Rated Structural – Use Panels. *The Engineered Wood Association;* Tacoma, WA.

Cook, R. D, Malkus, D. S., and Plesha, M. E. (1989). Concepts and Applications of Finite Element Analysis. *John Wiley and Sons Ltd*.

CSA S16-01.(2003). Handbook of Steel Construction. Canadian Institute of Steel Construction. Toronto, Ontario.

ER-6151. (2003). Sure-board 200 series structural panels. *ICC Evaluation Service, Inc*. Legacy report. Retrieved July 15, 2006, from http://www.icc-es.org/.

FEMA 273. (1997). NEHRP Guidelines for the Seismic Rehabilitation of Buildings. *Federal Emergency Management Agency*.

FEMA 274. (1997). NEHRP Commentary on the Guidelines for the Seismic Rehabilitation of Buildings. *Federal Emergency Management Agency*.

FEMA 450. (2003). NEHRP Recommended provisions for Seismic Regulations for new Buildings and other Structures. *Federal Emergency Management Agency*.

Filiatrault, A., and Folz, B. (2002). Performance-Based Seismic Design of Wood Framed Buildings. *Journal of Structural Engineering*, ASCE; Vol. 128 No. 1, pp. 39-47.

Fulop, L., and Dubina, D. (2004). Performance of wall-stud cold-formed shear panels under monotic and cyclic loading Part I: Experimental research. *Thin-Walled Structures*; Vol. 42, pp. 321-338.

Fulop, L., and Dubina, D. (2004b). Performance of wall-stud cold-formed shear panels under monotonic and cyclic loading Part II: Numerical modelling and performance analysis. Thin-Walled Structures; Vol. 42, pp. 339-349.

GA-235. (2002). Gypsum Board Typical Mechanical and Physical Properties. *Gypsum Association*; Washington, DC.

Gad, E.F., Chandler, A. M., Duffield, and C.F., Stark, G. (1999). Lateral Behaviour of Plasterboard-Clad residential Steel Frames. *Journal of Structural Engineering*, ASCE; pp. 32-39.

Ghobarah, A. (2001). Performance-based deign in earthquake engineering: State of development. *Engineering Structures;* Vol. 23, pp. 878-884.

Gong, Y. (2003). Perfomance-Based Design of Steel Building Frameworks Under Seismic Loading. *University of Waterloo,* PhD Thesis.

Grierson, D.E., Xu, L., and Liu, Y. (2005). Progressive-Failure Analysis of Buildings Subjected to Abnormal Loading. *Computer-Aided Civil and Infrastructure Engineering;* Vol. 20, pp. 155-171.

Grierson, D.E., Gong, Y., and Xu, L. (2006). Optimal performance-based seismic design using modal pushover analysis. *Journal of Earthquake Engineering;* Vol. 10, pp. 73-96.

Hasan, R., Xu, L., and Grierson, D. E. (2002). Push-over analysis for performance-based seismic design. *Computers and Structures;* Vol. 80, pp. 483-2493.

Krawinkler, H., and Senervitna, G. D. P. K. (1998). Pros and cons of a pushover analysis of seismic performance evaluation. *Engineering Structures;* Vol. 20, pp. 42-464.

Lee K., and Foutch D. A. (2002). Performance evaluation of new steel frame buildings for seismic loads. *Earthquake Engineering and Structural Dynamics;* Vol. 31, pp. 653-670.

Lee Y.K. (1999). Behavior of Gypsum-Sheathed Cold-Formed Steel Wall Stud Panels. *Oregon State University,* PhD Thesis.

Liew, Y. R., and Chen, H. (2004). Direct analysis for performance-based design of steel and composite structures. *Prog. Struct. Engng Mater*; Vol. 6, pp. 213-228.

NAHBRC. (1997). Monotonic tests of cold-formed steel shear walls with openings. Report prepared by NAHB Research Center, Inc. AISI; Washington, DC.

NBCC, (2005). National Building Code of Canada. *Canadian Commission on Building and fire Codes*. National Research Council; Ottawa, Ontario.

Okasha, A. F. (2004). Performance of steel frame / wood sheathing screw connections subjected to monotonic and cyclic loading. *University of McGill,* MSc Thesis.

OSB. (1995). OSB Design Manual, Design Rated Oriented Strand Board. *Structural Board Association*, Willowdale, ON.

S136-01. (2002). North American Specification for the Design of Cold-formed Steel Structural Members. *Canadian Standards Association*.

SAP2000. (2006). Integrated software for structural analysis and design. *Computers and Structures Inc*; Berkeley, California.

SEAOC. (1995). VISION 2000 – A Framework for Performance Based Earthquake Engineering. *Structural Engineers Association of California*; Vol. 1.

SEAOC. (1997). Standard Method of Cyclic (reversed) Load Test for Shear Resistance of Framed Walls for Buildings. *Structural Engineers Association of California*; Whittier, USA.

SEAOC and COLA-UCI. (2001). Report of a Testing Program of Light-Framed Walls with Wood-Sheathed Shear Panels. *Structural Engineers Association of California, COLA-UCI Light Frame Test Committee, and Department of Civil Eng. University of California, Irvine*. Research award: FEMA-DR-1008-8011.

SODA (1999). Structural Optimization Design Analysis. *Acronym Software, Inc.* Waterloo, On., Canada.

Serrette, R. L., Morgan, K. A., and Sorhouet, M. A. (2002). Performance of Cold-Formed Steel-Framed Shear Walls: Alternative Configurations. *Santa Clara University*; Final Report LGSRG-06-02.

Serrette, R. L, and Ogunfunmi, K. (1996). Shear Resistance of Gypsum-Sheathed Light-Gauge Steel Stud Walls. *Journal of Structural Engineering*, ASCE; pp. 383-389.

SSMA. (2001). Product technical information. *Steel Stud Manufacturers Association,* Report ICBO ER-4943P. Retrieved January 10, 2004, from http://www.ssma.com.

Sureboard (2004). Product technical information. *Sure-Board, Intermat, Inc.* http://www.sureboard.com

Telue, Y.K., and Mahendran, M. (2001). Behaviour of cold-formed steel wall frames lined with plasterboard. *Journal of Constructional Steel Research*; Vol. 57, pp. 435-452.

Thomas, W.H. (2004). Poisson's ratios of an oriented strand board. Wood Science and Technology, Springer Berlin / Heidelberg; Vol. 37, pp. 259-268.

Troitsky, M., S. (1976). Stiffened Plates, Bending, Stability and Vibrations. *Elsevier Scientific Publishing Company*.

USGS. (2002). Interpolated Probabilistic Ground Motion for the Conterminous 48 States, 2002 Data. U.S. Geological Survey Earthquake Hazards program. Retrived August 2, 2006, from http://earthquake.usgs.gov/research/hazmaps/.

Zalka, K. A. (2001). A simplified method for calculation of the natural frequencies of wall-frame buildings. *Engineering Structures;* Vol. 23, pp. 1544-1555.

Zou, X. K., and Chan, C. M. (2005). Optimal Seismic Performance-Based Design of Reinforced Building using Nonlinear Pushover Analysis. *Engineering Structures;* Vol. 27, pp. 1289-1302.

Appendix A

Simplified method of calculating the structure period of vibration

Zalka (2001) developed a simplified method for calculating the natural period of vibration of structures built with frameworks and shear walls. It is assumed that the buildings have a uniform layout in all the storeys, and uniform geometry along their height. The method transforms each frame, including shear walls in the direction under consideration, into a column with equivalent mass and stiffness. Then, the natural period is computed for the equivalent column. Three types of building deformation are considered in the analysis: shear, full-height bending, and full-height bending of individual columns.

Several modifications are needed to use Zalka's method for CFS buildings. Instead of computing the frequency for each plane frame, the frequency is computed for the entire three-dimensional building simultaneously. This is accomplished by taking into account all the elements in the building, instead of only a plane frame. The stiffness equations are modified to include the stiffness of the SWP made of CFS. The method still requires that the building plan distribution is the same for all the storeys. The procedure to determine the period of vibration of CFS buildings with frame elements and SWP is described in the following.

1. The global shear stiffness associated with the building beams and SWP is,

$$K_b = \sum_i^{n_{co}} 12 \frac{E_b I_{b,i}}{l_i h} + \sum_i^{n_p} 12 \frac{G_{s,i} A_S}{1.2h} \qquad \textbf{(A. 1)}$$

where: i is the number of the beams; the parameters n_{co} and n_p are respectively the numbers of columns and SWP in the building; the parameters E_b and I_b are respectively the modulus of elasticity and moment of inertia for the beams; l is the SWP length; h is the storey height; G_s is the sheathing shear modulus of elasticity; and A_S is the sheathing cross-sectional area.

2. The columns' shear stiffness is given by,

$$K_c = \sum_{i}^{n_{co}} 12 \frac{E_c I_{c,i}}{h^2} \quad \textbf{(A. 2)}$$

where I_c is the column i moment of inertia, and E_c is the column modulus of elasticity.

3. The stiffness combination factor is calculated as,

$$r_c = \frac{K_c}{K_c + K_b} \quad \textbf{(A. 3)}$$

4. The building's shear stiffness is,

$$K = r_c K_b \quad \textbf{(A. 4)}$$

5. The building's shear frequency is given by,

$$f_{s'}^2 = \frac{1}{(4H)^2} \frac{r_f^2 K}{m} \quad \textbf{(A. 5)}$$

where: H is the building height; m is the mass density per unit of the building height; and r_f is a reduction factor whose value depends on the number of storeys, (see Table A.1).

6. The bending frequency associated with the building full height is defined as,

$$f_g^2 = \frac{0.313 r_f^2 E_c I_g}{H^4 m} \quad \textbf{(A. 6)}$$

where

$$I_g = \sum_i^{n_{co}} A_{c,i} d_{f,i}^2 \quad \textbf{(A. 7)}$$

in which A_c is the column cross-sectional area, and d_f is the distance from the column centroid to the floor plan centroid.

7. The shear stiffness effectiveness factor is,

$$s^2 = \frac{f_g^2}{f_{s'}^2 + f_g^2} \quad \textbf{(A. 8)}$$

8. The building effective shear stiffness is,

$$K_e = s^2 K_j \quad \textbf{(A. 9)}$$

9. The building lateral frequency associated with shear deformation is,

$$f_s^2 = \frac{1}{(4H)^2} \frac{r_f^2 K_e}{m} \quad \textbf{(A. 10)}$$

10. The building equivalent bending stiffness, taking into account the columns and SWP, is given by,

$$EI = EI_{Columns} + EI_{SWP} = E_c I_c r + \sum_{n_p} \left(E_{Sy} I_S + \sum_{Studs} E_F I_F \right) \quad \textbf{(A. 11)}$$

where E_{Sy} is the sheathing modulus of elasticity in the y direction such that

$$I_S = \frac{t_p l^3}{12} \quad \textbf{(A. 12)}$$

11. The frequency associated with the bending stiffness of the building is defined as,

$$f_b^2 = \frac{0.313 r_f^2 EI}{H^4 m} \quad \textbf{(A. 13)}$$

12. The non-dimensional parameter is,

$$k_p = H \sqrt{\frac{K_e}{EI}} \quad \textbf{(A. 14)}$$

13. The building natural frequency is calculated as,

$$f = \sqrt{s \cdot f_b^2 \left(\frac{\eta_s^2}{0.313} - \frac{k_p^2}{5} - 1 + \frac{1}{s} \right) + f_s^2} \qquad \textbf{(A. 15)}$$

where η is obtained from Table A.2.

14. The building lateral period of vibration is,

$$T = \frac{1}{f} \qquad \textbf{(A. 16)}$$

If the CFS building being analyzed is built with SWP only, without frame elements, the procedure of analysis is slightly different. In fact, the stiffness equations are the only difference with respect to the procedure described in the foregoing for buildings that also include frame elements. To determine the natural frequency of vibration of a building having only SWP, calculate the following quantities.

1. The global shear stiffness associated with the building's SWP is,

$$K_b = \sum_i^{n_p} 12 \frac{G_{s,i} A_s}{1.2h} \qquad \textbf{(A. 17)}$$

2. The building equivalent bending stiffness including columns and SWP is,

$$EI = EI_{SWP} = \sum_{n_p} \left(E_{Sy} I_S + \sum_{Studs} E_F I_F \right) \qquad \textbf{(A. 18)}$$

3. The frequency associated with the bending stiffness of the building is given by,

$$f_b^2 = \frac{0.313 r_f^2 EI}{H^4 m} \qquad \textbf{(A. 19)}$$

4. The building lateral frequency associated with shear deformation is computed as,

$$f_s^2 = \frac{1}{(4H)^2} \frac{r_f^2 K_b}{m} \qquad \textbf{(A. 20)}$$

5. The non-dimensional parameter is,

$$k_p = H\sqrt{\frac{K_b}{EI}} \qquad \textbf{(A. 21)}$$

6. The building lateral frequency is defined as,

$$f = \sqrt{s \cdot f_b^2\left(\frac{\eta_s^2}{0.313} - \frac{k_p^2}{5} - 1 + \frac{1}{s}\right) + f_s^2} \qquad \textbf{(A. 22)}$$

7. The building lateral period of vibration is,

$$T = \frac{1}{f} \qquad \textbf{(A. 23)}$$

Table A. 1 Reduction factor r_f, Zalka (2001).

n[1]	1	2	3	4	5	6	7
r_f	0.493	0.653	0.770	0.812	0.842	0.863	0.879
n[1]	8	9	10	11	12	13	14
r_f	0.892	0.902	0.911	0.918	0.924	0.929	0.934
n[1]	15	16	18	20	19	20	21
r_f	0.938	0.941	0.947	0.952	0.961	0.967	0.98
n > 50	$\sqrt{n}/(n+2.06)$						

[1] Building number of storeys

Table A. 2. Frequency parameter, Zalka (2001)

k_p	η_s	k_p	η_s	k_p	η_s	k_p	η_s	k_p	η_s
0.0	0.5596	4.5	1.465	9.5	2.680	14.5	3.913	20	5.278
0.1	0.5606	5.0	1.586	10.0	2.803	15.0	4.036	30	7.769
0.5	0.5851	5.5	1.706	10.5	2.926	15.5	4.160	40	10.26
1.0	0.6542	6.0	1.827	11.0	3.049	16.0	4.284	50	12.76
1.5	0.7511	6.5	1.949	11.5	3.172	16.5	4.408	60	15.26
2.0	0.8628	7.0	2.070	12.0	2.295	17.0	4.532	70	17.26

2.5	0.9809	7.5	2.192	12.5	3.418	17.5	4.656	80	20.26
3.0	1.1014	8.0	2.313	13.0	3.542	18.0	4.781	90	22.76
3.5	1.2226	8.5	2.435	13.5	3.665	18.5	4.905	100	25.26
4.0	1.3437	9.0	2.558	14.0	3.789	19.0	5.029	>100	kp/4

Appendix B

Calibration of the α_b and α_v coefficients

The purpose of the coefficients α_b and α_v, introduced in Section 3.3, is to transform the elastic stiffness of the sheathing to the secant stiffness at the ultimate load and displacement level. Thus, the framing contribution to the SWP lateral strength is accounted for at the ultimate limit state. The coefficients α_b and α_v have been calibrated using experimental data obtained by Branston et al. (2006) from monotonic and cyclic testing of SWP. The results reported by Branston for a SWP length of 1219mm (4 ft) have been used in the calibration. The results for other SWP lengths have not been used because the variation in length of the SWP is accounted by the parameter η, which is less than unity for SWP lengths smaller than 1219 mm (4ft), and larger than unity otherwise.

Listed in Table B.1 are the SWP stiffnesses at the ultimate load level, K, derived from experimental data (Branston et al. 2006). Also, presented in the table are the elastic shear and bending stiffnesses of the SWP, K_v and K_b, respectively. The calibration of the coefficients α_b and α_v has been carried out "manually" since there are three variables that affect the stiffness reduction of the SWP, and the author did not have the appropriate software to make the calibration on a computer. These variables are screw spacing s_C, number of screws n_C, and ultimate strength factor C_u.

Since the experimental stiffness of the SWP at the ultimate load level is known, as is the elastic stiffness of the SWP, several equations which account for the variables that affect the stiffness of the SWP were proposed. Then, it was found that the equations that fit best the experimental data are Eqs. (3.10) and (3.11) repeated below,

$$\alpha_V = \left(\frac{C_u}{3.3 \cdot n_C} \right)^{1.8} \cdot \left(\frac{6in}{s_C} \right)$$

$$\alpha_B = \left(\frac{6}{C_u}\right)^2 \cdot \left(\frac{6in}{s_C}\right)^{\frac{1.3 \cdot n_C}{C_u}}$$

Presented in the fist column of Table B.1 is a description of the specimens tested by Branston (2004), in the second to the fourth columns are the SWP experimental lateral resistance, maximum displacement and ultimate lateral stiffness. The K_v and K_b values in the table are the elastic shear and bending stiffnesses of the SWP, computed from principles of mechanics. The ultimate lateral stiffness of the SWP, K_S , is computed by multiplying the elastic stiffnesses K_v and K_b by the coefficients α_b and α_v, respectively, as described for Eq. (3.8). Listed in the last column is the ratio of the experimental and predicted ultimate lateral stiffness. Also given are statistical results obtained, such as average of the predicted-to-experimental ratio, the standard deviation and the correlation.

Table B.1 Calibration of coefficients α_b and α_v using experimental data (Branston, 2004)

		Assembly maximum:											
		Resistance	Disp.	K	C_u	n_C	s_C	α_v	α_b	K_v	K_b	K_S	K_S/K
Specimen		kN/m	mm	kN/mm						kN/mm			
1 – A,B,C	CSP	16.6	60.6	0.27	39.04	74	102	0.06	0.06	2.59	2.88	0.33	1.20
5 – A,B,C,D	DFP	23.8	60.6	0.39	39.04	74	102	0.06	0.06	4.30	4.08	0.50	1.27
7 – A,B,C	CSP	12.7	50.7	0.25	26.19	50	152	0.04	0.05	2.59	2.88	0.25	0.98
9 – A,B,C	CSP	25.1	61	0.41	51.89	98	76	0.07	0.07	2.59	2.88	0.40	0.98
11 – A,B,C	DFP	16	54.8	0.29	26.19	50	152	0.04	0.05	4.30	4.08	0.37	1.27
13 – A,B,C[2]	DFP	29.7	58.2	0.51	51.89	98	76	0.07	0.07	4.30	4.08	0.62	1.21
21 – A,B,C	OSB	13.2	41.1	0.32	26.19	50	152	0.04	0.05	4.24	3.41	0.33	1.04
23 – A,B,C	OSB	19.3	39.5	0.49	39.04	74	102	0.06	0.06	4.24	3.41	0.45	0.93
25 – A,B,C	OSB	23.5	40.7	0.58	51.89	98	76	0.07	0.07	4.24	3.41	0.56	0.98
4 – A,B,C	CSP	17.5	-15.3	0.33	39.04	74	102	0.06	0.06	2.59	2.88	0.33	1.00
6 – A,B,C	DFP	22.6	-19.6	0.41	39.04	74	102	0.06	0.06	4.30	4.08	0.50	1.21
8 – A,B,C	CSP	11.9	-10.6	0.26	26.19	50	152	0.04	0.05	2.59	2.88	0.25	0.96
10 – A,B,C	CSP	26.2	-23.1	0.51	51.89	98	76	0.07	0.07	2.59	2.88	0.40	0.78
12 – A,B,C	DFP	14.6	-13.4	0.31	26.19	50	152	0.04	0.05	4.30	4.08	0.37	1.20
14 – A,B,C,D	DFP	29.7	-26.2	0.53	51.89	98	76	0.07	0.07	4.30	4.08	0.62	1.17
22 – A,B,C	OSB	11.7	-10.5	0.31	26.19	50	152	0.04	0.05	4.24	3.41	0.33	1.06
24 – A,B,C	OSB	17.2	-15.7	0.51	39.04	74	102	0.06	0.06	4.24	3.41	0.45	0.89
26 – A,B,C	OSB	23.5	-22.4	0.67	51.89	98	76	0.07	0.07	4.24	3.41	0.56	0.85
												Average	1.05
												Standard Deviation	0.15
												Correlation	0.85

Appendix C

Calibration of the β exponent

In the stiffness degradation model presented in Section 4.6, the loss of lateral stiffness of the SWP is determined as the ratio of the lateral loads applied on the SWP over their lateral strength. Since the loss of stiffness of the SWP is not linear, the exponent β has been introduced in Eq. 4.52 to characterize the nonlinear loss of SWP stiffness. It has been observed in experimental tests (Rogers, 2004) that the nonlinear stiffness degradation of SWP depends on several factors, the most important being the sheathing material and the screw spacing on the edge of the panel. However, the parameter β is calibrated taking into account the screw spacing only. The stiffness degradation model is intended to be used for any type of wood sheathing, so the exponent β is calibrated using the lowest force-displacement values obtained from the experimental testing for different types of wood sheathing materials.

Since the ratio of lateral force over lateral strength (P_a/P_R) in Eq. 4.52 is linear, the first condition that β must satisfy to characterize the nonlinear behaviour similar to that obtained from the experimental results is that it must be less than unity (otherwise the shape of the curve would be convex). Another condition is that β must decrease as the screw spacing increases because, as observed in the experimental data, the "radius" of the force-displacement curve becomes smaller as the screw spacing increases. With these two conditions in mind, it is determined that the screw spacing must be a reciprocal parameter in the equation for β. Thus β can be expressed as,

$$\beta = x / s_C \qquad \textbf{(C. 1)}$$

where s_C is the screw spacing on the edge of the panel, and x is a constant to be found from the experimental results. Depicted in Figures C.1, C.2, and C.3 are the experimental plots for the normalized force-displacement curves for screw spacings of 76 mm (3 in), 101 mm (4 in), and 152 mm (6 in), respectively. Then, different values for the constant x were tested, and the value that fits best with the experimental results

was found to be x = 38.1 mm (1.5 in). Figures C.1, C.2 and C.3 also show the normalized force-displacement curve predicted for β.

The experimental data used to calibrate β accounted for SWP lengths of 609 mm (2 ft), 1219 mm (4 ft), and 2438 mm (8 ft), and height of 2438 mm (8ft). Also, the three types of sheathing OSB, CSP and DFP were accounted for. For all SWP, the sheathing was attached to the framing with No. 8 screws.

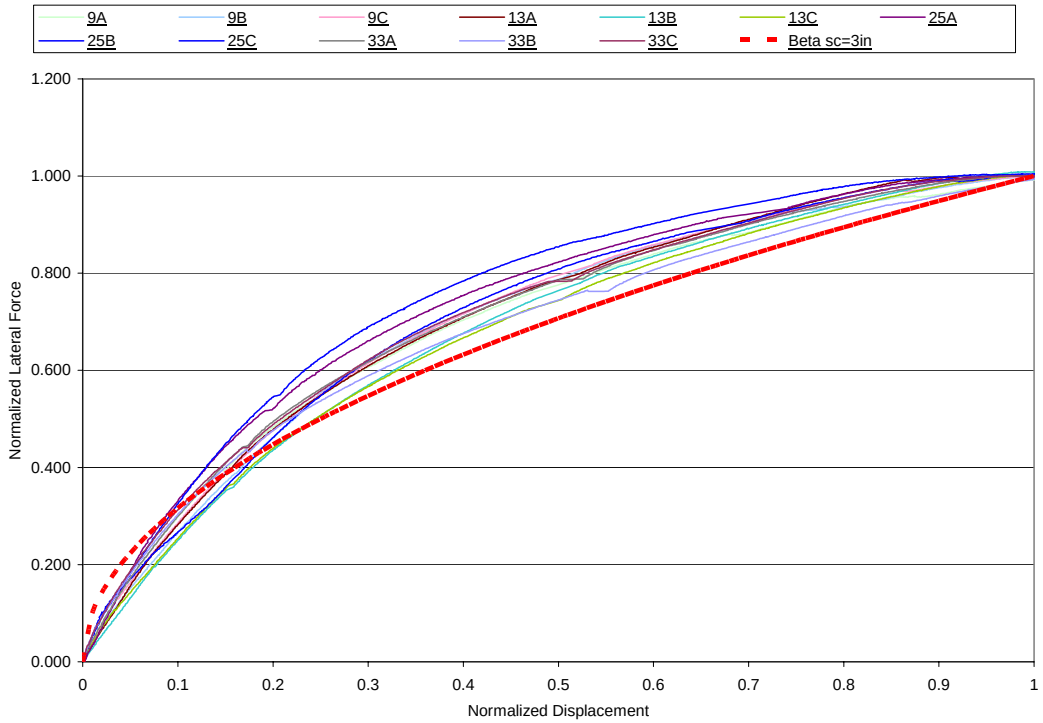

Figure C.1 Experimental (Branston et al., 2004) vs. predicted SWP response for screw spacing s_C=76 mm (3 in)

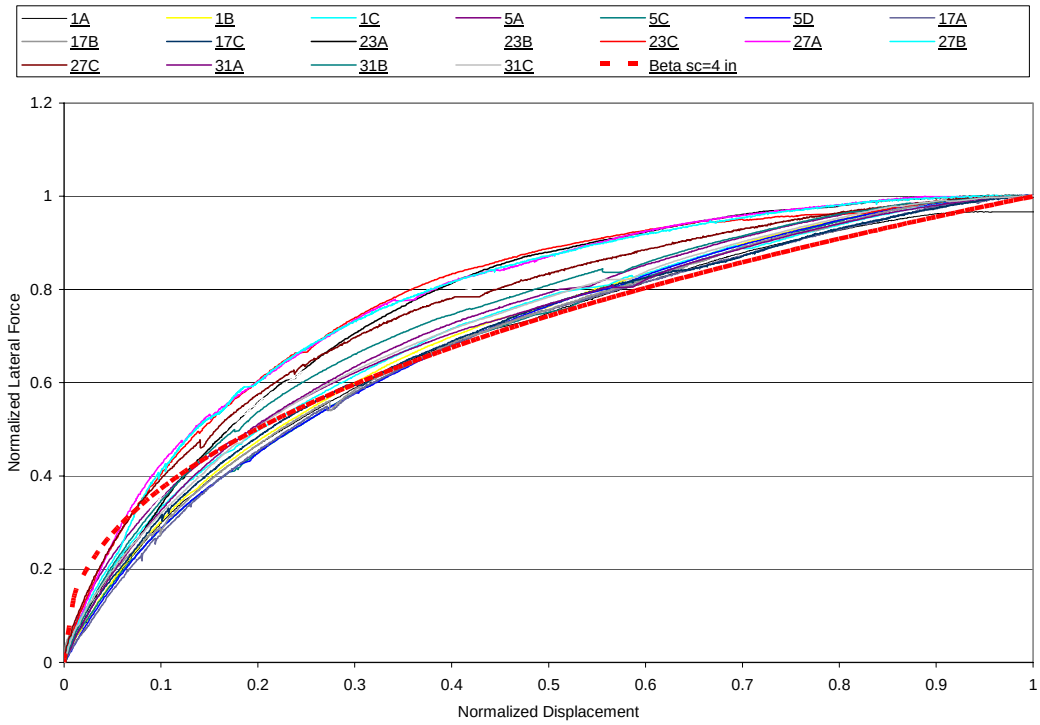

Figure C.2 Experimental (Branston et al., 2004) vs. predicted SWP response for screw spacing s_C=101 mm (4 in)

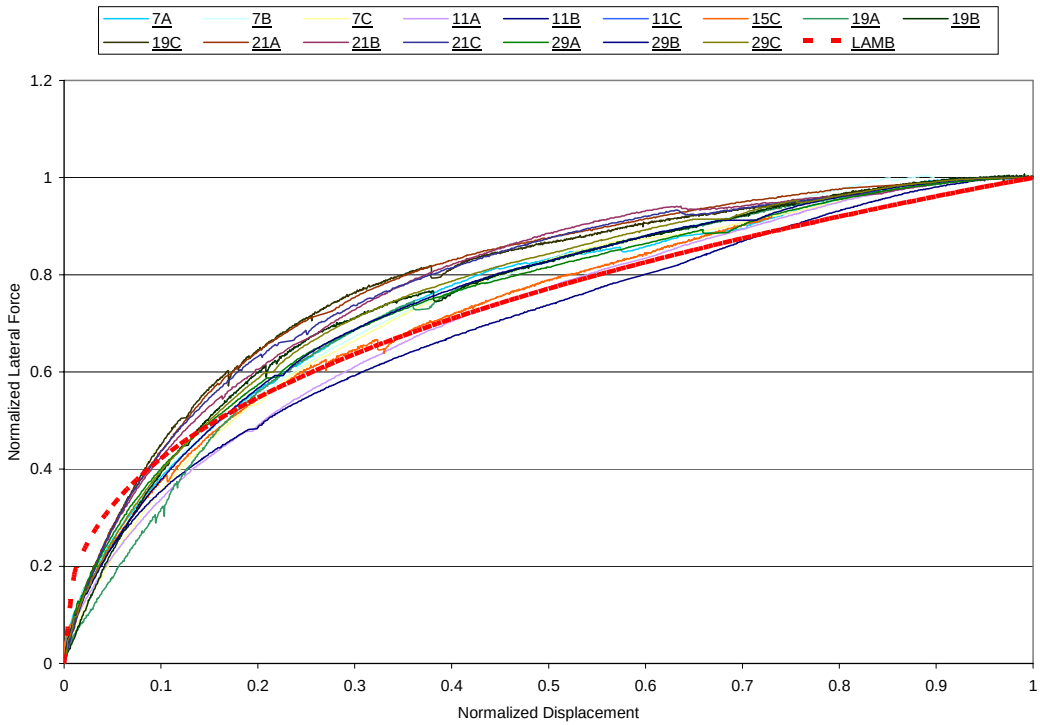

Figure C.3 Experimental (Branston et al., 2004) vs. predicted SWP response for screw spacing s_C=152 mm (6 in)